Appendices

- **Electronic Supplement A: Ground-motion data**
- **Electronic Supplement B: Site-characterization data**
- **Electronic Supplement C: Profiles and site factors**
- **Electronic Supplement D: Systematic residuals for all sites**
- **Electronic Supplement E: Additional considerations and results**

A Electronic Supplement A: Ground-motion data

Figure A.1 presents the distribution of observed ground motions in terms of peak ground acceleration (PGA) versus earthquake magnitude and V_{S30}.

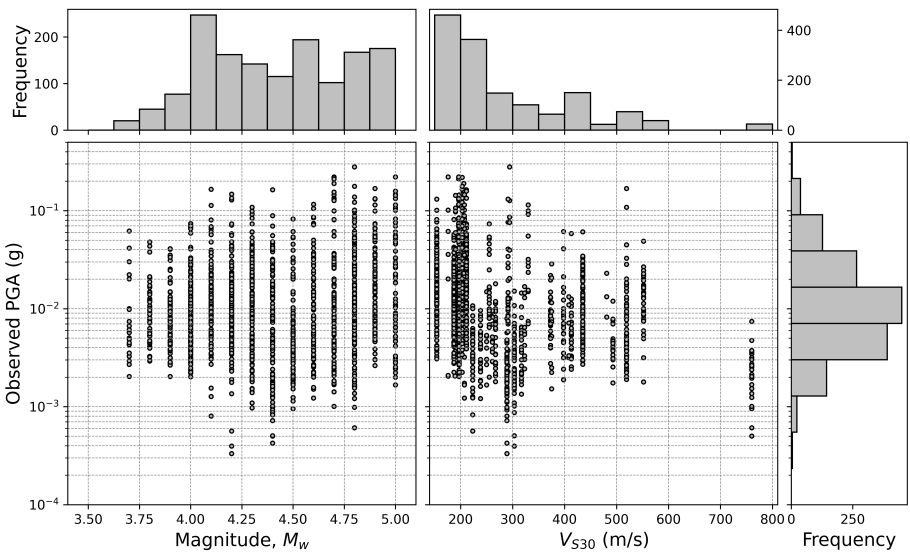

Figure A.1. Ground motion distribution in terms of observed peak ground acceleration (PGA) versus earthquake magnitude and V_{S30}.

Figure A.2 and Figure A.3 present the distribution of the PGV/V_{S30} index, which has been proposed as a proxy for the induced level of shear strain (Idriss, 2011). These figures suggest that (1) soil nonlinearity may be present at several sites in the Canterbury cluster, but (2) the degree of soil nonlinearity should be minor in most cases. The last point is illustrated in Figure A.3, where no appreciable systematic reduction in PGA is observed as PGV/V_{S30} increases (an exception can be noted for some ground motions at REHS).

Figure A.4 shows the relative locations of the seismic sources considered for the REHS and WEMS sites, which are representative sites of the Canterbury and Wellington clusters, respectively.

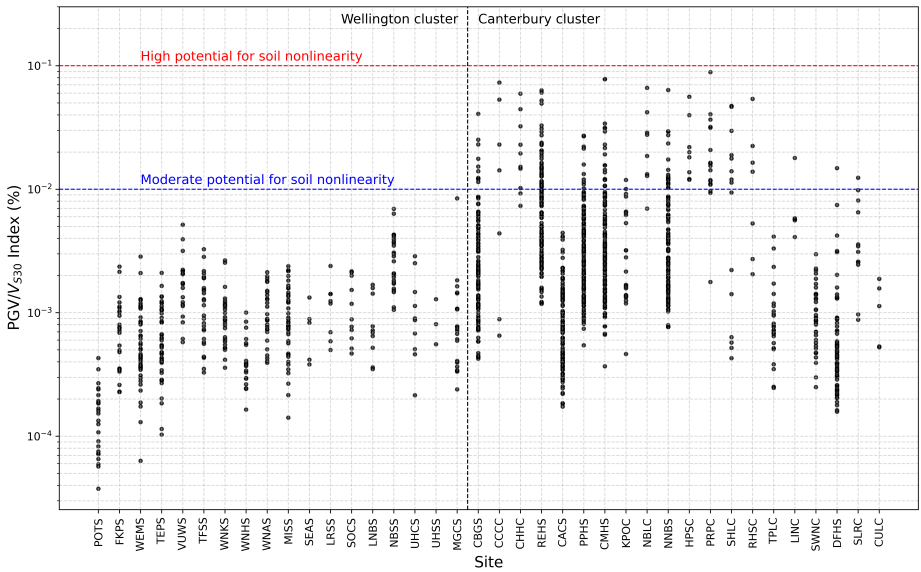

Figure A.2. PGV/V_{S30} index for all observed ground motions at each site.

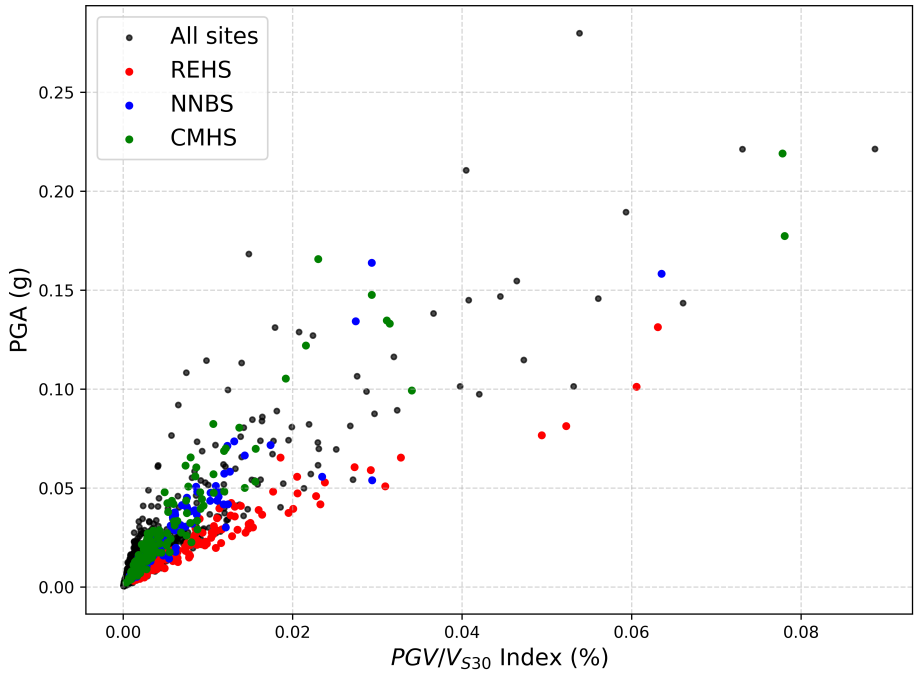

Figure A.3. Observed peak ground acceleration (PGA) versus PGV/V_{S30} index.

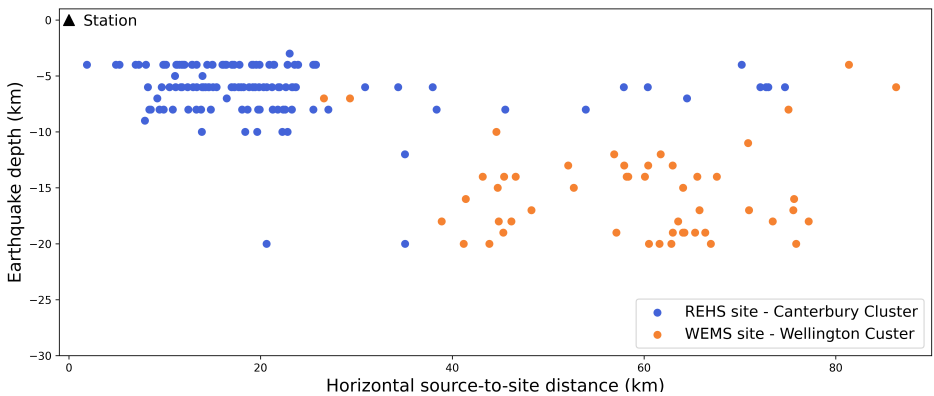

Figure A.4. Relative location of the seismic sources considered for the REHS and WEMS sites.

B Electronic Supplement B: Site-characterization data

B.1 Site data used

The data used to characterize the sites was obtained from several references, summarized in Table B.1. They include boreholes (BHs), standard penetration tests (SPTs), cone penetration tests (CPTs), seismic CPTs (sCPTs), surface-wave (SW) and downhole (DH) seismic testing. Table B.2 summarizes the data used at each site and the corresponding references considered (using the codes presented in Table B.1). The "best estimate of V_S" considered at each station, along with he underlying site data used, are presented in Figures B.1 to B.38.

Table B.1. References considered for obtaining site characterization data.

Reference	Code
Wotherspoon et al. (2015)	W15
Deschenes et al. (2018)	D18
Teague et al. (2018)	T18
Cox and Vantassel (2018)	CV18
Unpublish data collected by QuakeCoRE; Stolte et al. (2021)	QC
NZ Geotechnical Database	NZGD
NZ Geological Survey	NZGS

Table B.2. Sites considered and available site-characterization data.

Station ID	Cluster	Lat	Lon	V_{S30} (m/s)	Site-characterization data			Sources
					V_S	CPT	BH/SPT	
POTS	Wellington	-41.2722	174.7746	760	X			QC
FKPS	Wellington	-41.2879	174.7788	317	X	X	X	CV18, QC, NZGD
WEMS	Wellington	-41.2743	174.7793	303	X	X	X	QC, NZGD
TEPS	Wellington	-41.2906	174.7811	289	X		X	CV18, NZGD
VUWS	Wellington	-41.2799	174.7784	291	X		X	CV18, NZGD
TFSS	Wellington	-41.2754	174.7831	267	X	X	X	QC
WNKS	Wellington	-41.2848	174.7421	373	X	X	X	QC, NZGD
WNHS	Wellington	-41.3008	174.7755	493	X	X	X	QC, NZGD
WNAS	Wellington	-41.3264	174.8090	238	X	X		QC
MISS	Wellington	-41.3149	174.8184	223	X	X	X	QC, NZGS
SEAS	Wellington	-41.3264	174.8376	317	X	X		QC
LRSS	Wellington	-41.2294	174.9042	250	X	X	X	QC, NZGD
SOCS	Wellington	-41.2043	174.9159	261	X			QC
LNBS	Wellington	-41.2050	174.9266	323	X		X	QC, NZGD
NBSS	Wellington	-41.2023	174.9538	189	X		X	QC, NZGD
UHCS	Wellington	-41.1268	175.0409	375	X	X		QC
UHSS	Wellington	-41.1264	175.0651	481	X	X	X	QC, NZGD
MGCS	Wellington	-41.5077	173.9444	413	X	X	X	QC, NZGD
CBGS	Canterbury	-43.5293	172.6199	197	X	X	X	W15
CCCC	Canterbury	-43.5381	172.6474	176	X	X		W15
CHHC	Canterbury	-43.5359	172.6275	206	X	X	X	W15
REHS	Canterbury	-43.5219	172.6351	154	X	X	X	W15, NZGD
CACS	Canterbury	-43.4832	172.5300	435	X		X	W15
PPHS	Canterbury	-43.4928	172.6069	187	X	X	X	W15
CMHS	Canterbury	-43.5656	172.6242	203	X	X	X	W15, T18
KPOC	Canterbury	-43.3765	172.6638	255	X		X	W15
NBLC	Canterbury	-43.5069	172.7314	190	X	X		W15
NNBS	Canterbury	-43.4954	172.7180	211	X	X	X	W15, NZGD
HPSC	Canterbury	-43.5016	172.7022	207	X	X	X	W15
PRPC	Canterbury	-43.5258	172.6828	196	X	X	X	W15
SHLC	Canterbury	-43.5053	172.6634	207	X	X	X	W15
RHSC	Canterbury	-43.5362	172.5644	294	X		X	W15, T18
TPLC	Canterbury	-43.5500	172.4720	398	X			D18
LINC	Canterbury	-43.6232	172.4680	291	X			D18
SWNC	Canterbury	-43.3694	172.4954	552	X			D18
DFHS	Canterbury	-43.4897	172.1022	519	X			D18
SLRC	Canterbury	-43.6751	172.3175	330	X			D18
CULC	Canterbury	-42.7594	172.8026	408	X			QC

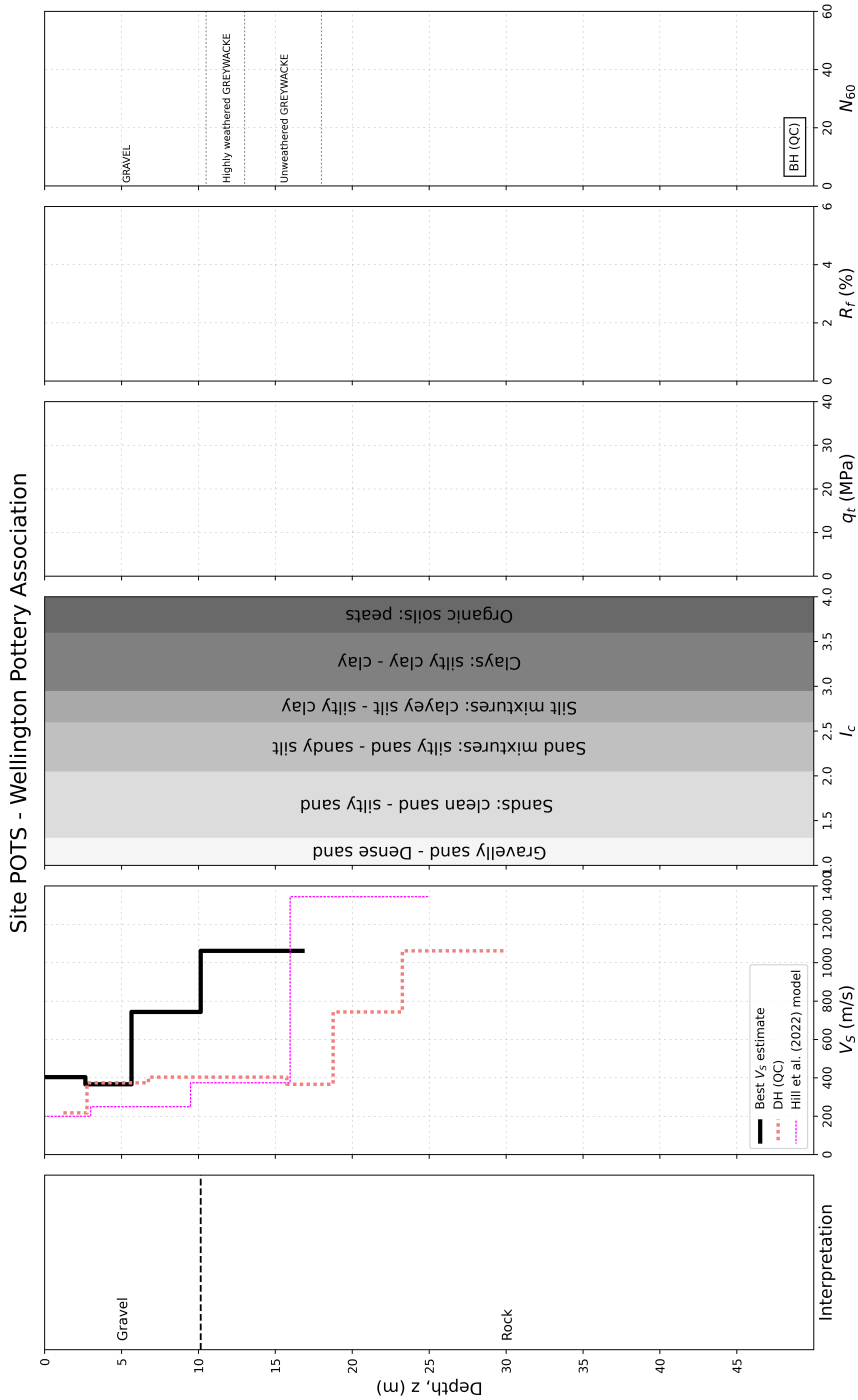

Figure B.1. Site data used to characterize the site POTS, located in the Wellington Region.

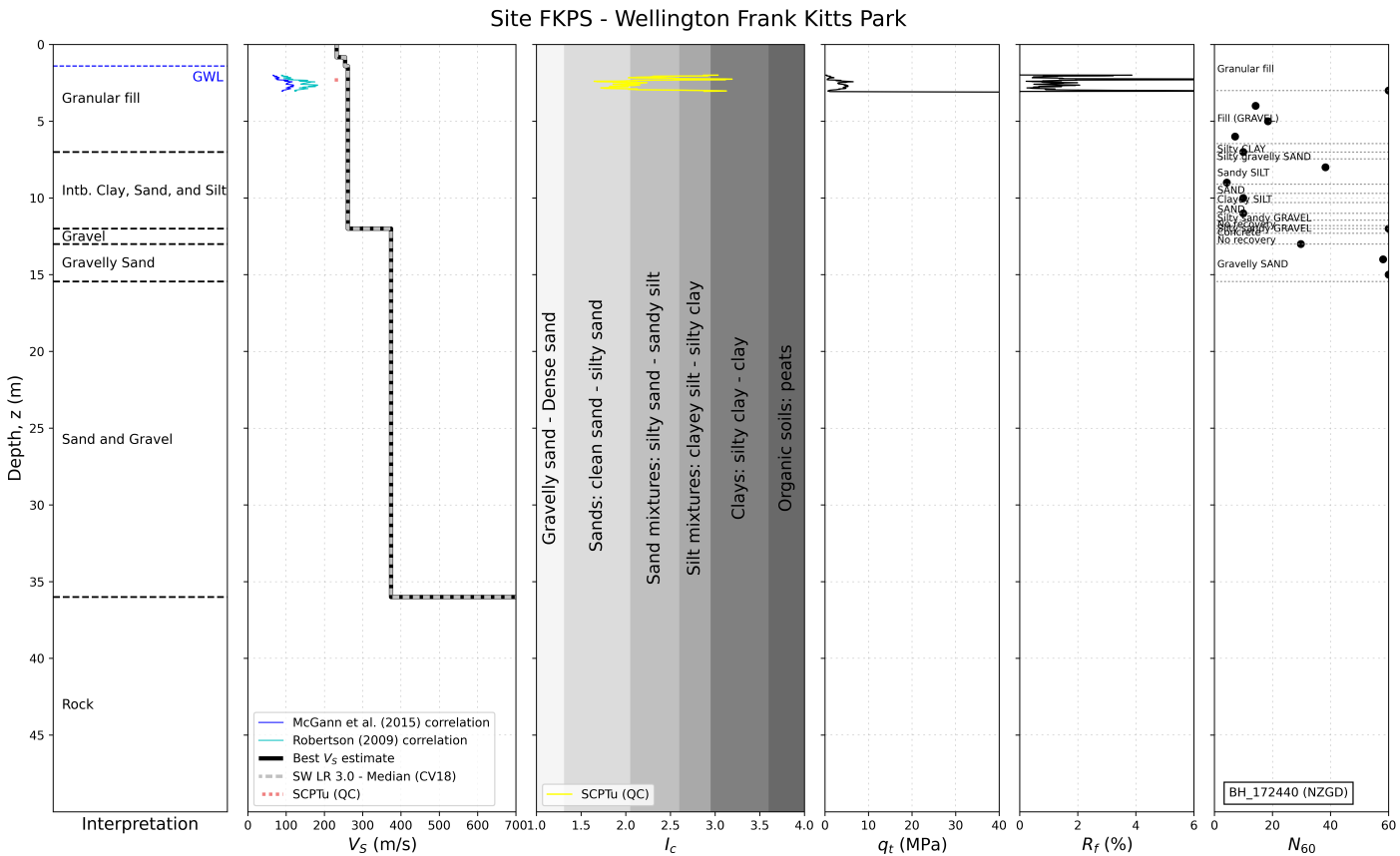

Figure B.2. Site data used to characterize the site FKPS, located in the Wellington Region.

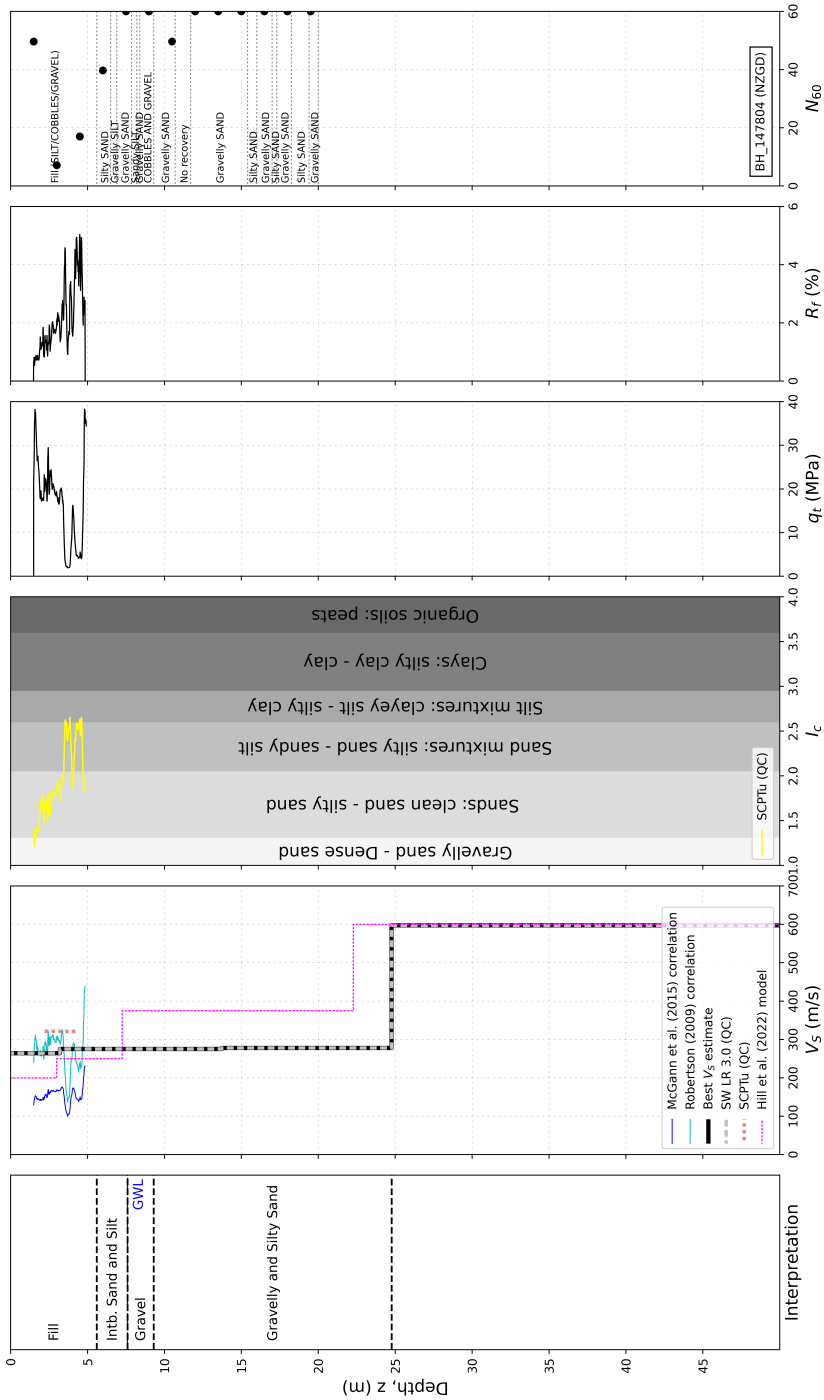

Figure B.3. Site data used to characterize the site WEMS, located in the Wellington Region.

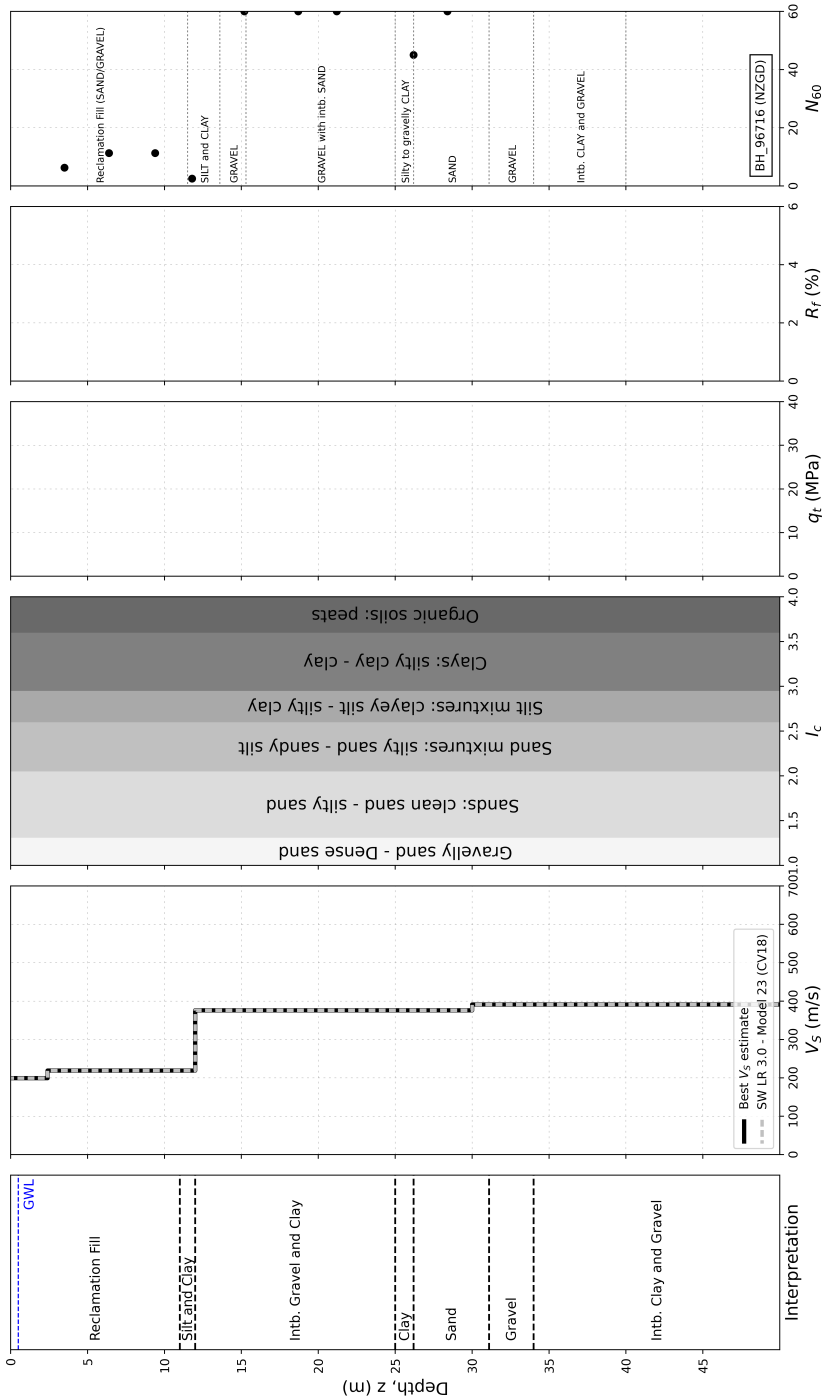

Figure B.4. Site data used to characterize the site TEPS, located in the Wellington Region.

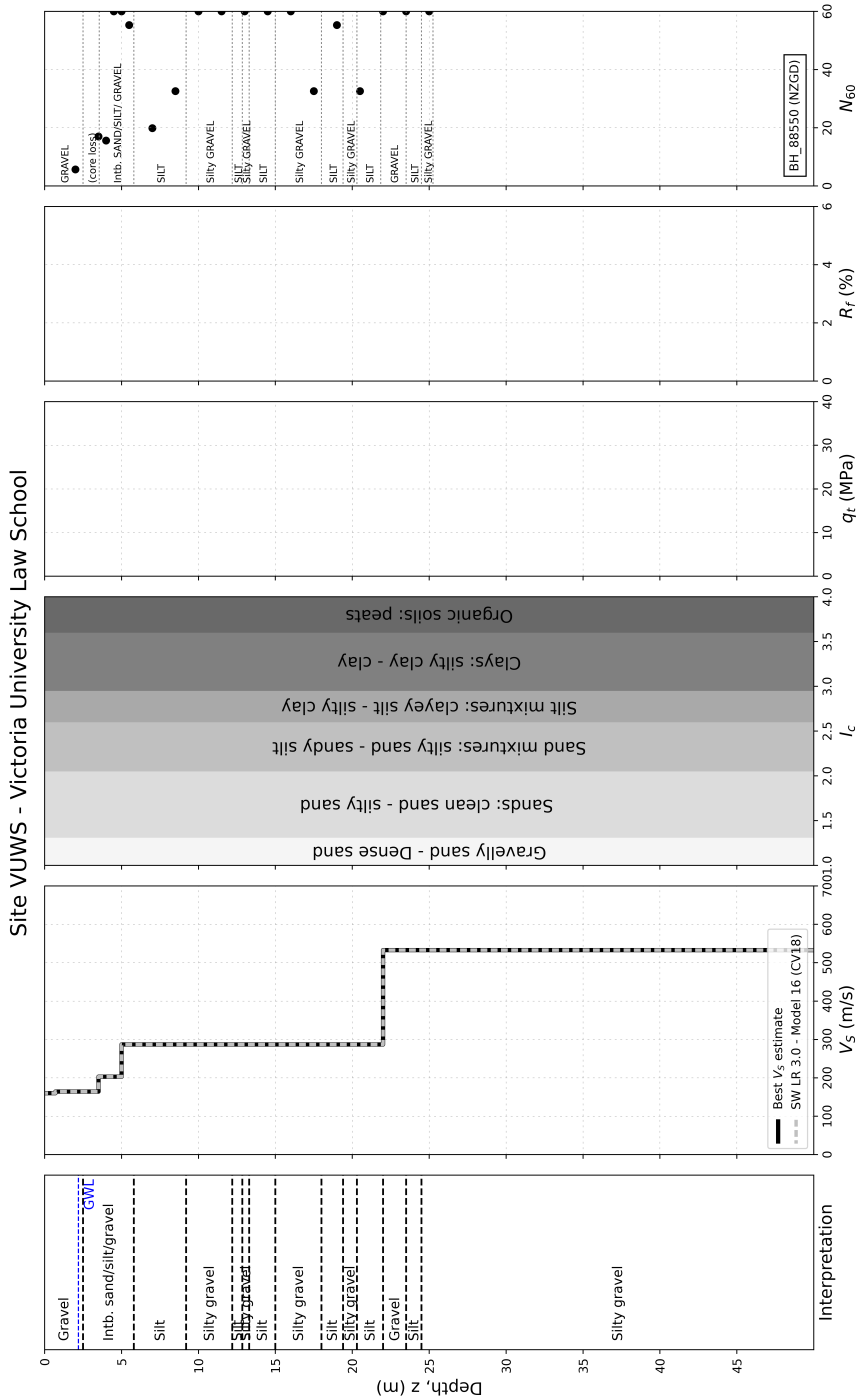

Figure B.5. Site data used to characterize the site VUWS, located in the Wellington Region.

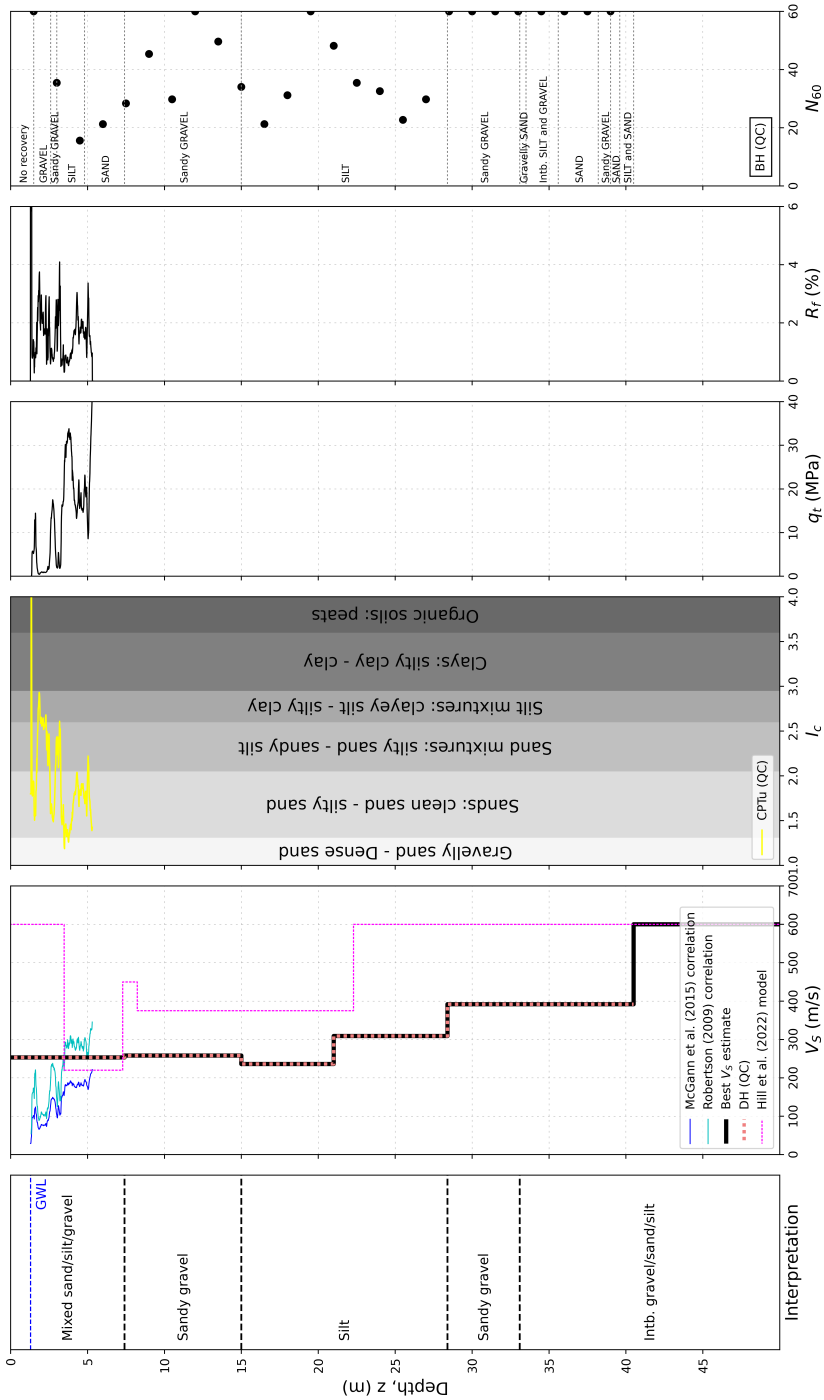

Figure B.6. Site data used to characterize the site TFSS, located in the Wellington Region.

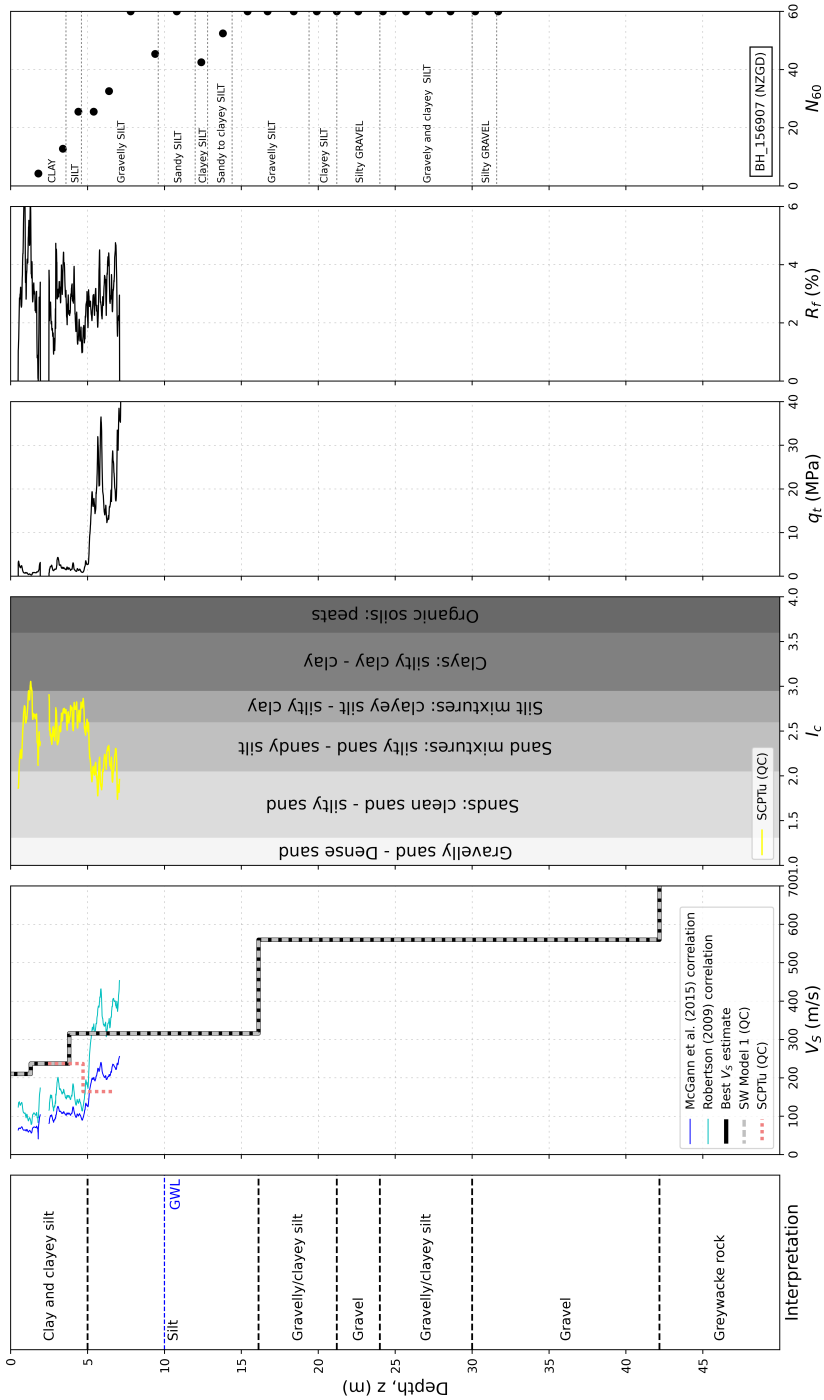

Figure B.7. Site data used to characterize the site WNKS, located in the Wellington Region.

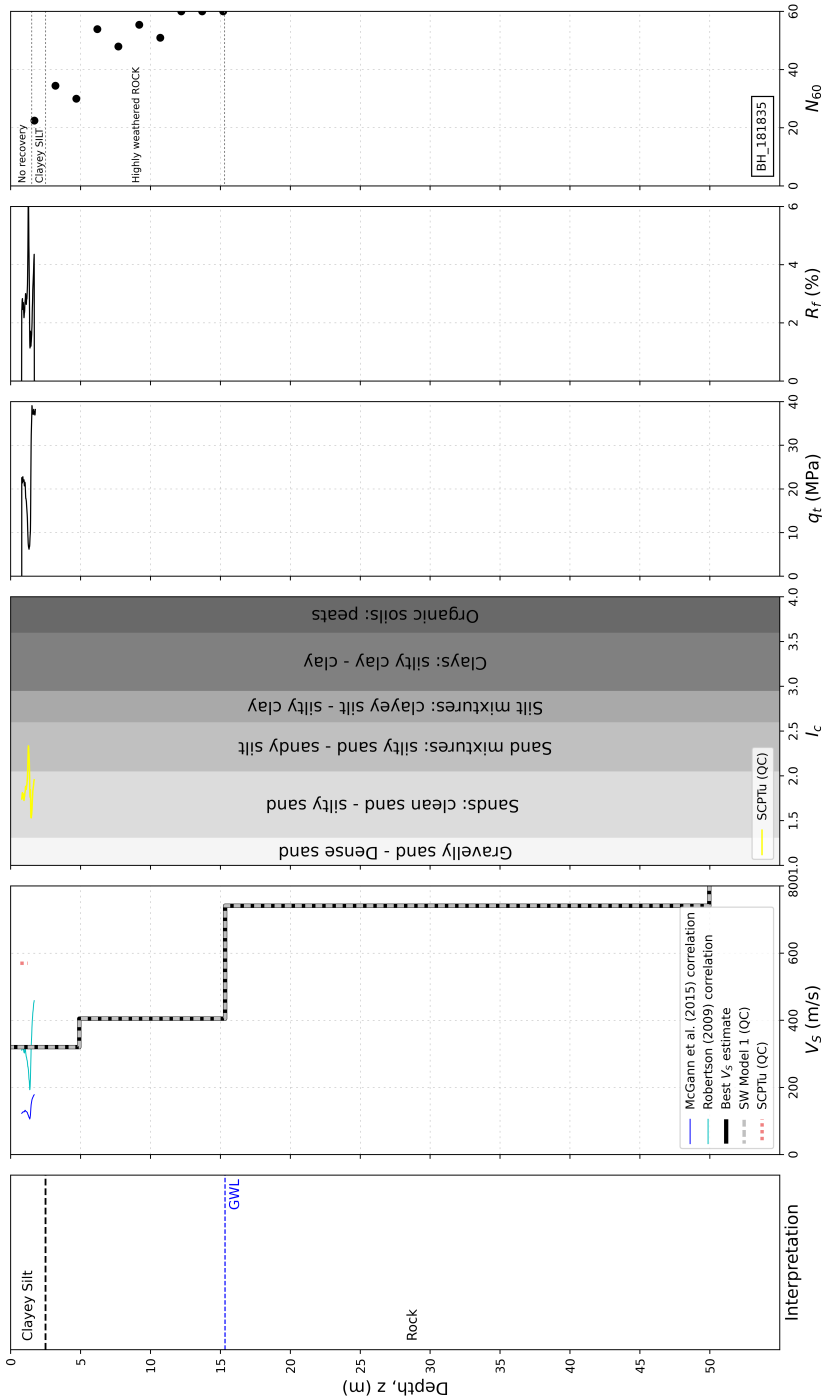

Figure B.8. Site data used to characterize the site WNHS, located in the Wellington Region.

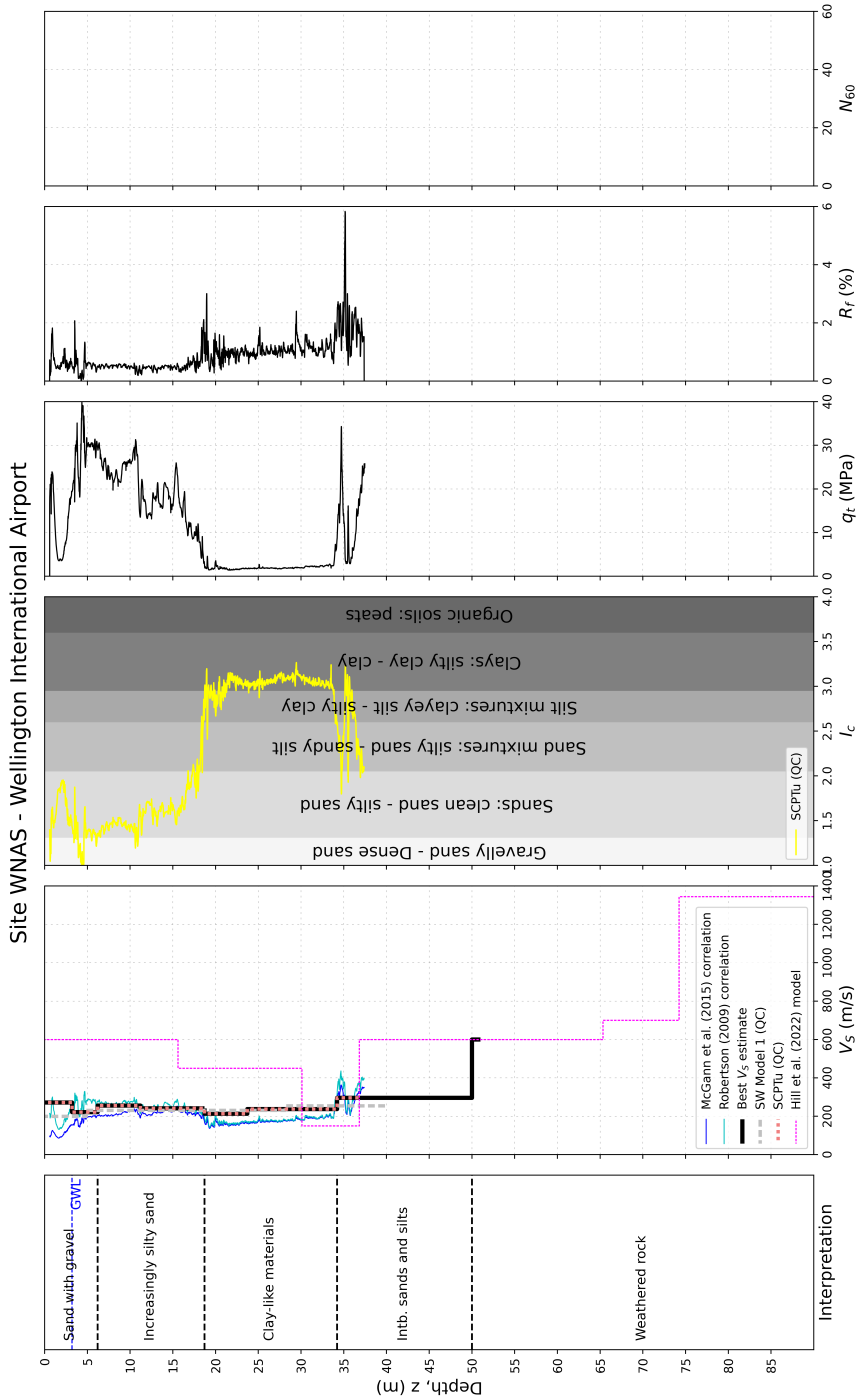

Figure B.9. Site data used to characterize the site WNAS, located in the Wellington Region.

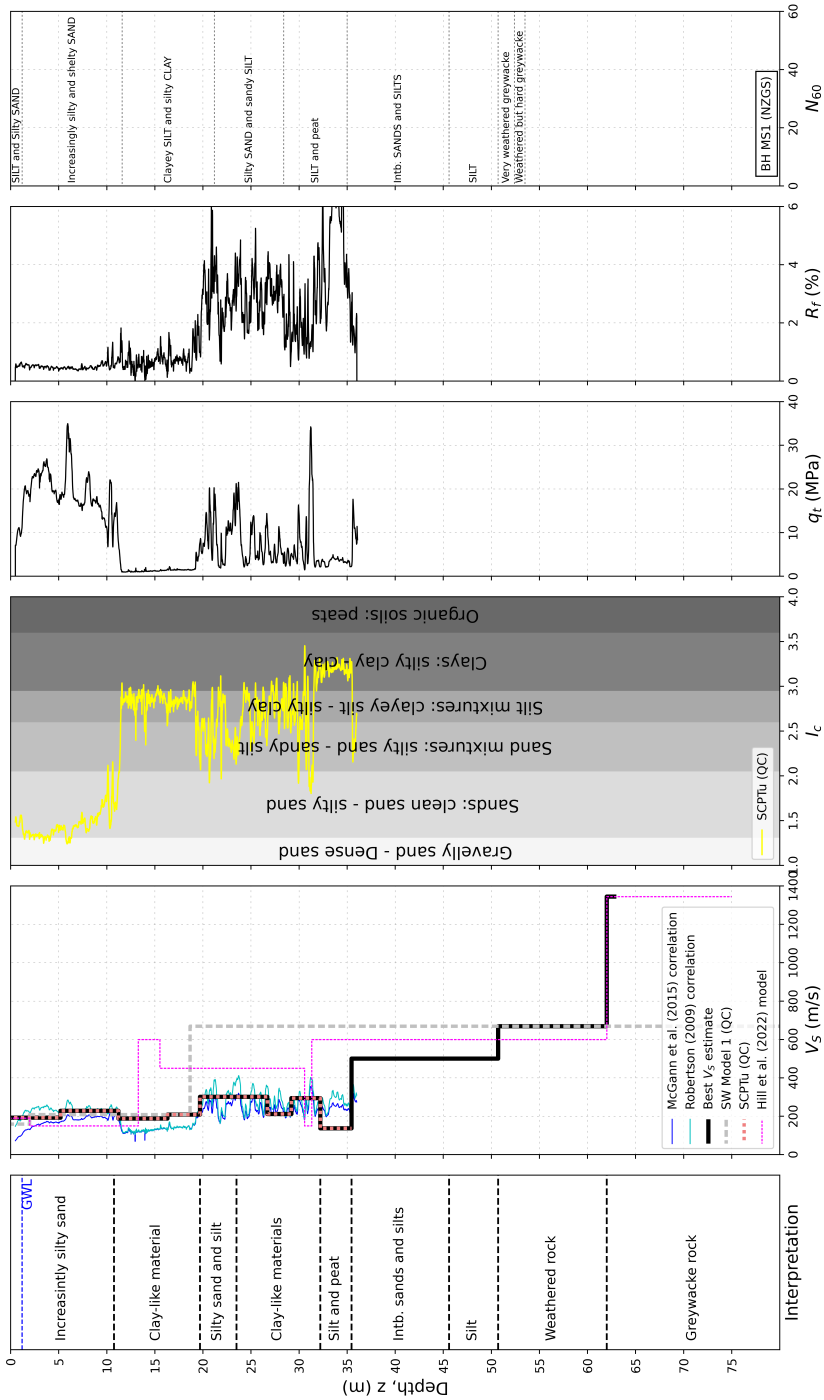

Figure B.10. Site data used to characterize the site MISS, located in the Wellington Region.

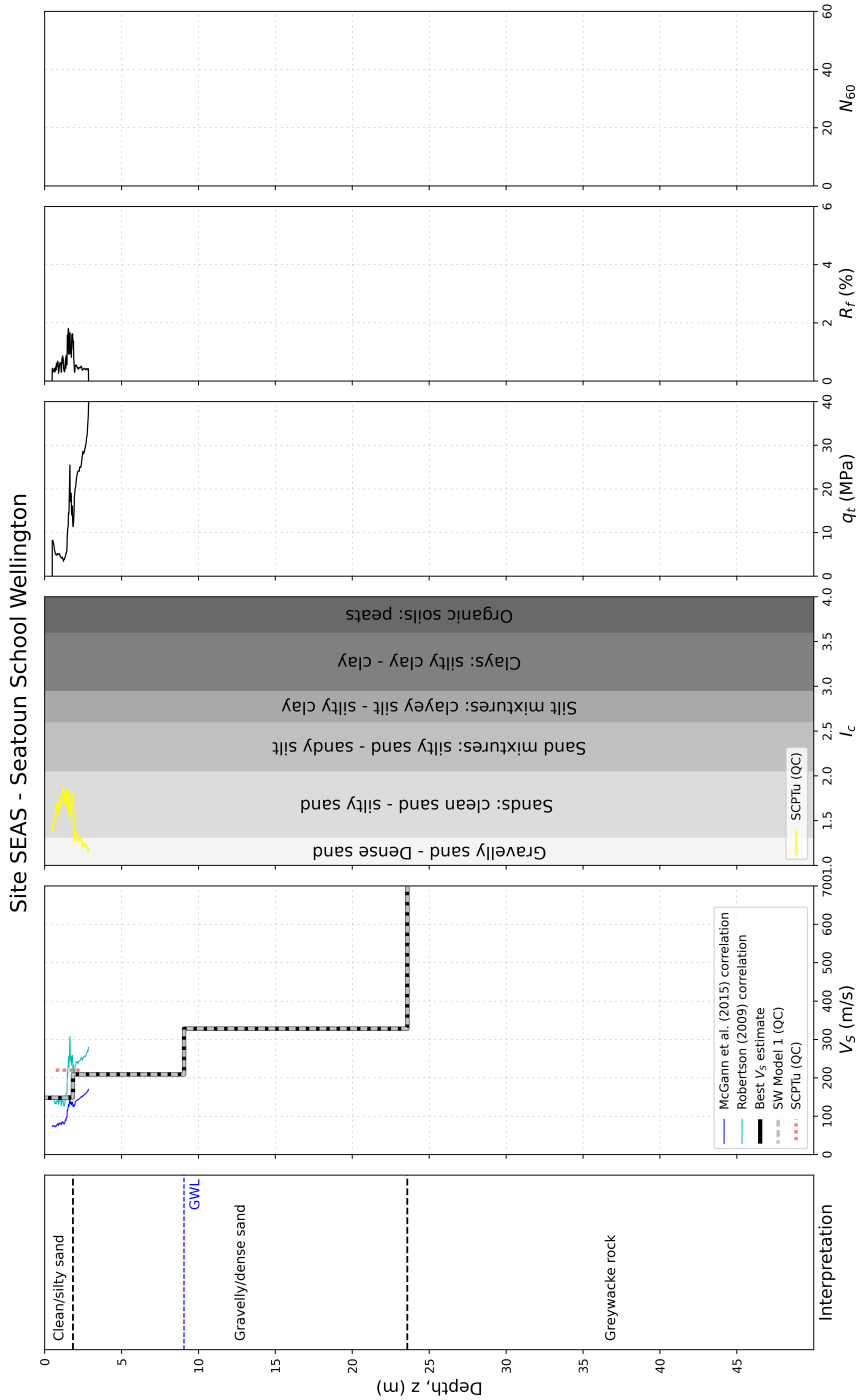

Figure B.11. Site data used to characterize the site SEAS, located in the Wellington Region.

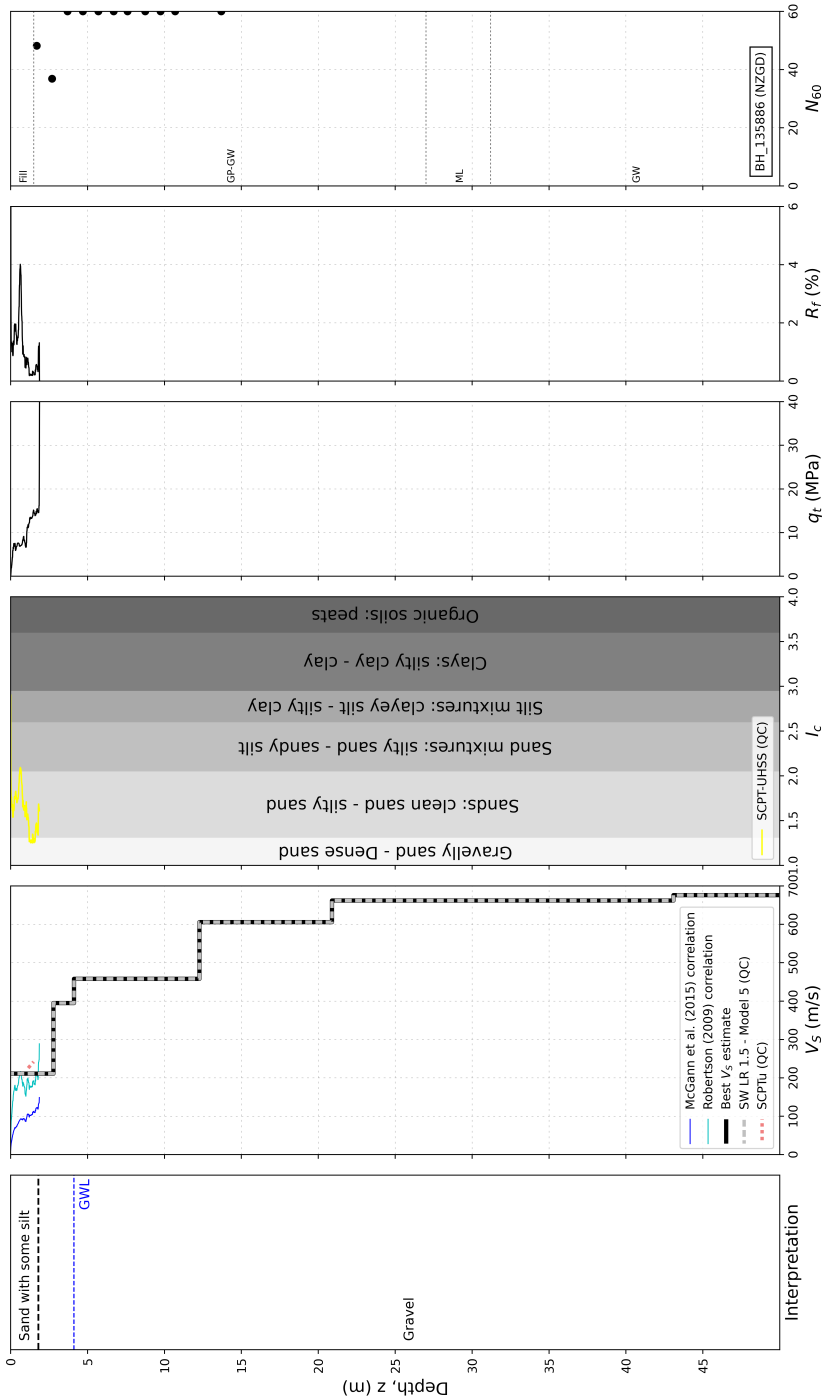

Figure B.12. Site data used to characterize the site UHSS, located in the Wellington Region.

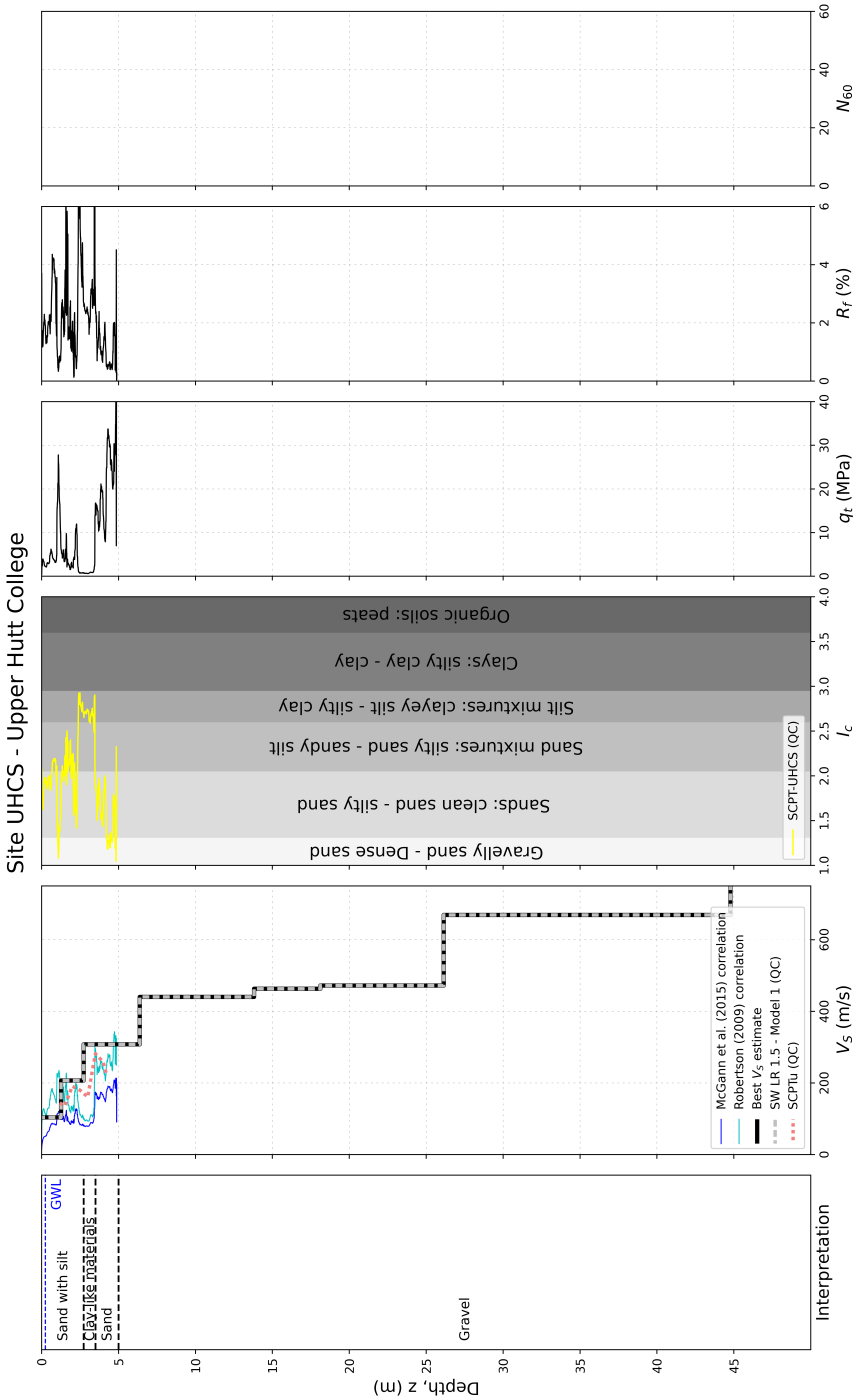

Figure B.13. Site data used to characterize the site UHCS, located in the Wellington Region.

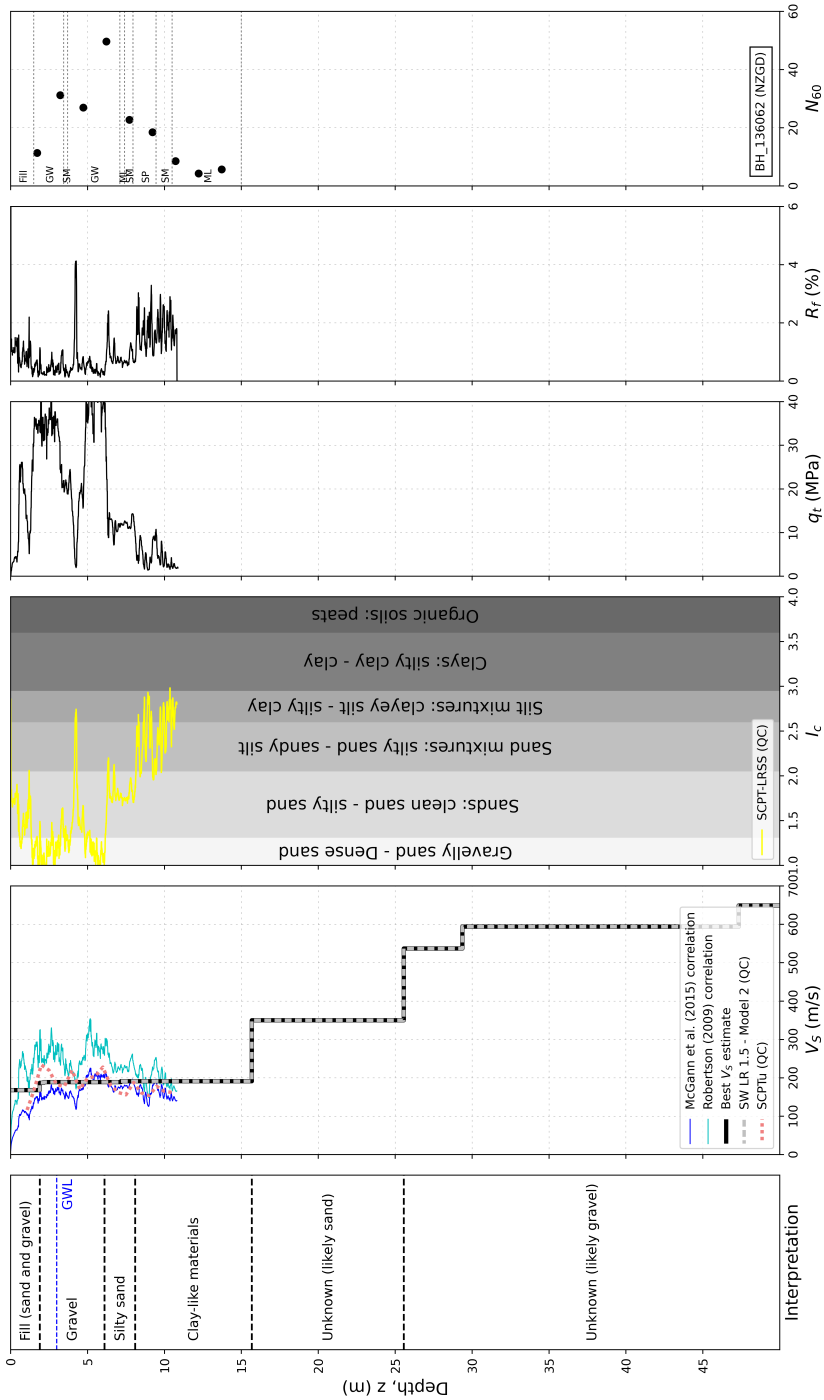

Figure B.14. Site data used to characterize the site LRSS, located in the Wellington Region.

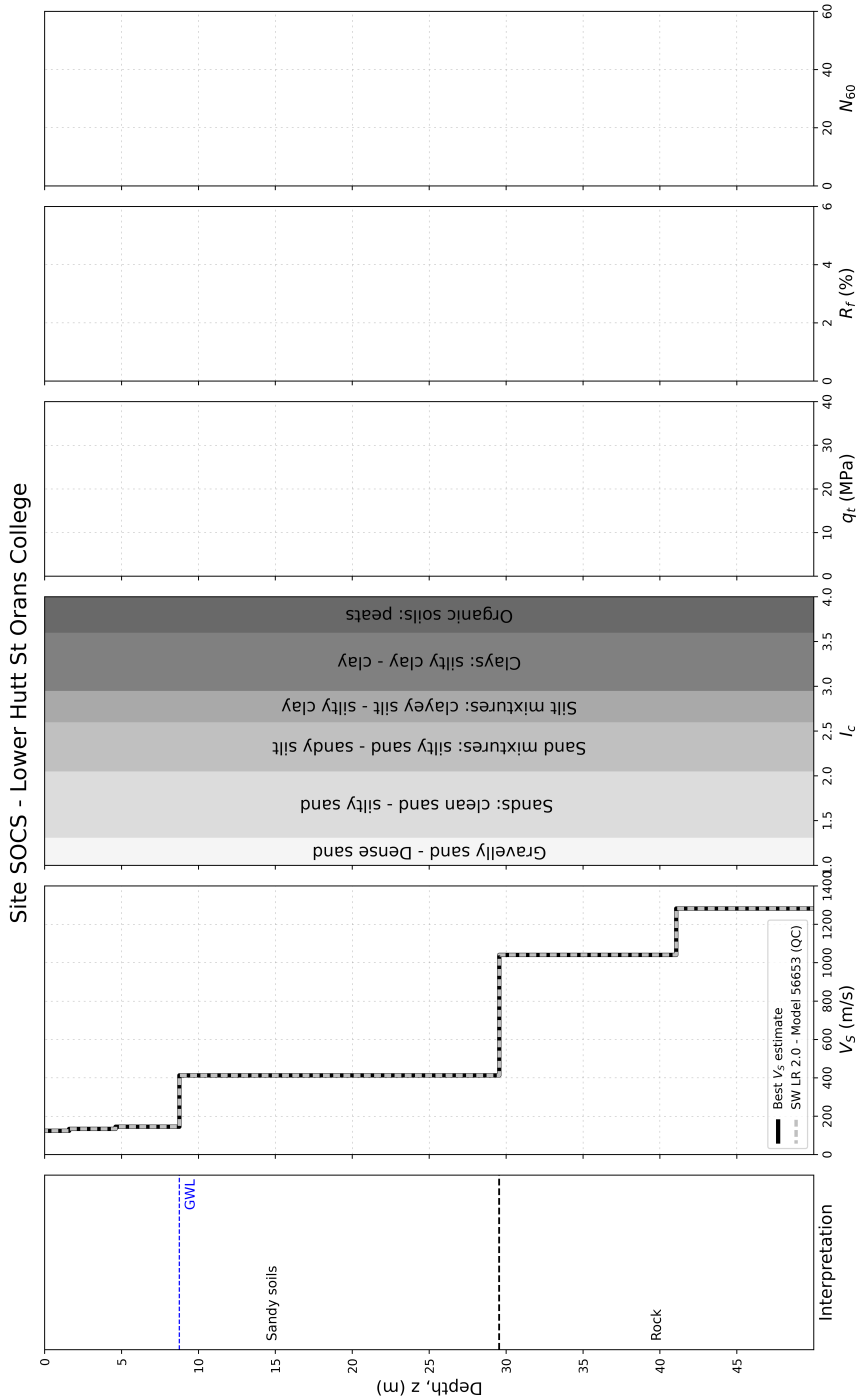

Figure B.15. Site data used to characterize the site SOCS, located in the Wellington Region.

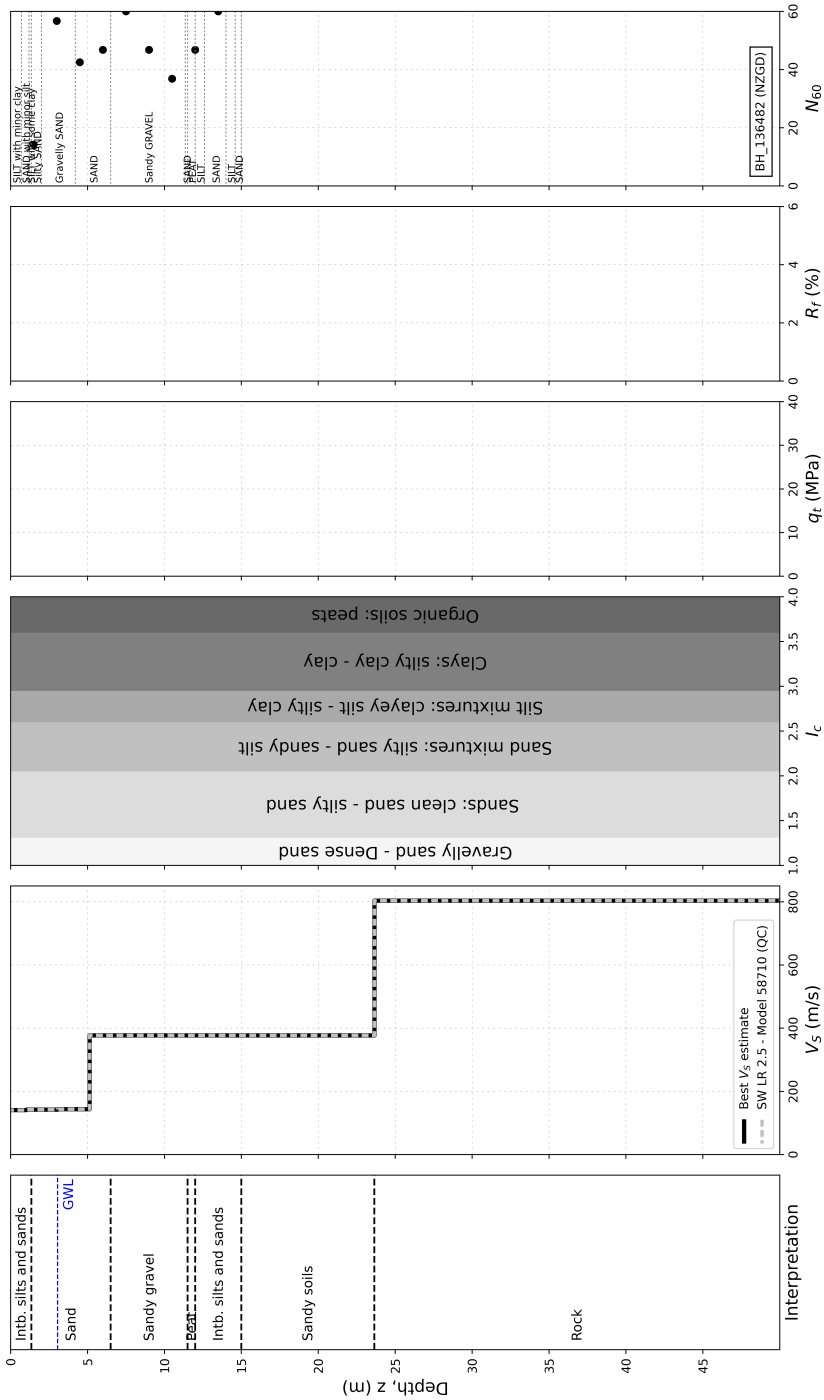

Figure B.16. Site data used to characterize the site LNBS, located in the Wellington Region.

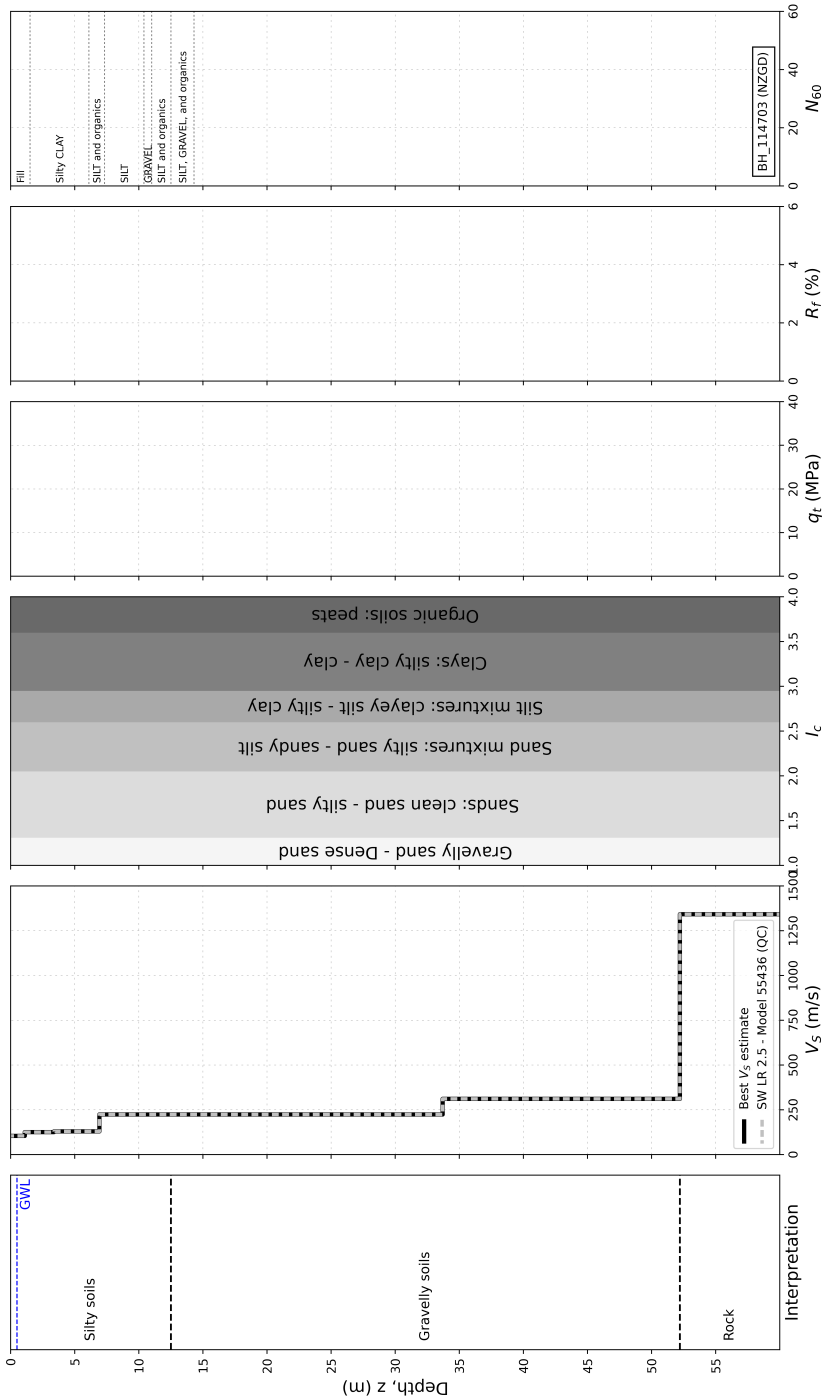

Figure B.17. Site data used to characterize the site NBSS, located in the Wellington Region.

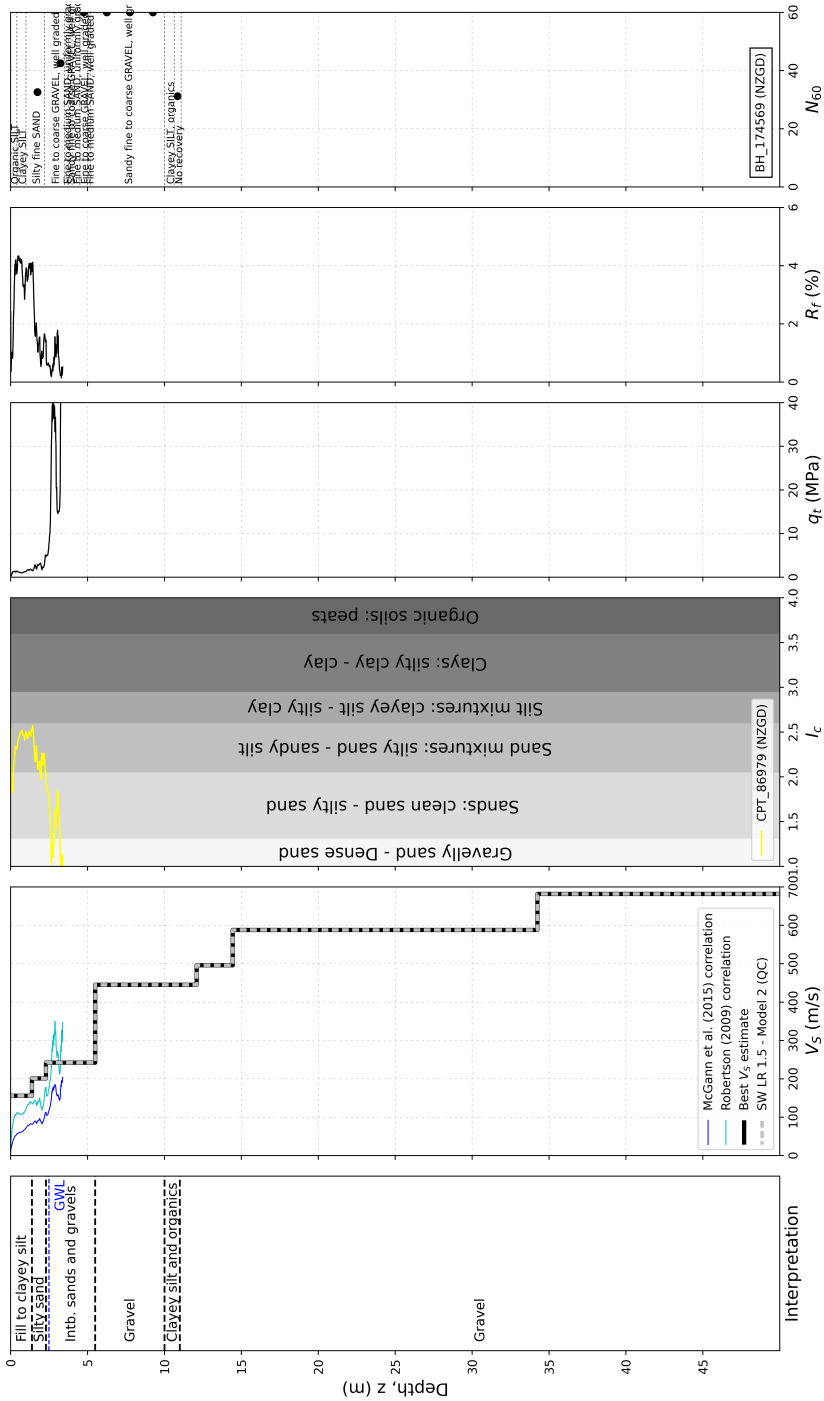

Figure B.18. Site data used to characterize the site MGCS, located in the Marlborough Region.

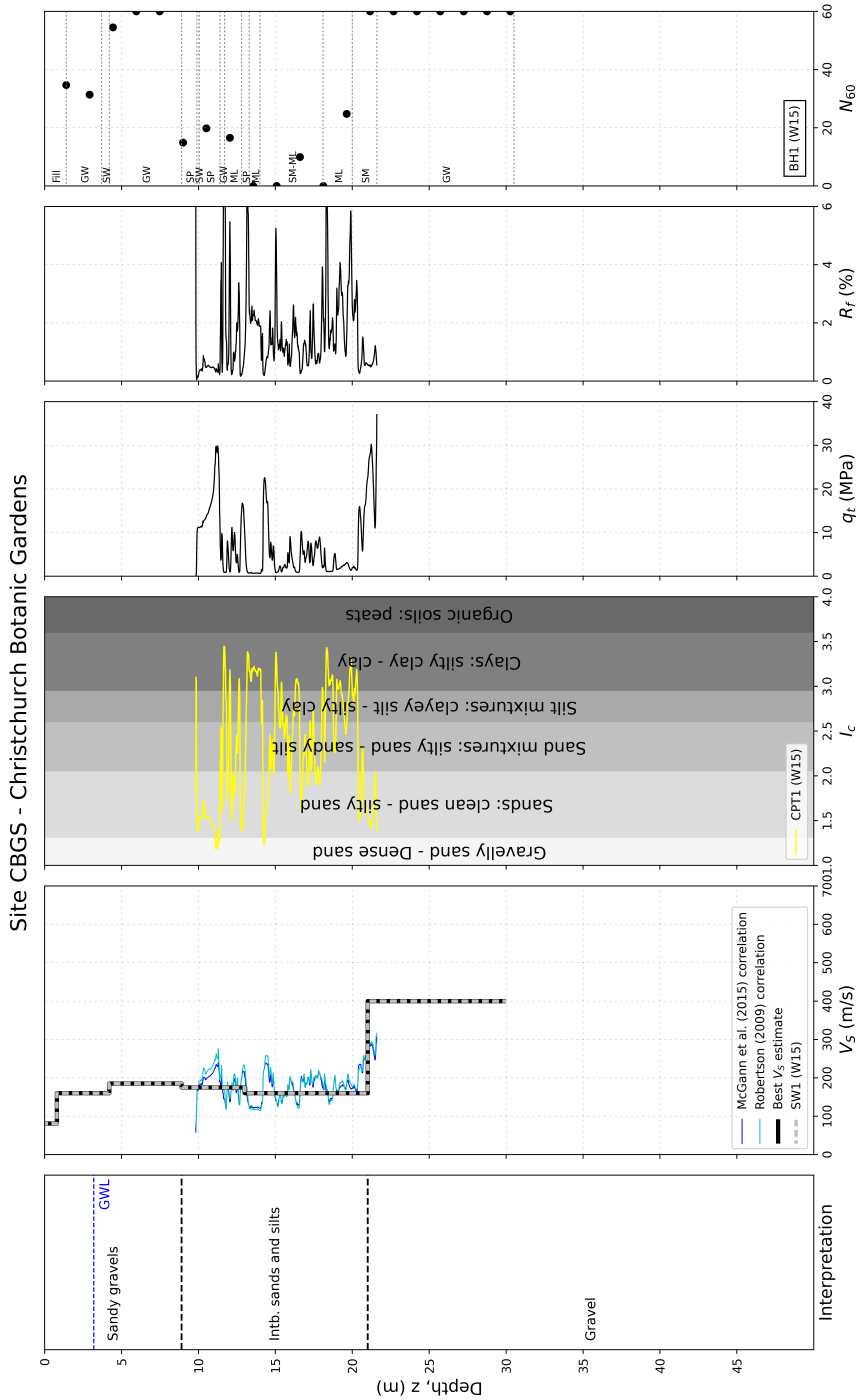

Figure B.19. Site data used to characterize the site CBGS, located in the Canterbury Region.

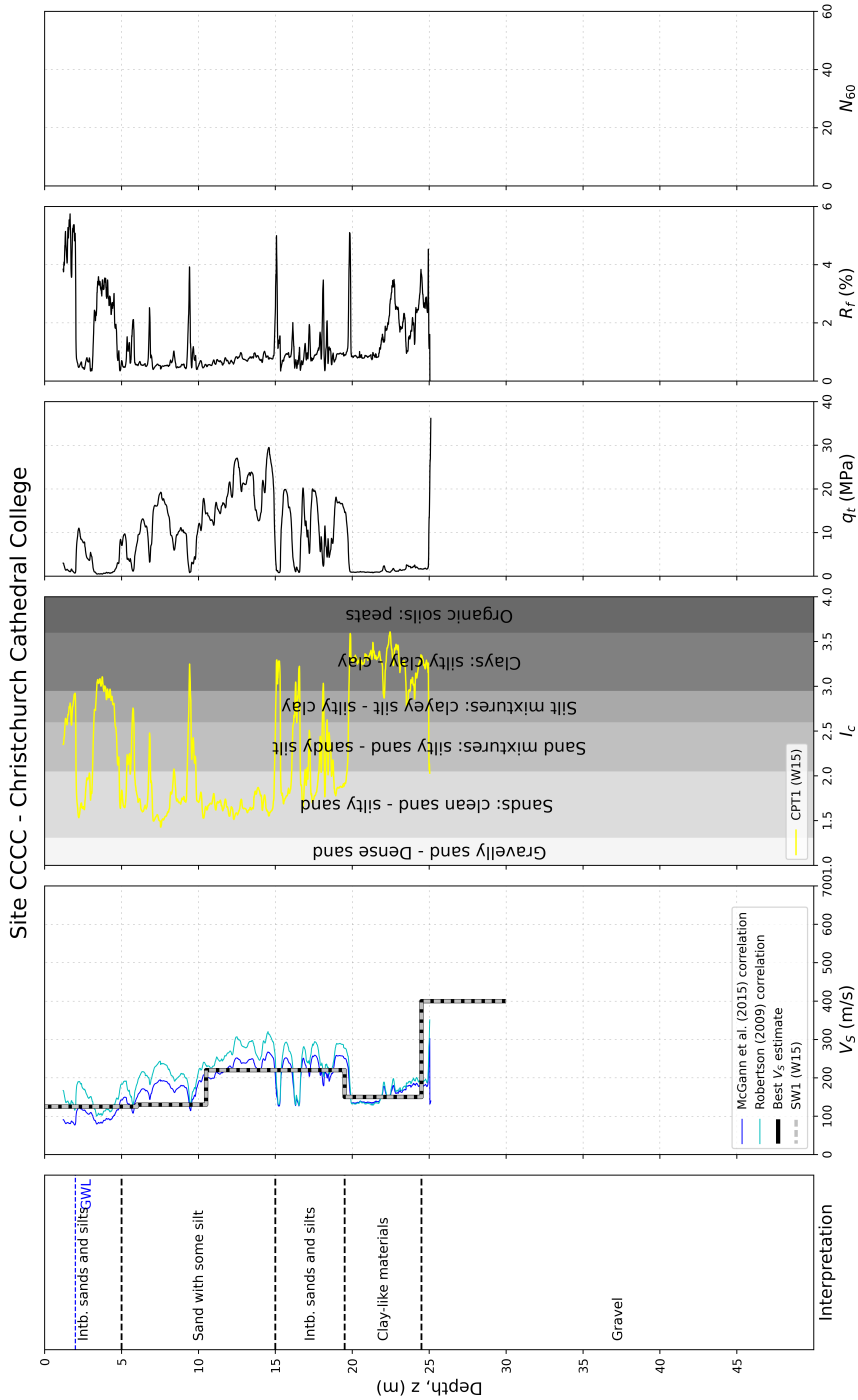

Figure B.20. Site data used to characterize the site CCCC, located in the Canterbury Region.

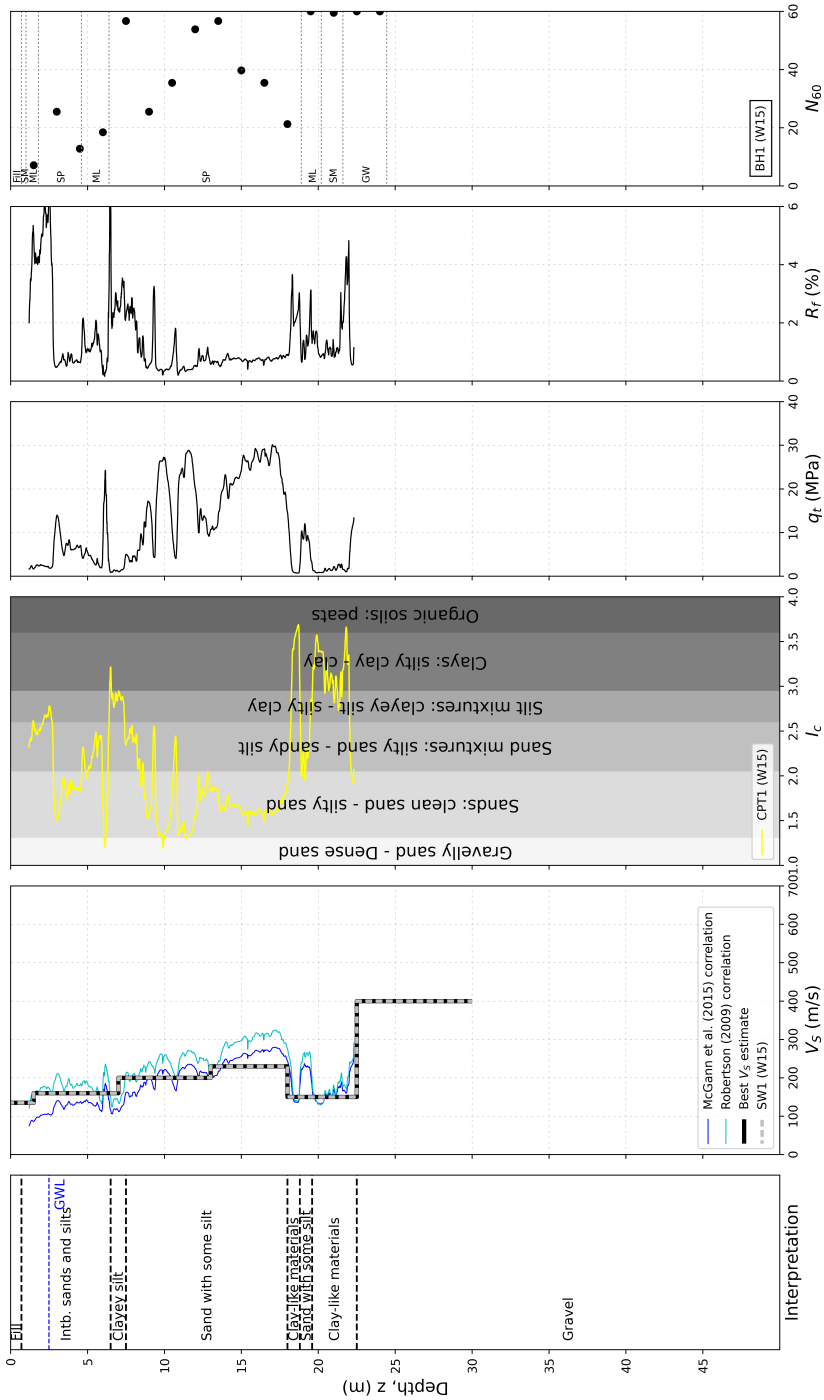

Figure B.21. Site data used to characterize the site CHHC, located in the Canterbury Region.

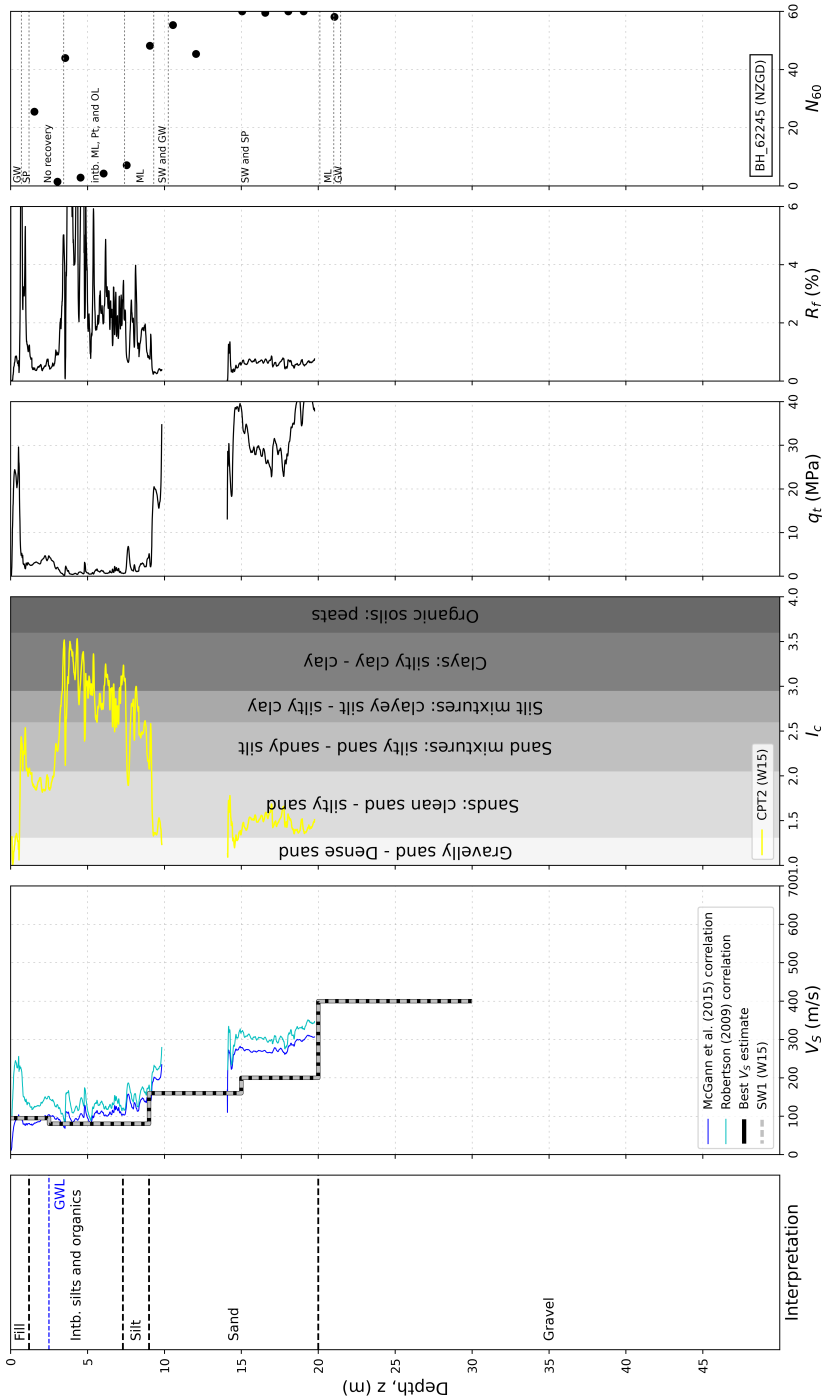

Figure B.22. Site data used to characterize the site REHS, located in the Canterbury Region.

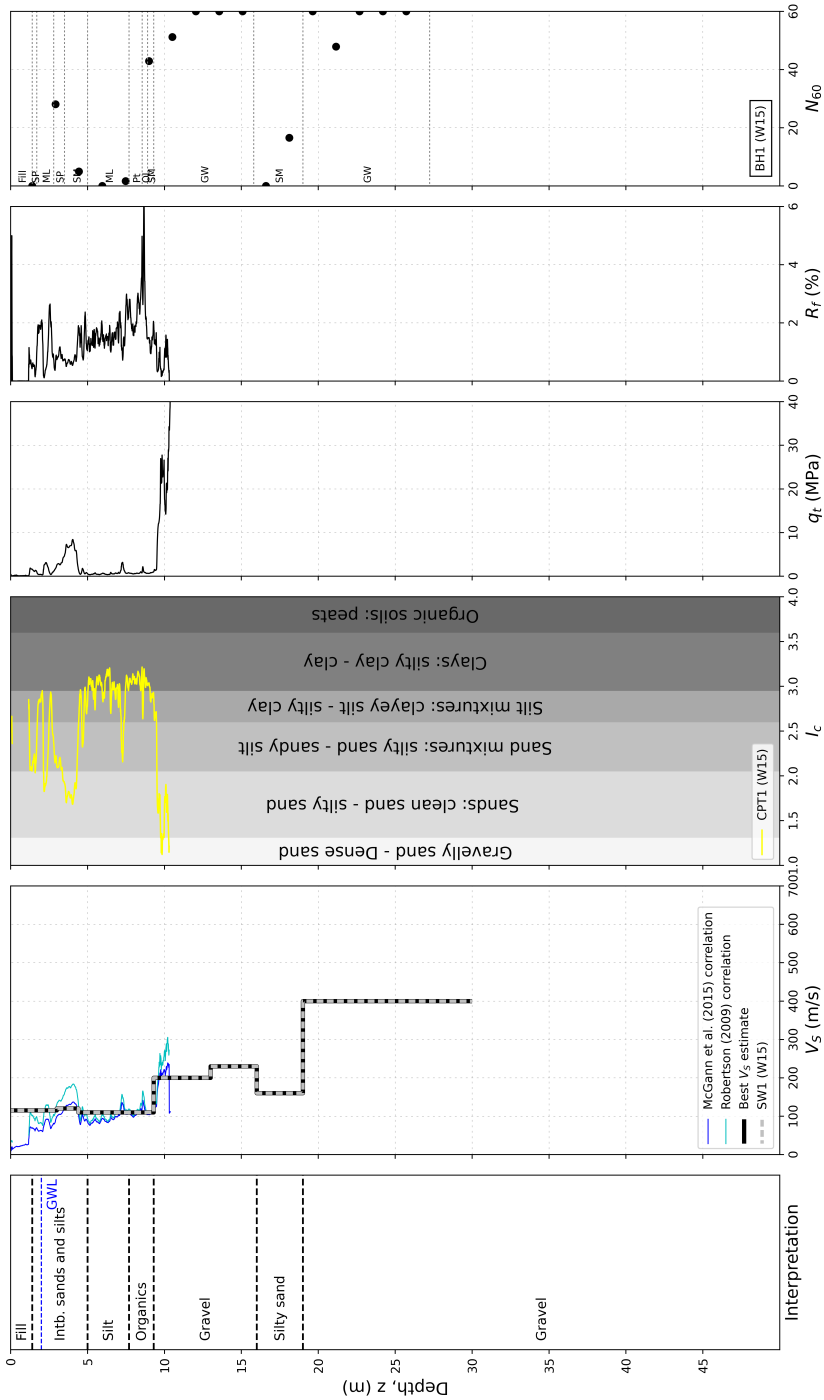

Figure B.23. Site data used to characterize the site PPHS, located in the Canterbury Region.

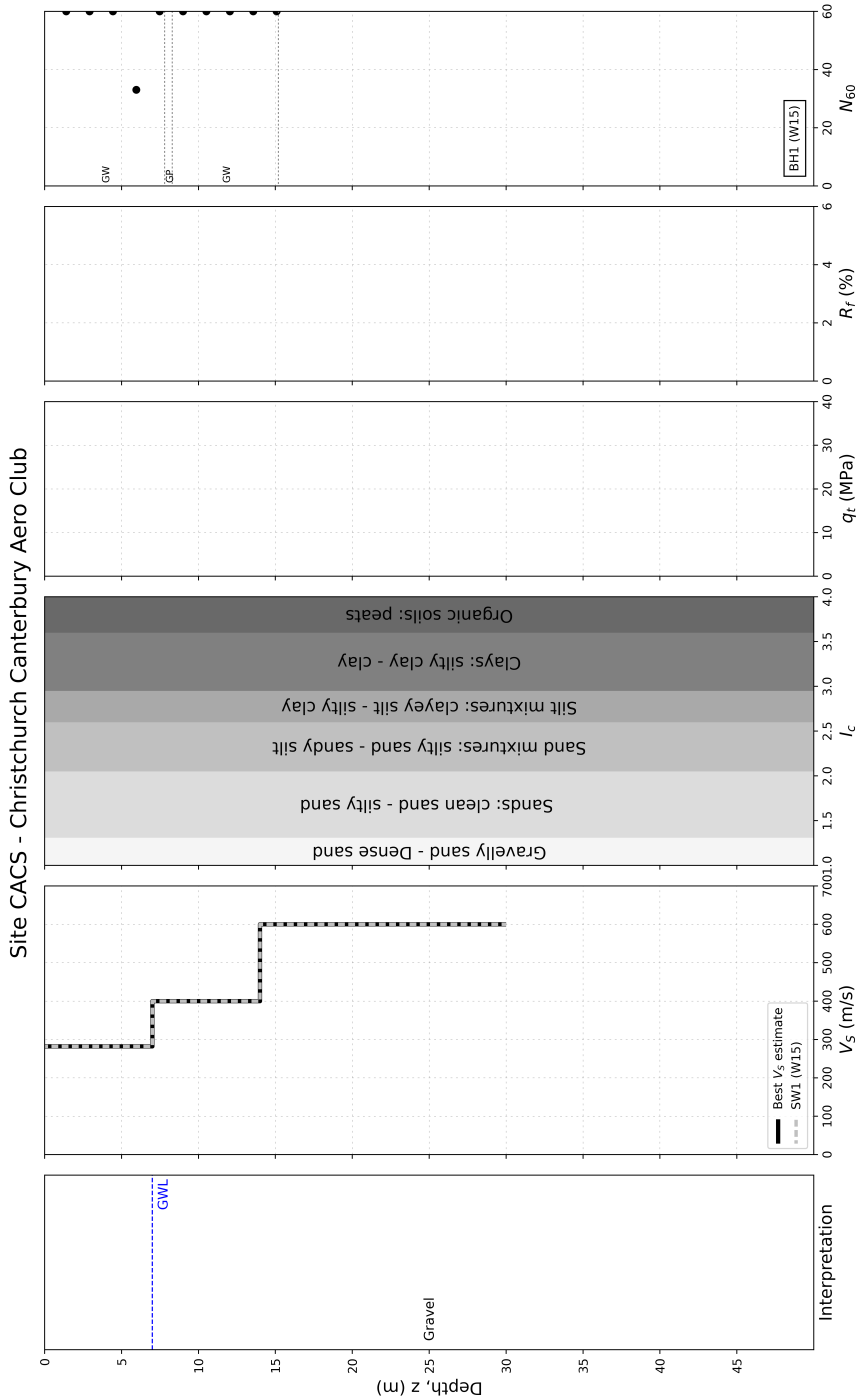

Figure B.24. Site data used to characterize the site CACS, located in the Canterbury Region.

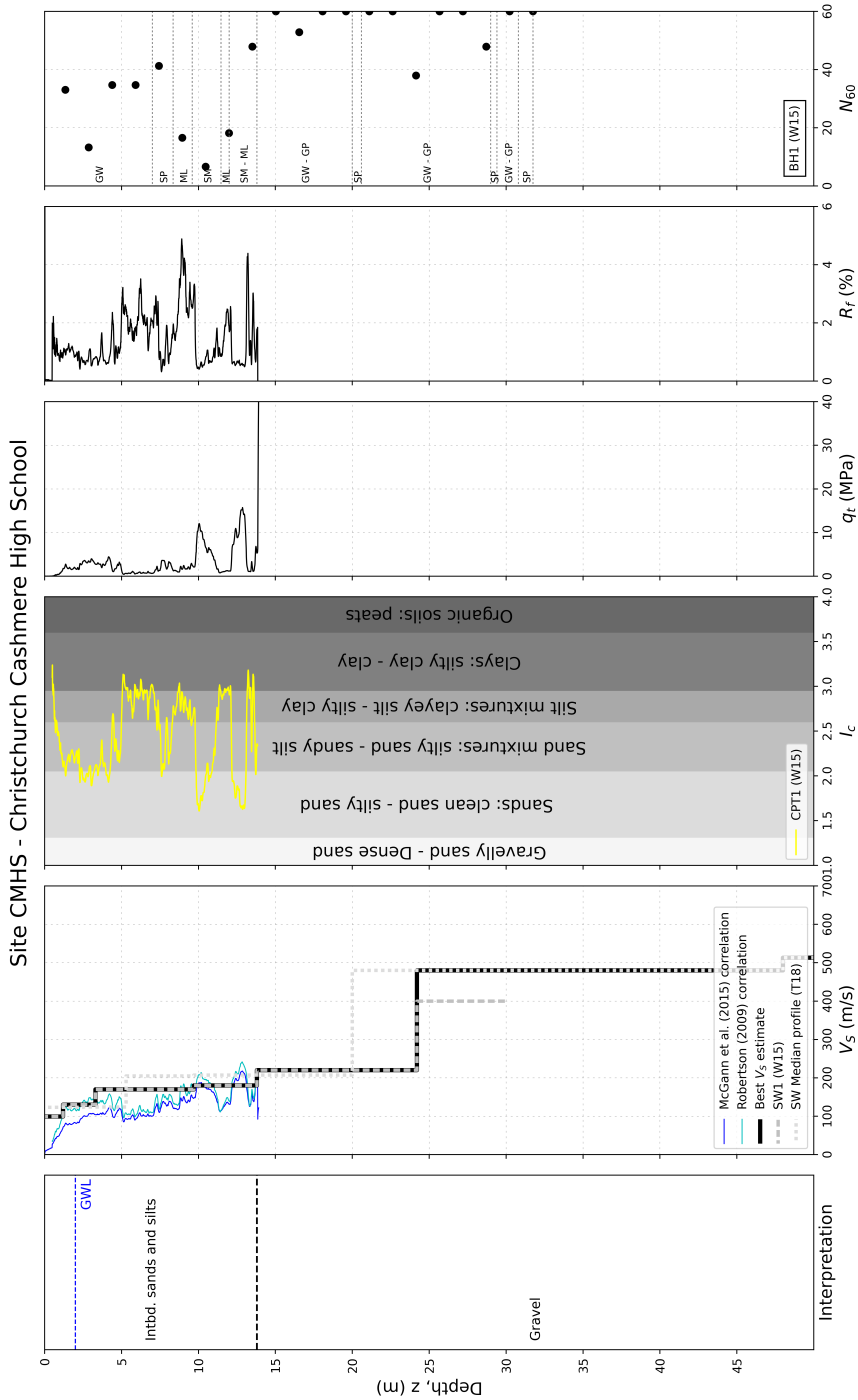

Figure B.25. Site data used to characterize the site CMHS, located in the Canterbury Region.

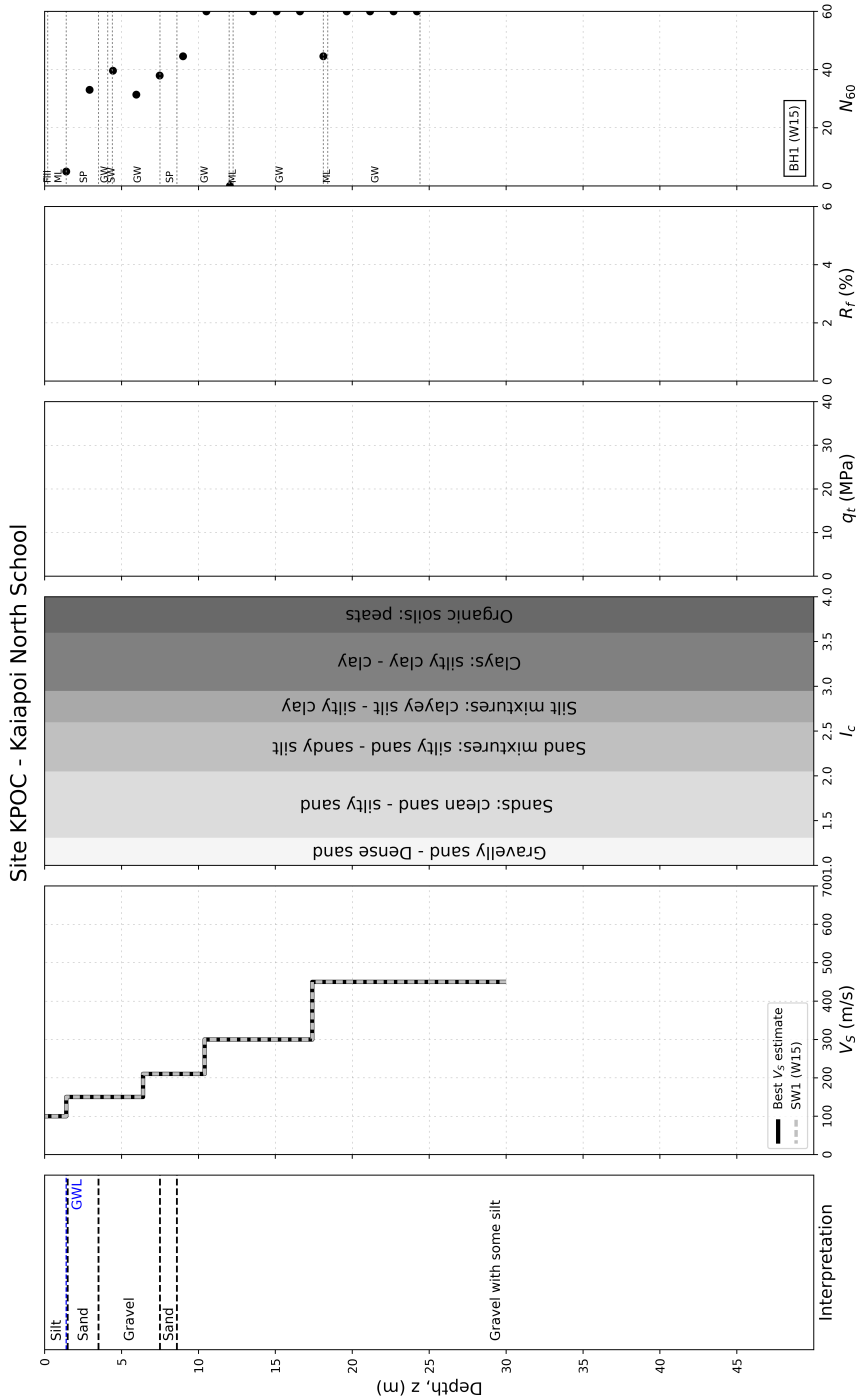

Figure B.26. Site data used to characterize the site KPOC, located in the Canterbury Region.

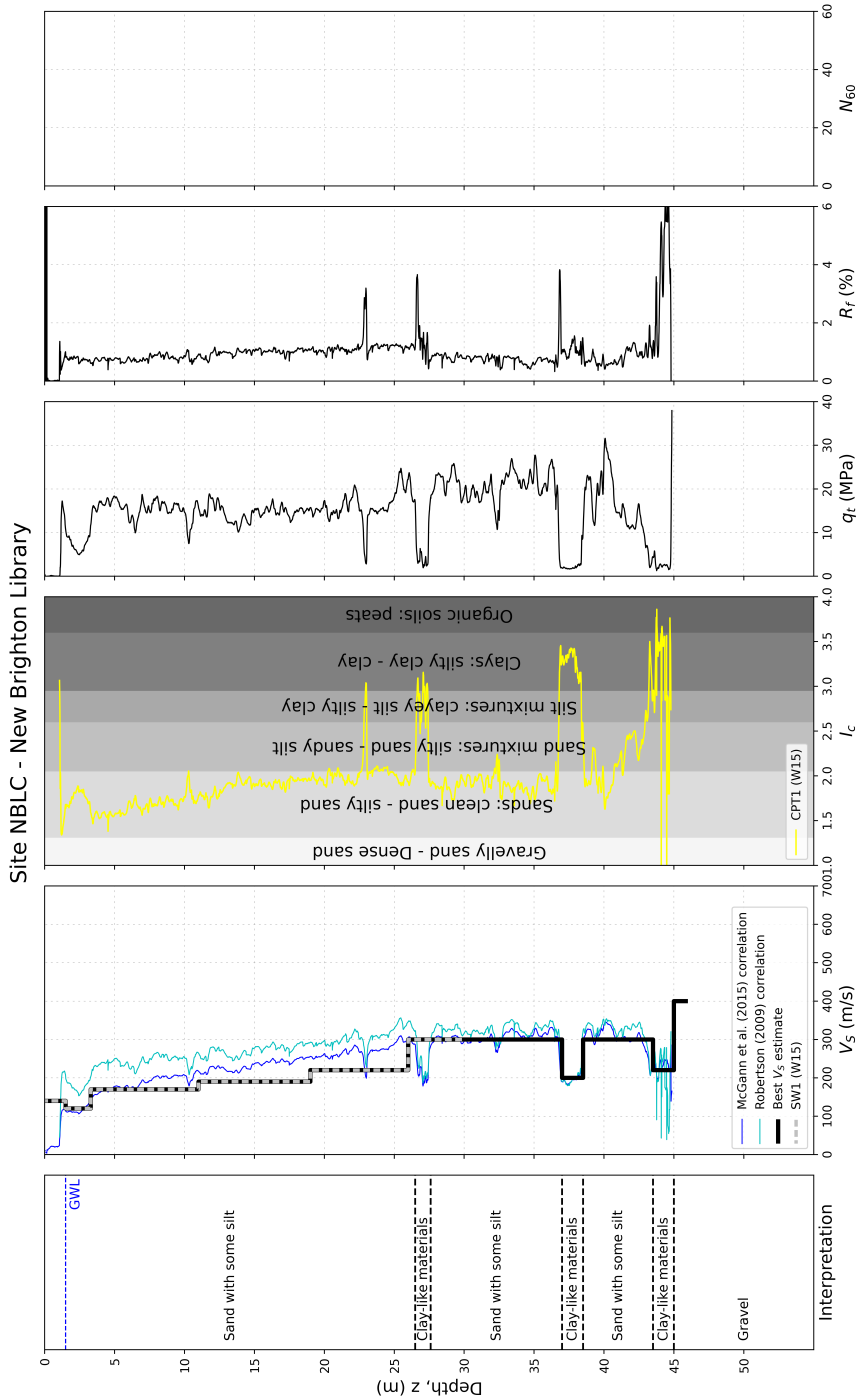

Figure B.27. Site data used to characterize the site NBLC, located in the Canterbury Region.

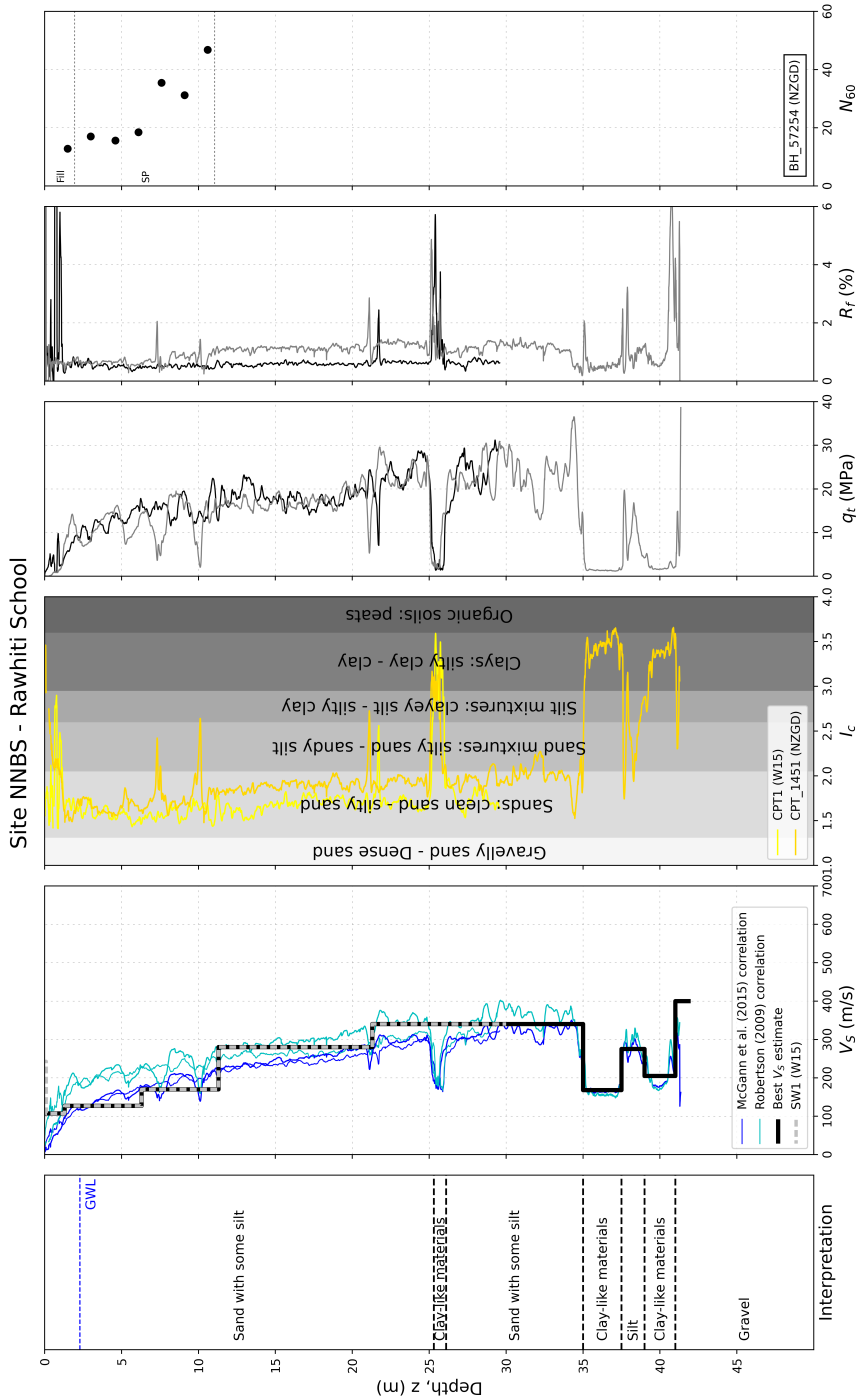

Figure B.28. Site data used to characterize the site NNBS, located in the Canterbury Region.

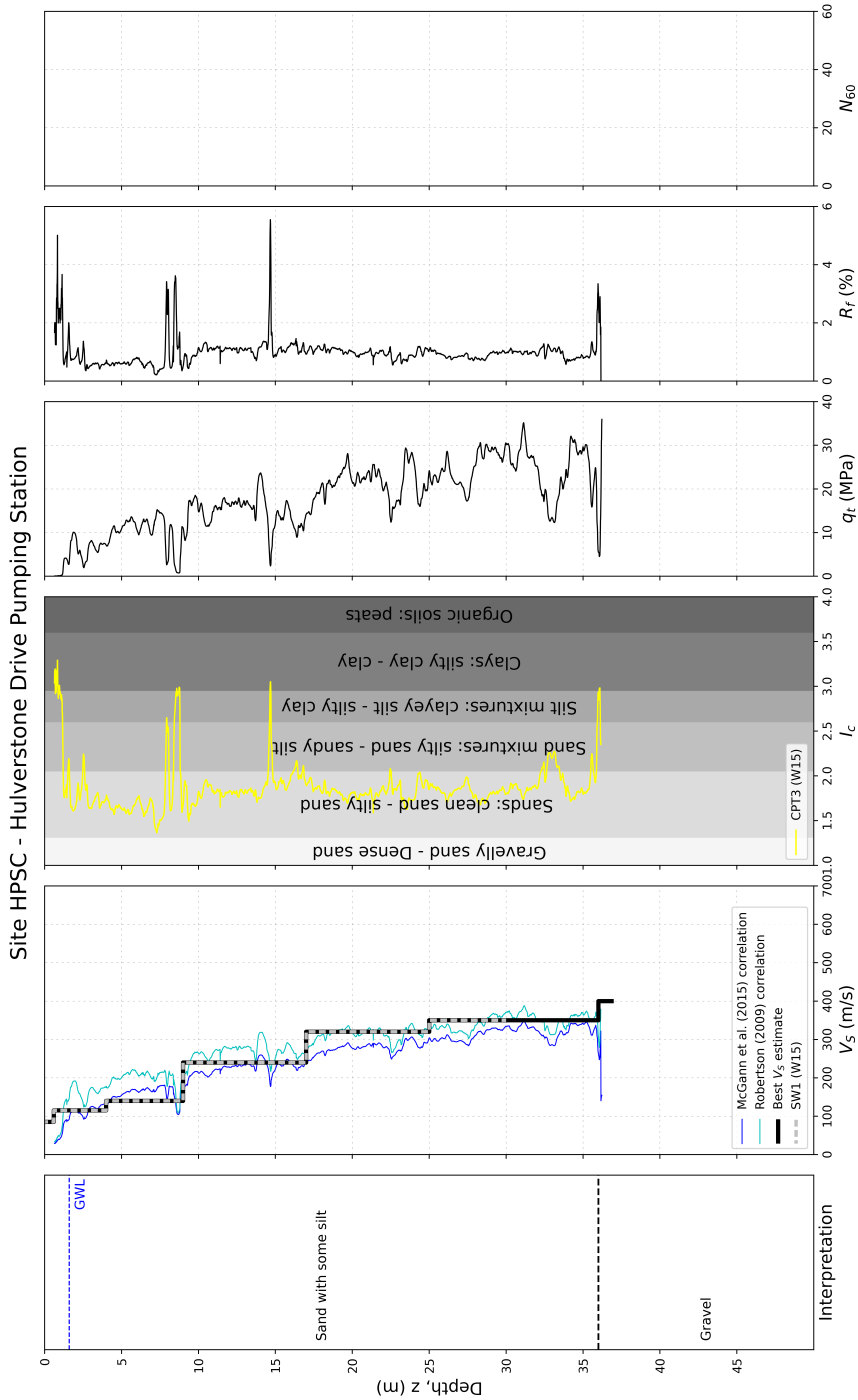

Figure B.29. Site data used to characterize the site HPSC, located in the Canterbury Region.

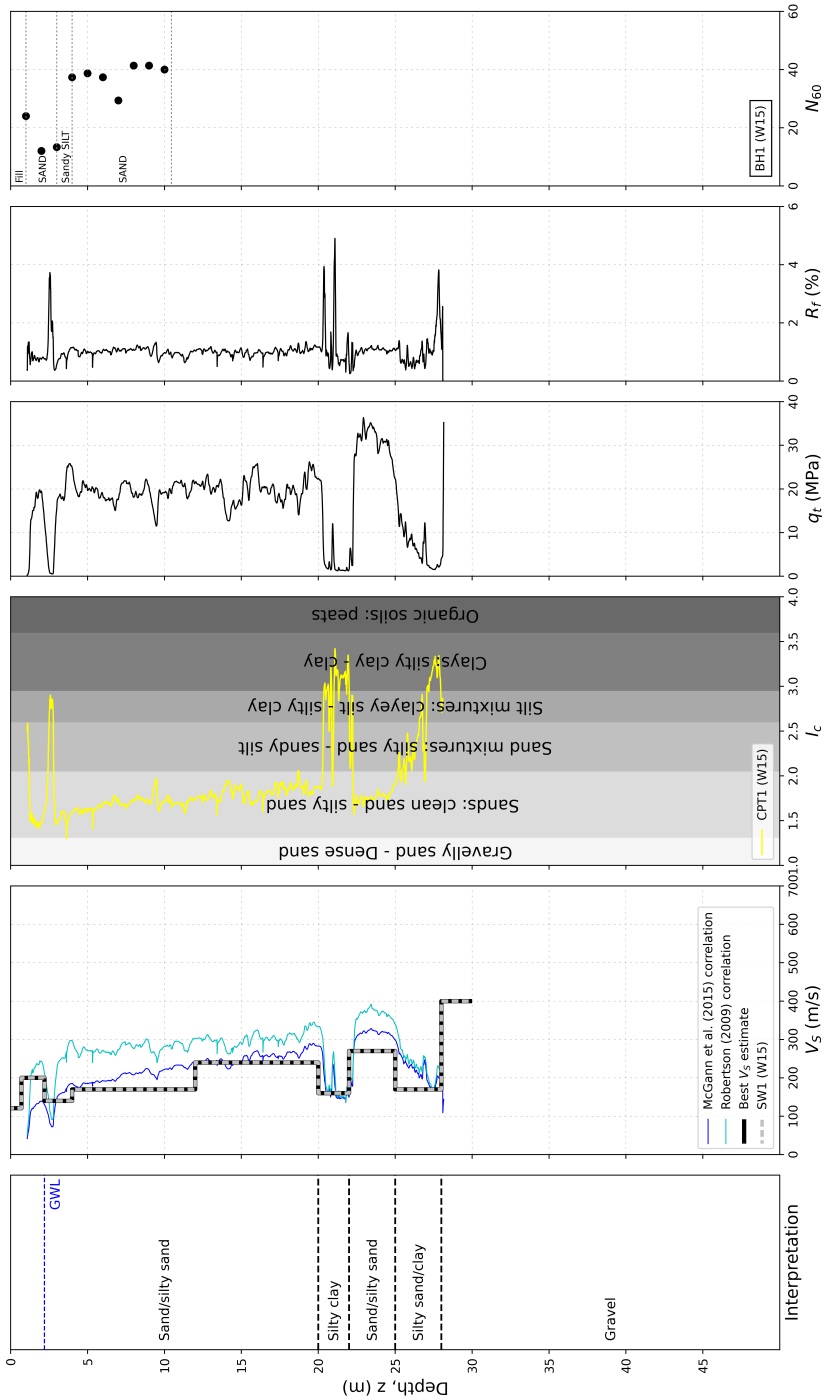

Figure B.30. Site data used to characterize the site PRPC, located in the Canterbury Region.

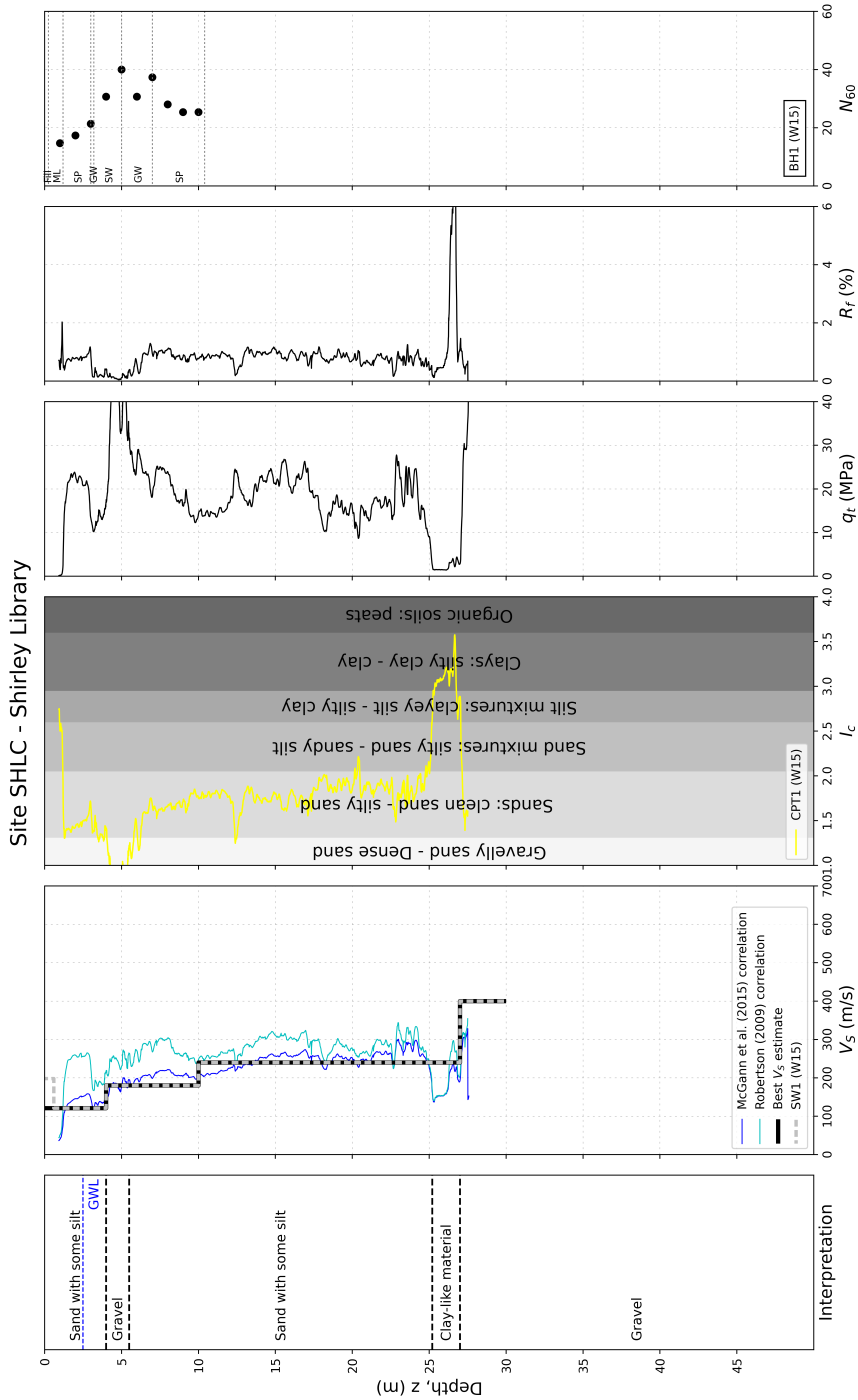

Figure B.31. Site data used to characterize the site SHLC, located in the Canterbury Region.

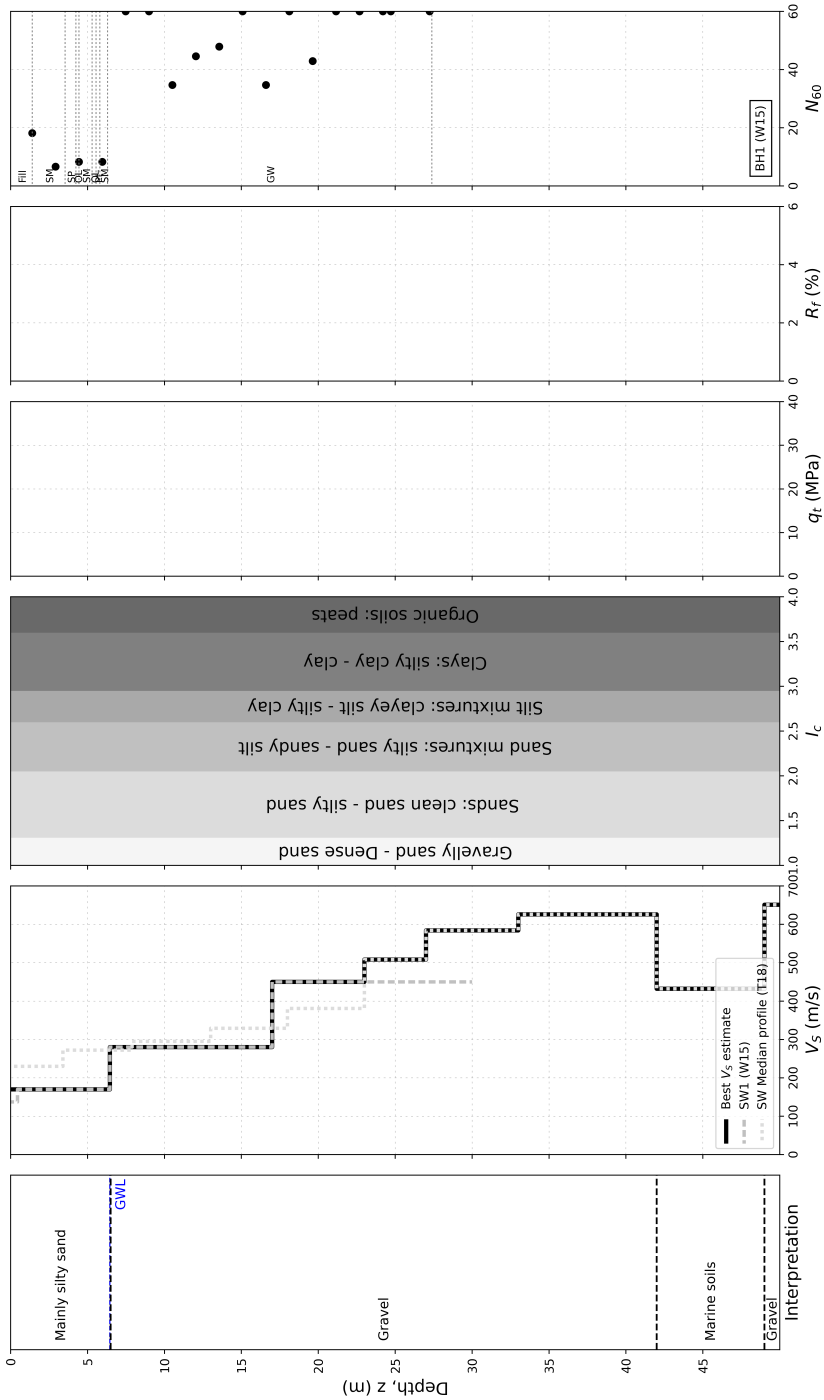

Figure B.32. Site data used to characterize the site RHSC, located in the Canterbury Region.

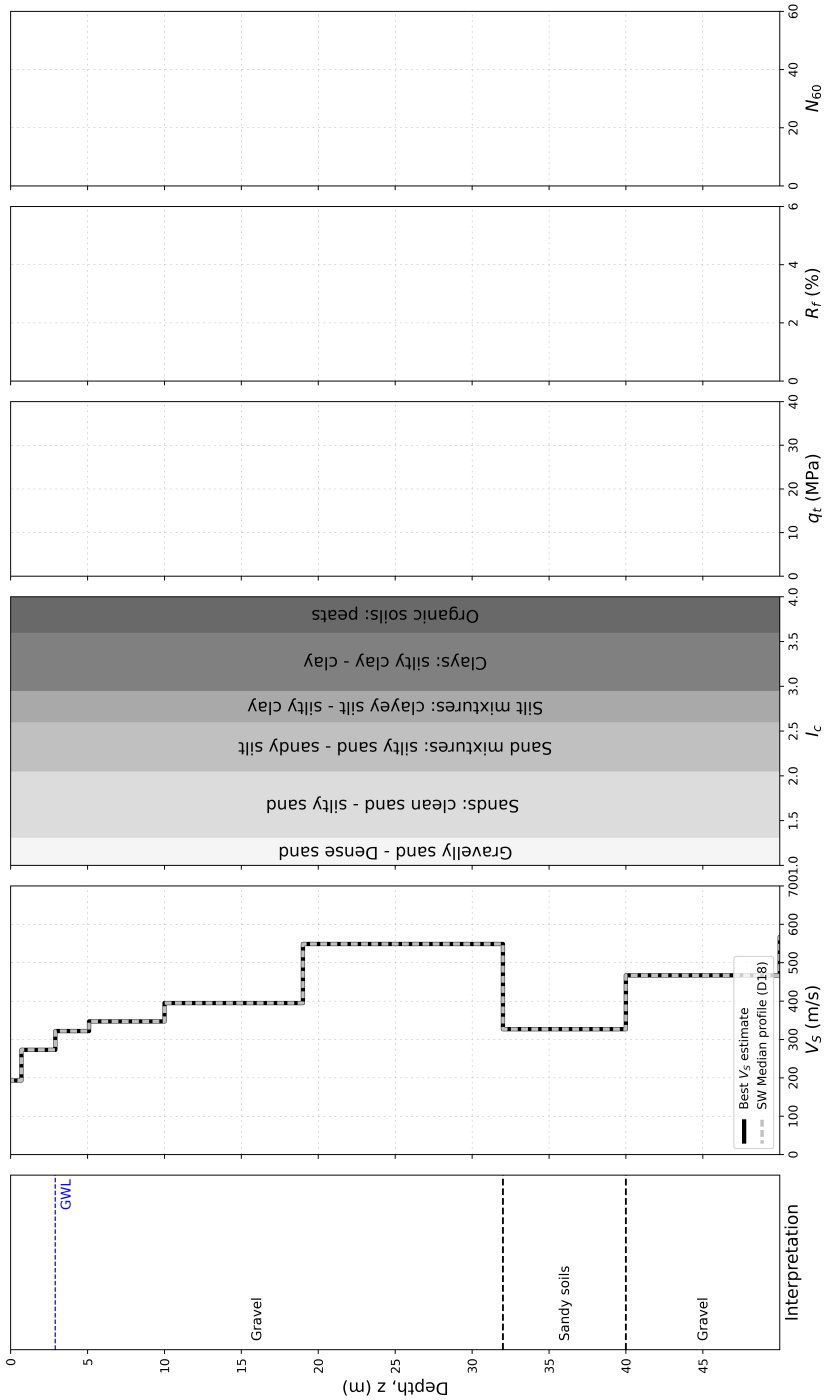

Figure B.33. Site data used to characterize the site TPLC, located in the Canterbury Region.

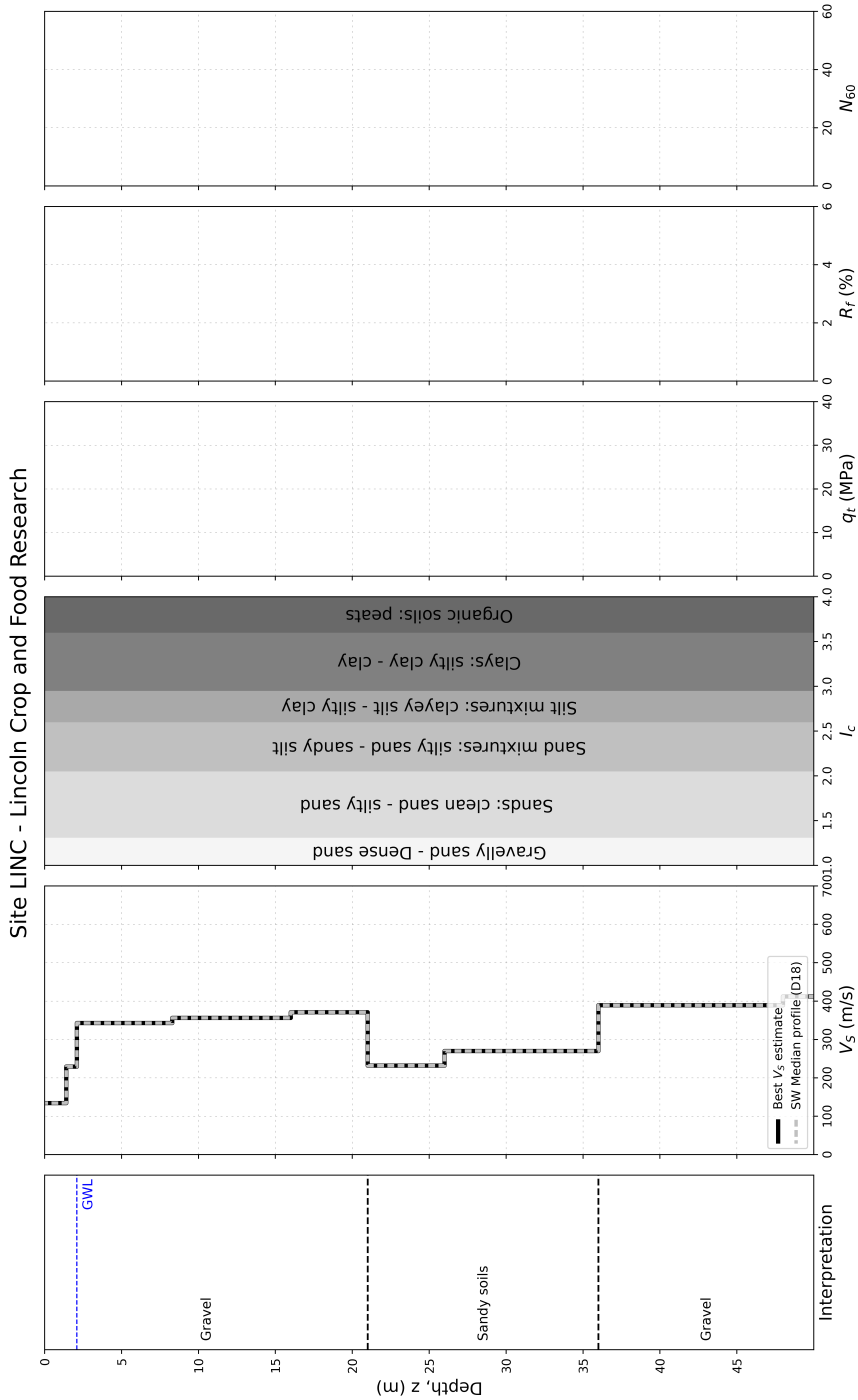

Figure B.34. Site data used to characterize the site LINC, located in the Canterbury Region.

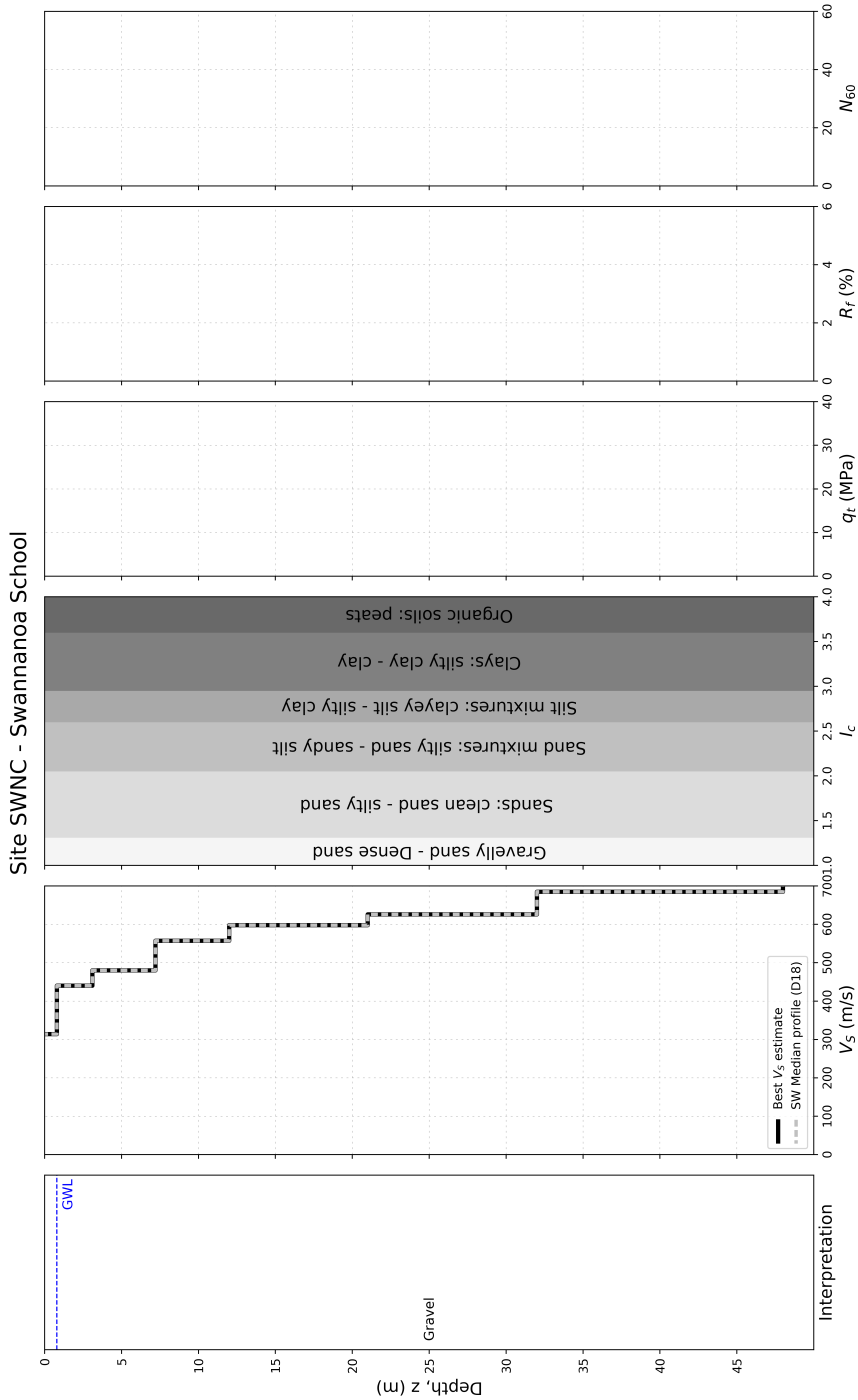

Figure B.35. Site data used to characterize the site SWNC, located in the Canterbury Region.

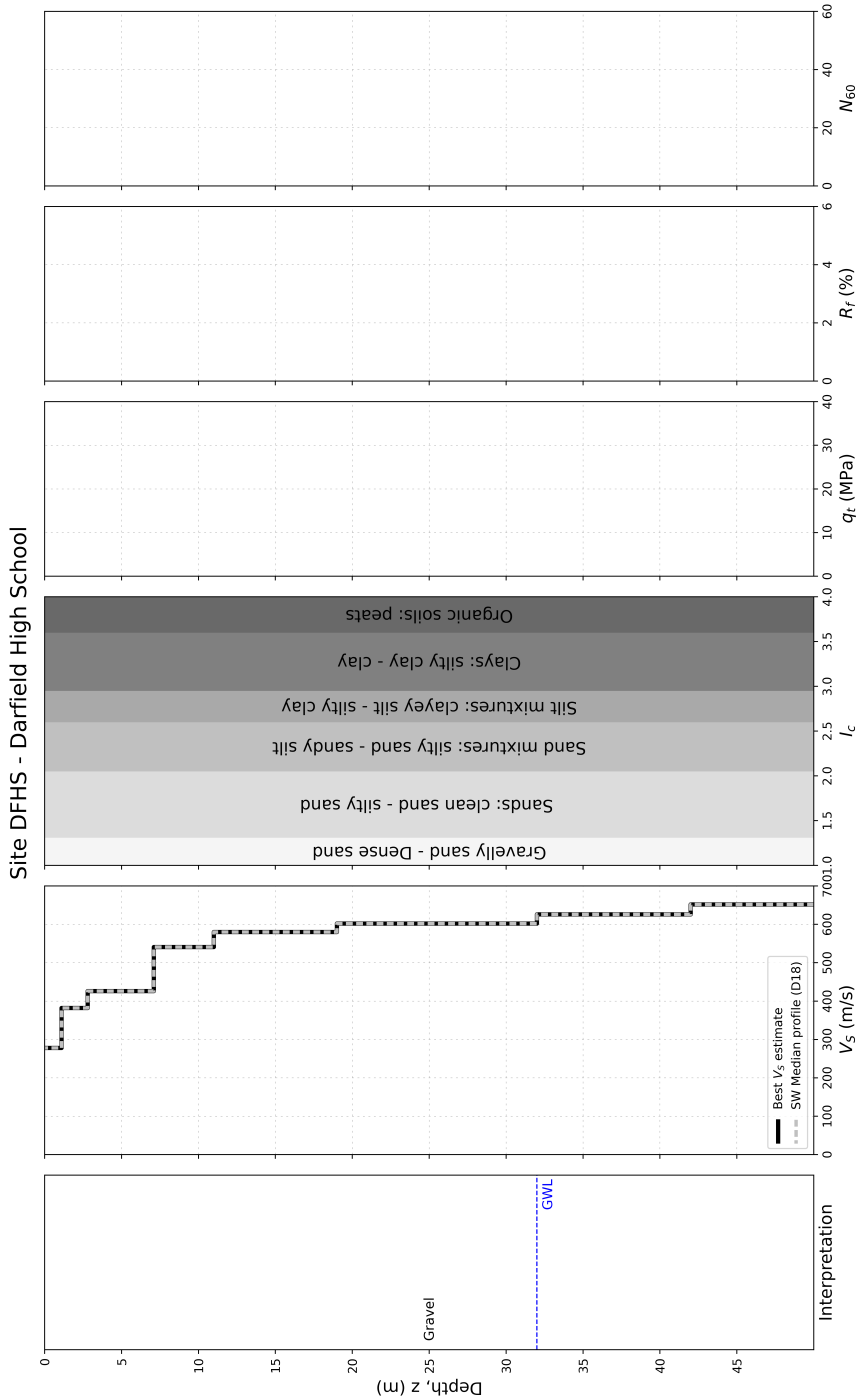

Figure B.36. Site data used to characterize the site DFHS, located in the Canterbury Region.

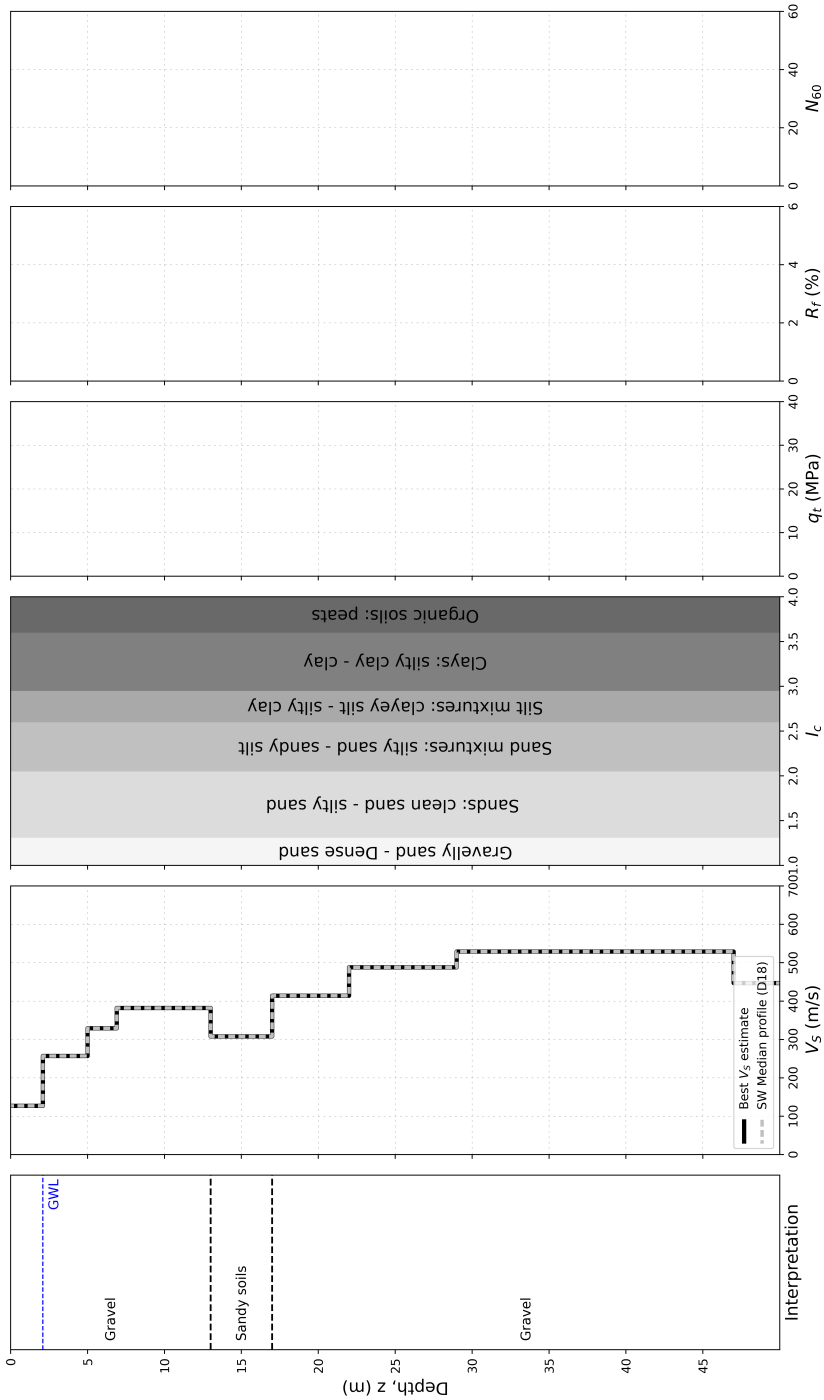

Figure B.37. Site data used to characterize the site SLRC, located in the Canterbury Region.

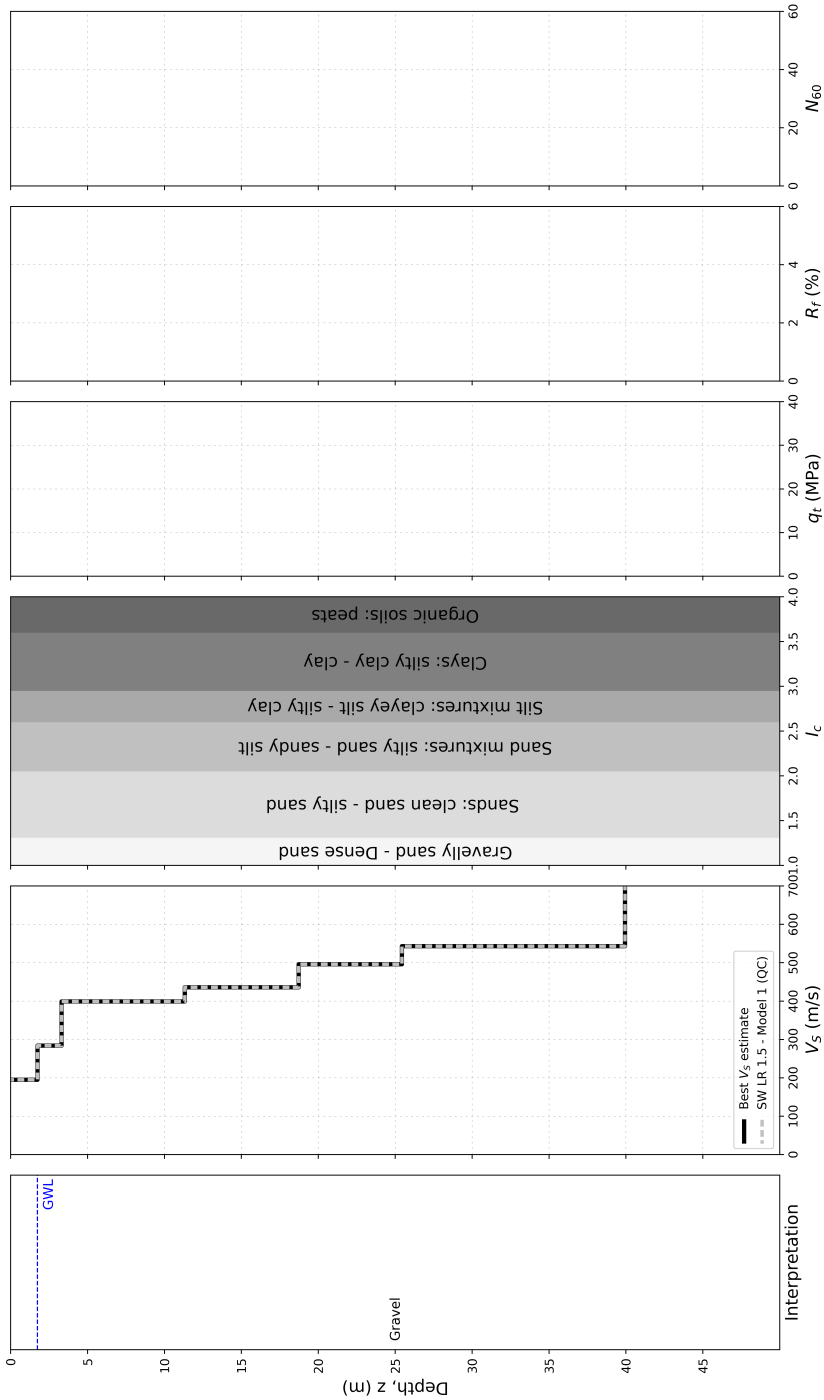

Figure B.38. Site data used to characterize the site CULC, located in the Canterbury Region.

B.2 CPT data availability

Figure B.39 illustrates that most of the CPT measurements available are relatively shallow. Only 14 sites (41% of the sites considered) have CPT measurements reaching a depth of at least 10 m. As observed in Figure B.39(a), these sites are mainly located in the Canterbury Region.

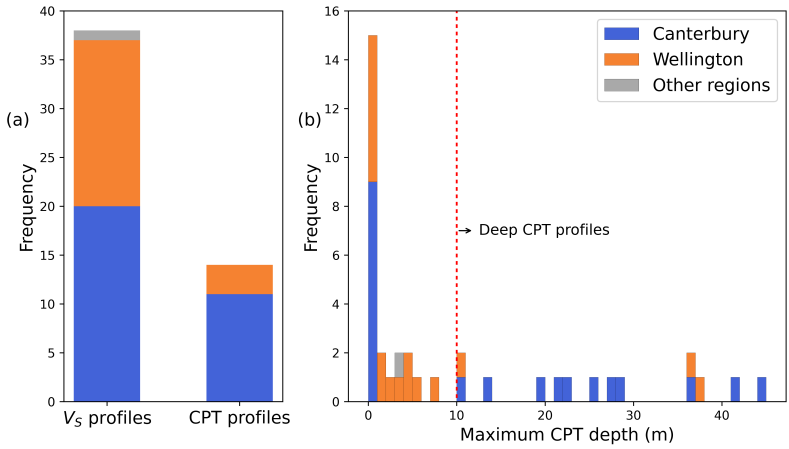

Figure B.39. Main site-characterization data considered. (a) Number of V_S and CPT profiles; (b) Distribution of maximum CPT depths and selection of CPT profiles.

B.3 Comparison of NZ NSHM site parameters and those in this study

Figure B.40 compares the values of the site parameters V_{S30} and $Z_{1.0}$ as computed from the "actual" profiles considered in this study and as provided in the New Zealand National Seismic Hazard Model (NSHM) site characterization database (Wotherspoon et al. 2024). $Z_{1.0}$ is only compared for sites whose actual $Z_{1.0}$ values are above the elastic half-space considered for the site factor computation. As observed, both site parameter estimates are relatively consistent, although with some expected differences. In the case of V_{S30}, the POTS site (located in Wellington) shows a significant difference between the two estimated values, which is due to the fact that the "actual" V_S profile for POTS was modified as explained in Electronic Supplement E. In the case of $Z_{1.0}$, the TFSS site (located in Wellington) presents a significant difference between the two estimated values, which is due to the fact that the "actual" V_S profile was constrained by the Hill et al. (2022) model, whereas the NSHM value is constrained by the NZVM (Thomson et al. 2020), which provides a shallower representation of the Wellington basin.

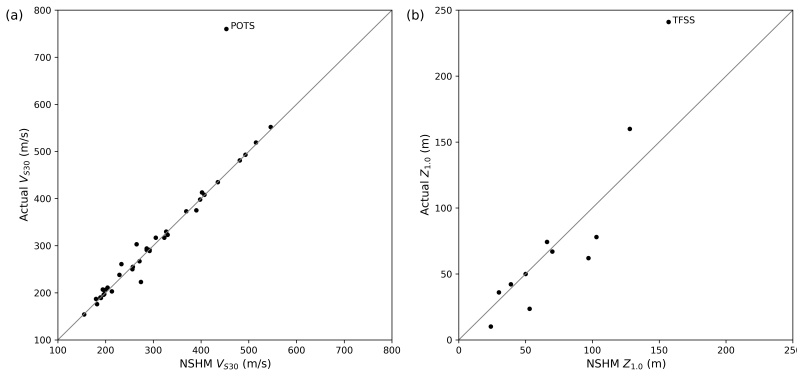

Figure B.40. Comparison between the site parameters considered for the "actual" profiles and the corresponding parameters considered in the NZ NSHM site characterization database (Wotherspoon et al. 2024). (a) V_{S30} and (b) $Z_{1.0}$ comparison.

B.4 mHVSR site frequencies and comparison to SH1D-based site frequencies

Figure B.41 compares the SH1D-based site frequencies, $f_{SH1D,0}$ and $f_{SH1D,max}$, with those obtained by mHSVR measurements (unpublished data provided by C. de la Torre). The figure illustrates that in several cases, mHVSR can identify resonances at relatively high frequencies, which are modeled by the 'SH1D-based' SF method. In the case of the Canterbury Cluster, it also illustrates how the site adjustment considered does not intend to capture the fundamental frequency of the site, but rather a shallower impedance contrast, which is usually also identify by mHVSR.

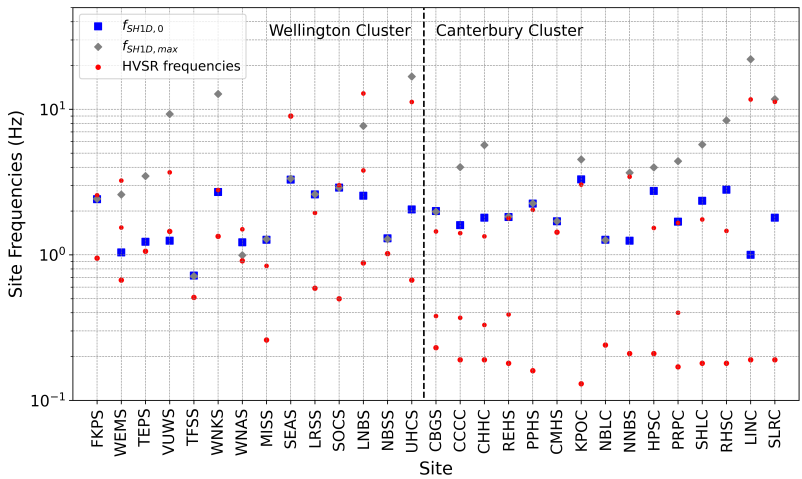

Figure B.41. SH1D-based site frequencies, $f_{SH1D,0}$ and $f_{SH1D,max}$, and those obtained by mHSVR measurements.

It is worth noting that mHVSR is often used to constrain the development of V_S profiles derived from surface-wave testing (e.g., Wotherspoon et al. 2015), and consequently, the resulting 'SH1D-based' SFs computed here. Besides this, these observations indicate that mHVSR measurements could be useful at sites without a measured V_S profile. Specifically, they could help inform site-response method selection and evaluate the need for obtaining a V_S profile. For example, detecting high-frequency resonances via mHVSR could indicate a lower performance of the 'V_{S30}-based' SF method relative to the 'SH1D-based' approach at high frequencies.

C Electronic Supplement C: Profiles and site factors

The following figures presents the V_S profiles used and site factors obtained with the different methods for all sites considered, using a representative HF PGA of 0.01g. The HF component of the V_S profile-based SFs is presented with the HF normalization factor applied (i.e., $NF \cdot SF$).

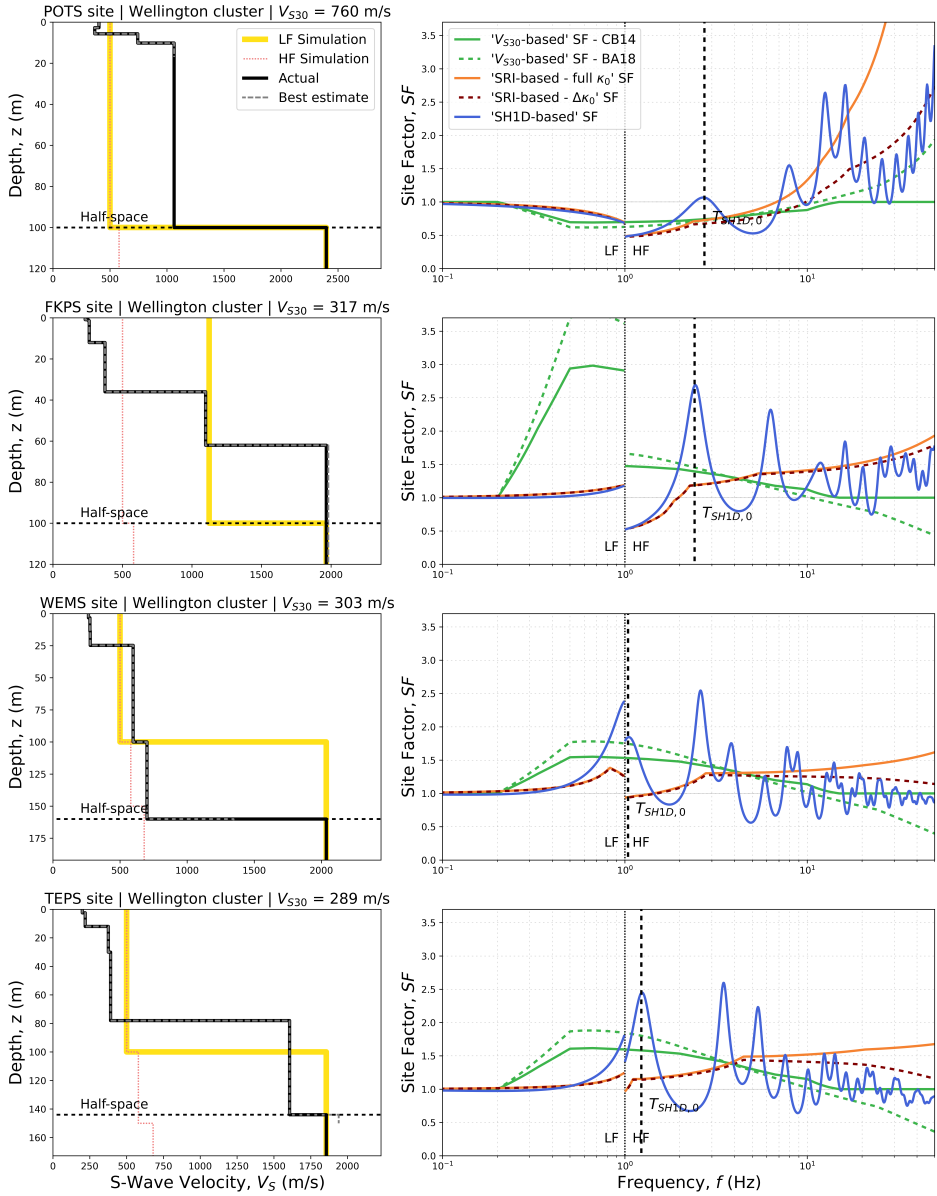

Figure C.1. V_S profiles considered and site factors obtained with the different methods, for the sites POTS, FKPS, WEMS, and TEPS. The site factors are computed for a HF PGA of 0.01g.

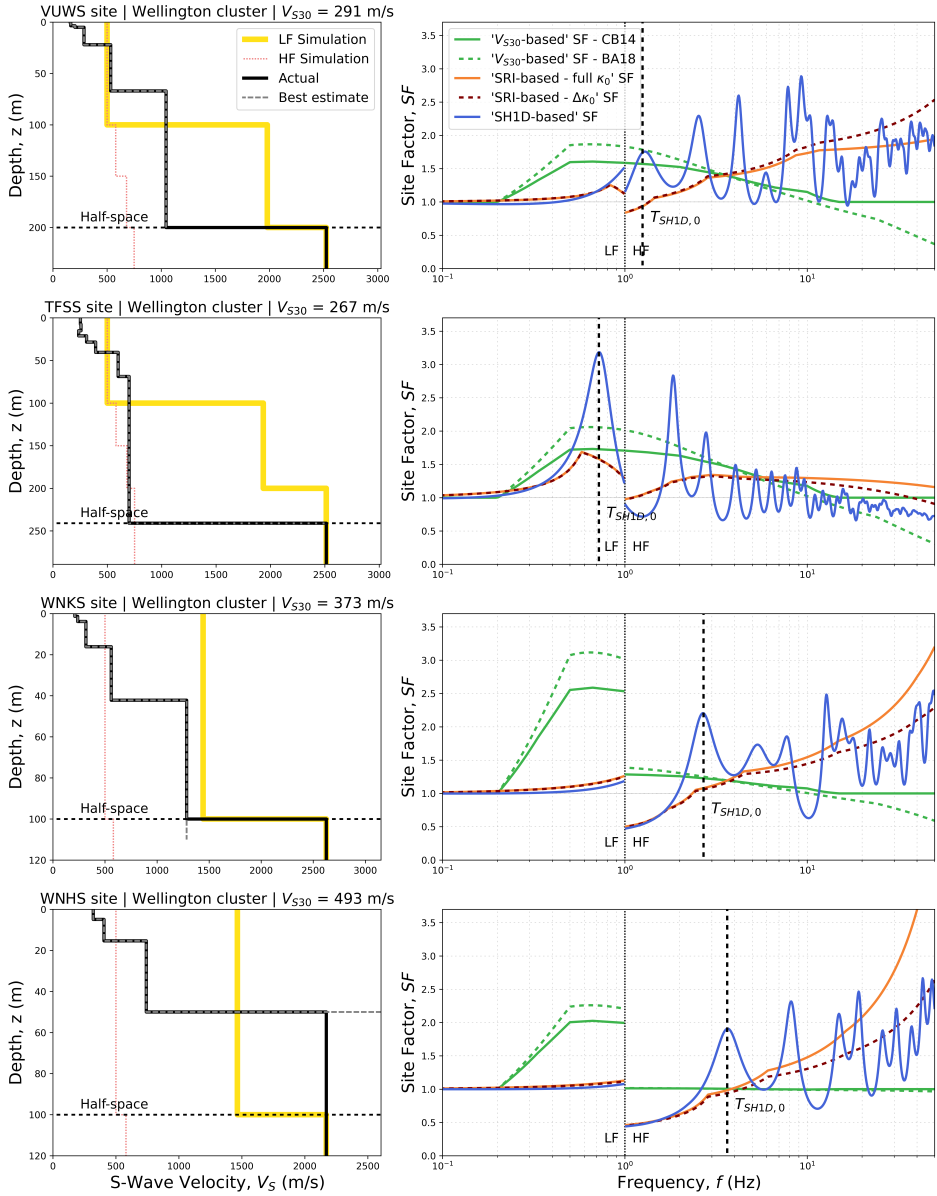

Figure C.2. V_S profiles considered and site factors obtained with the different methods, for the sites VUWS, TFSS, WNKS, and WNHS. The site factors are computed for a HF PGA of 0.01g.

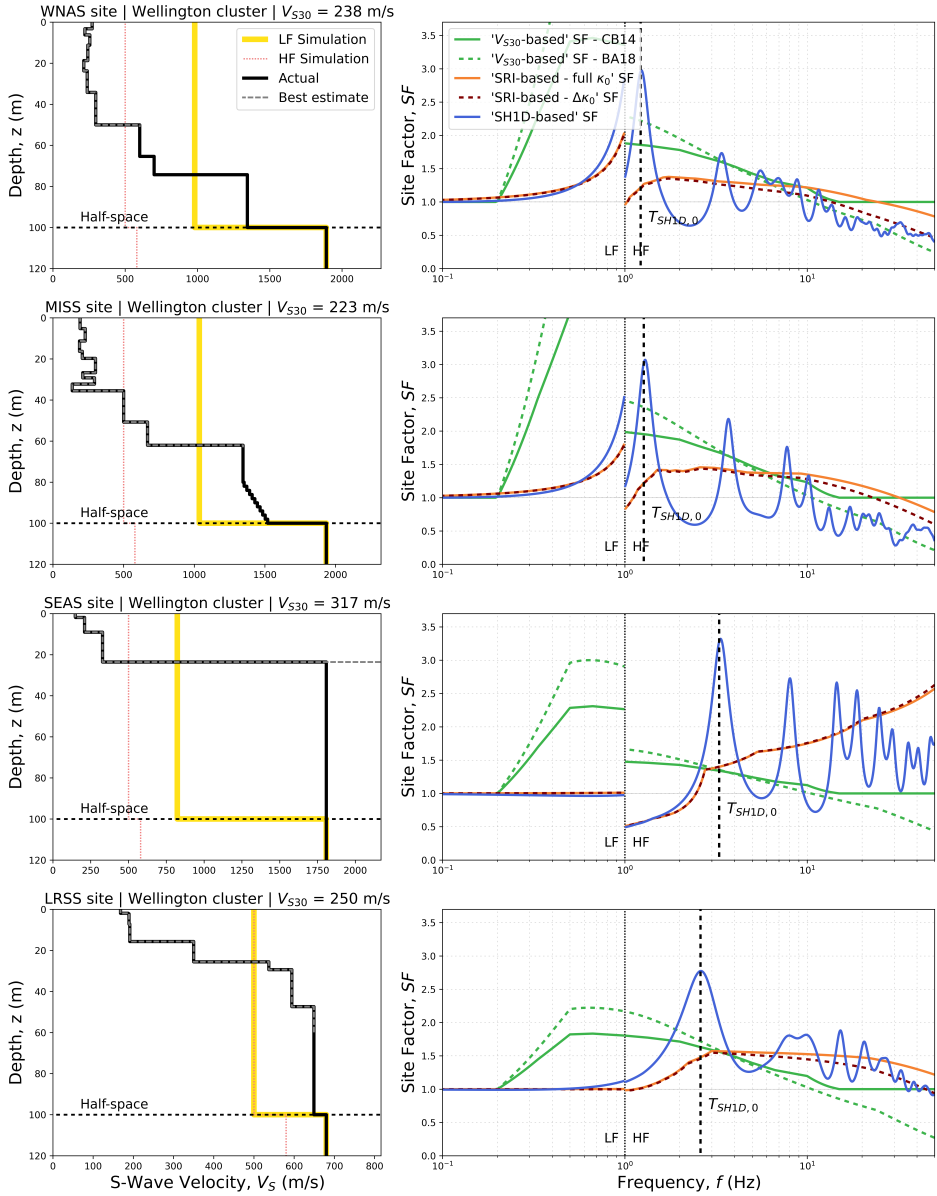

Figure C.3. V_S profiles considered and site factors obtained with the different methods, for the sites WNAS, MISS, SEAS, and LRSS. The site factors are computed for a HF PGA of 0.01g.

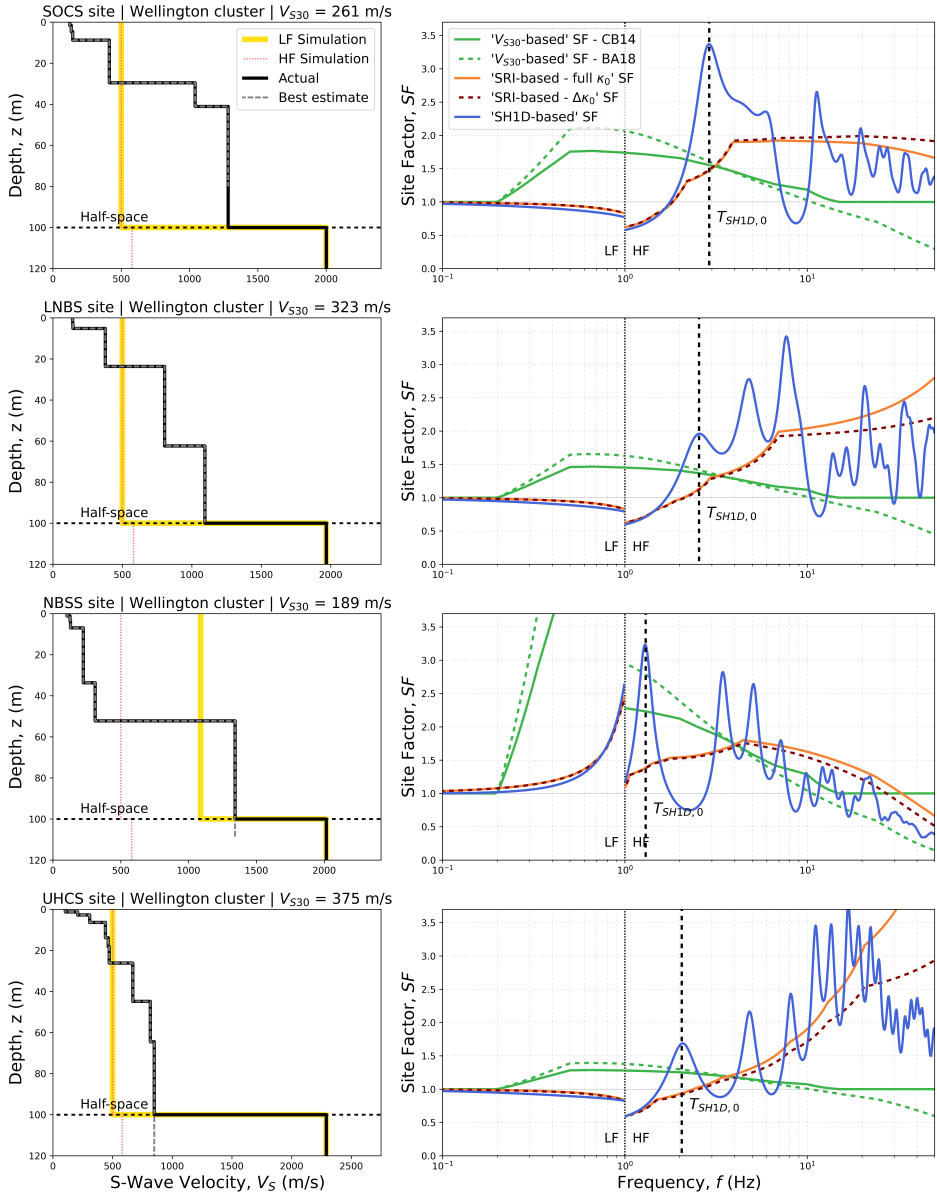

Figure C.4. V_S profiles considered and site factors obtained with the different methods, for the sites SOCS, LNBS, NBSS, and UHCS. The site factors are computed for a HF PGA of 0.01g.

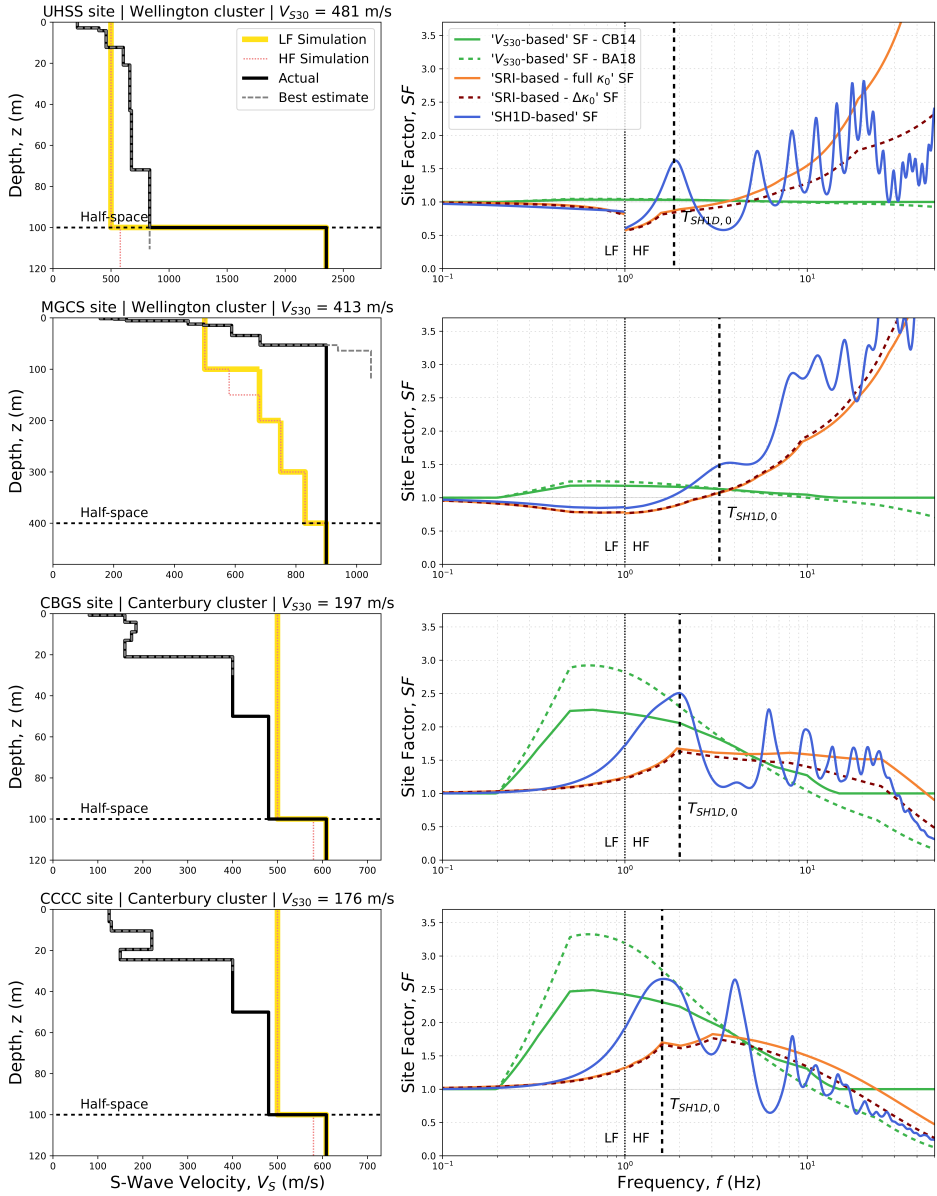

Figure C.5. V_S profiles considered and site factors obtained with the different methods, for the sites UHSS, MGCS, CBGS, and CCCC. The site factors are computed for a HF PGA of 0.01g.

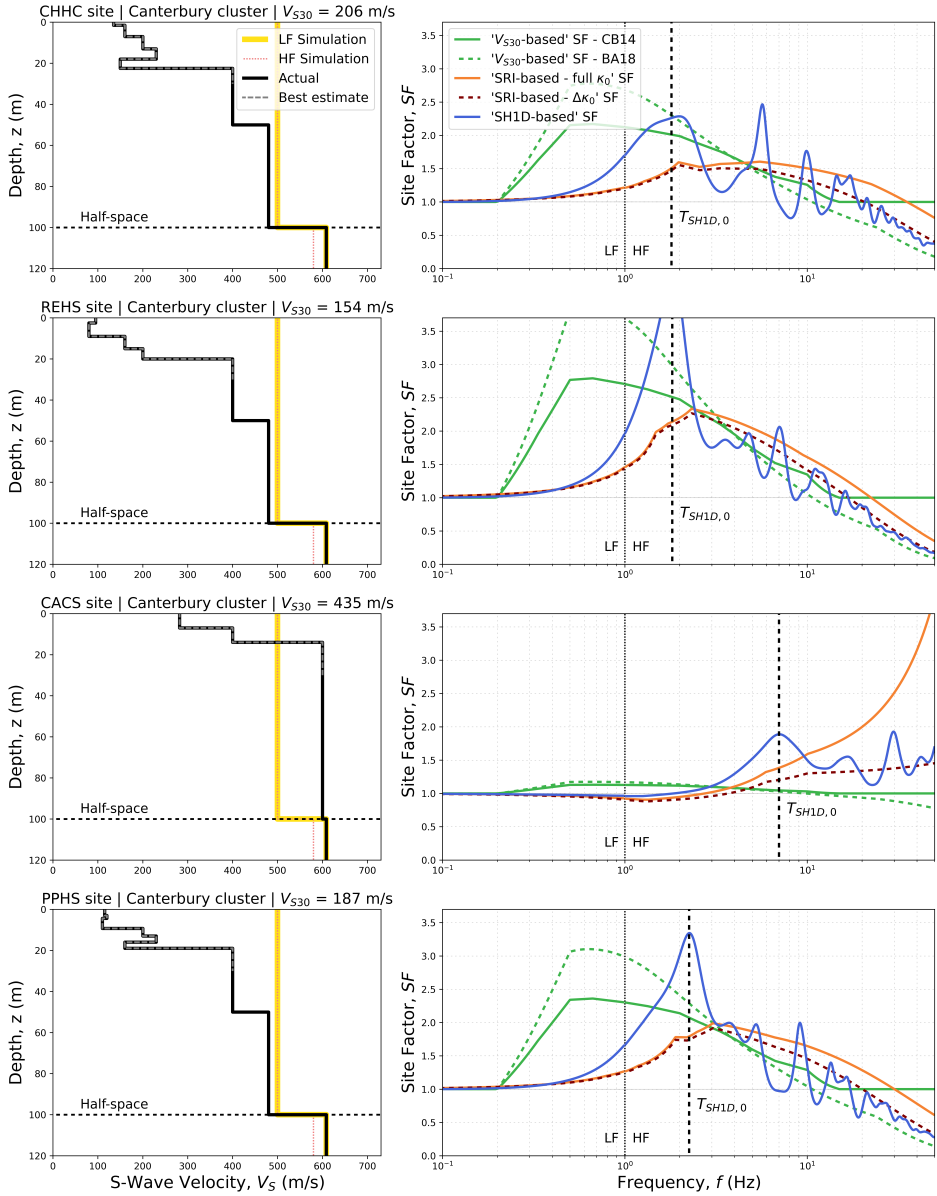

Figure C.6. V_S profiles considered and site factors obtained with the different methods, for the sites CHHC, REHS, CACS, and PPHS. The site factors are computed for a HF PGA of 0.01g.

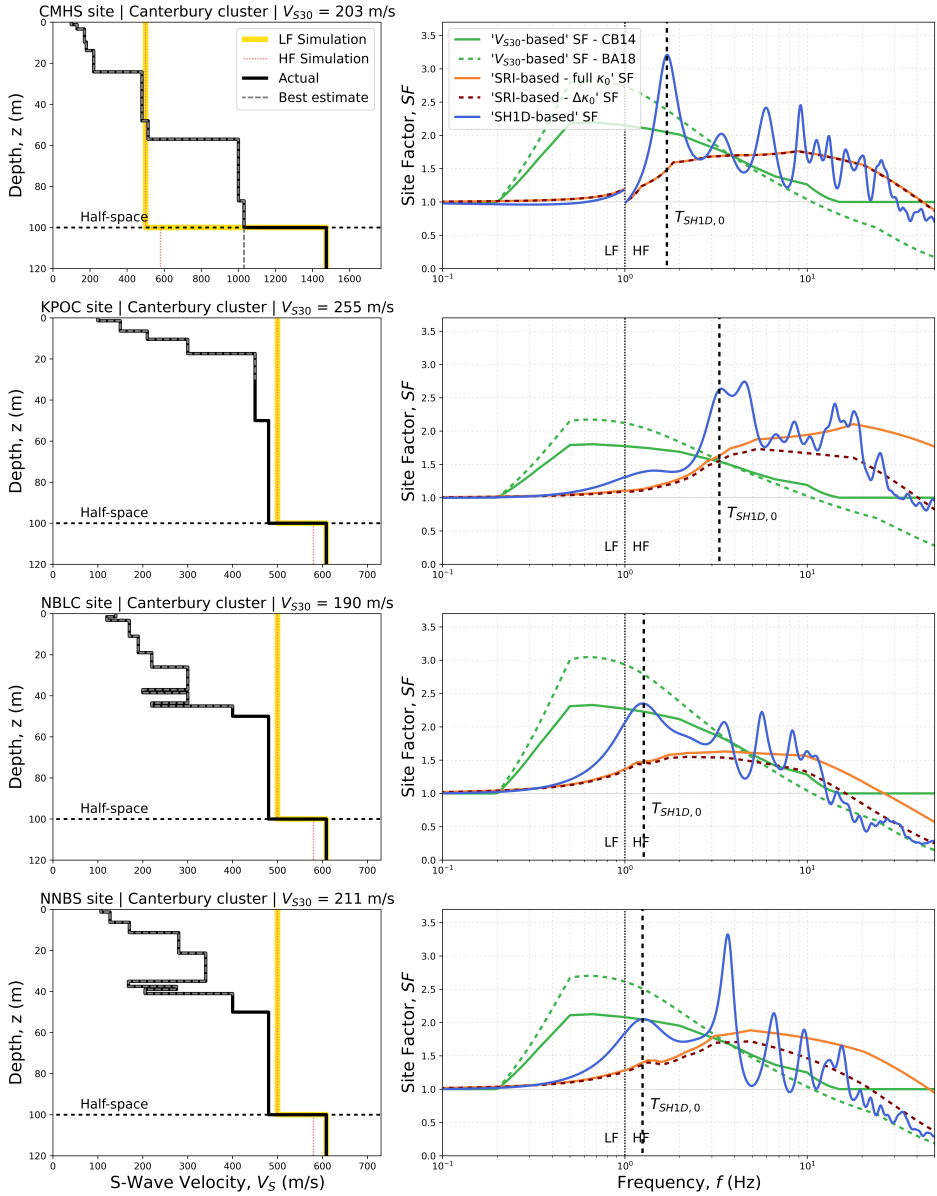

Figure C.7. V_S profiles considered and site factors obtained with the different methods, for the sites CMHS, KPOC, NBLC, and NNBS. The site factors are computed for a HF PGA of 0.01g.

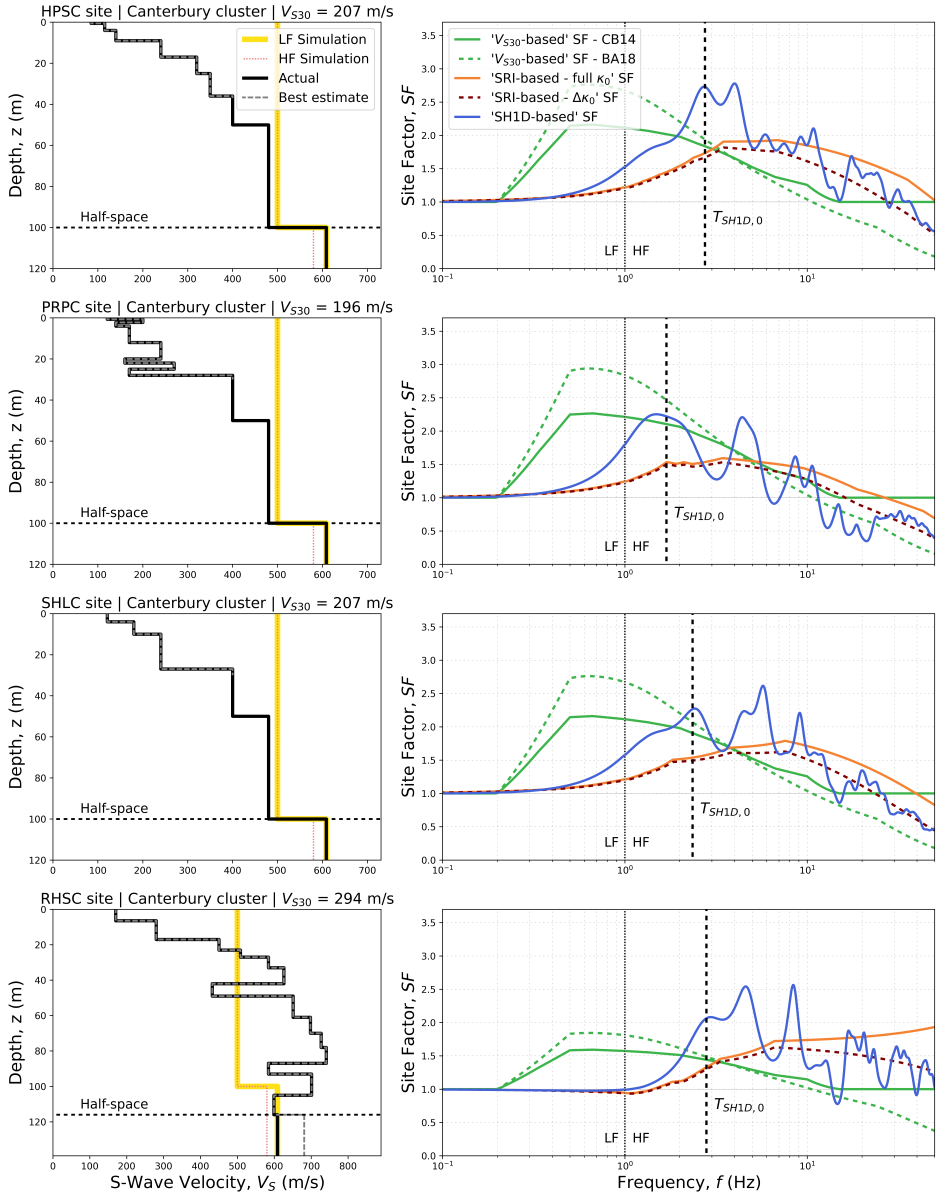

Figure C.8. V_S profiles considered and site factors obtained with the different methods, for the sites HPSC, PRPC, SHLC, and RHSC. The site factors are computed for a HF PGA of 0.01g.

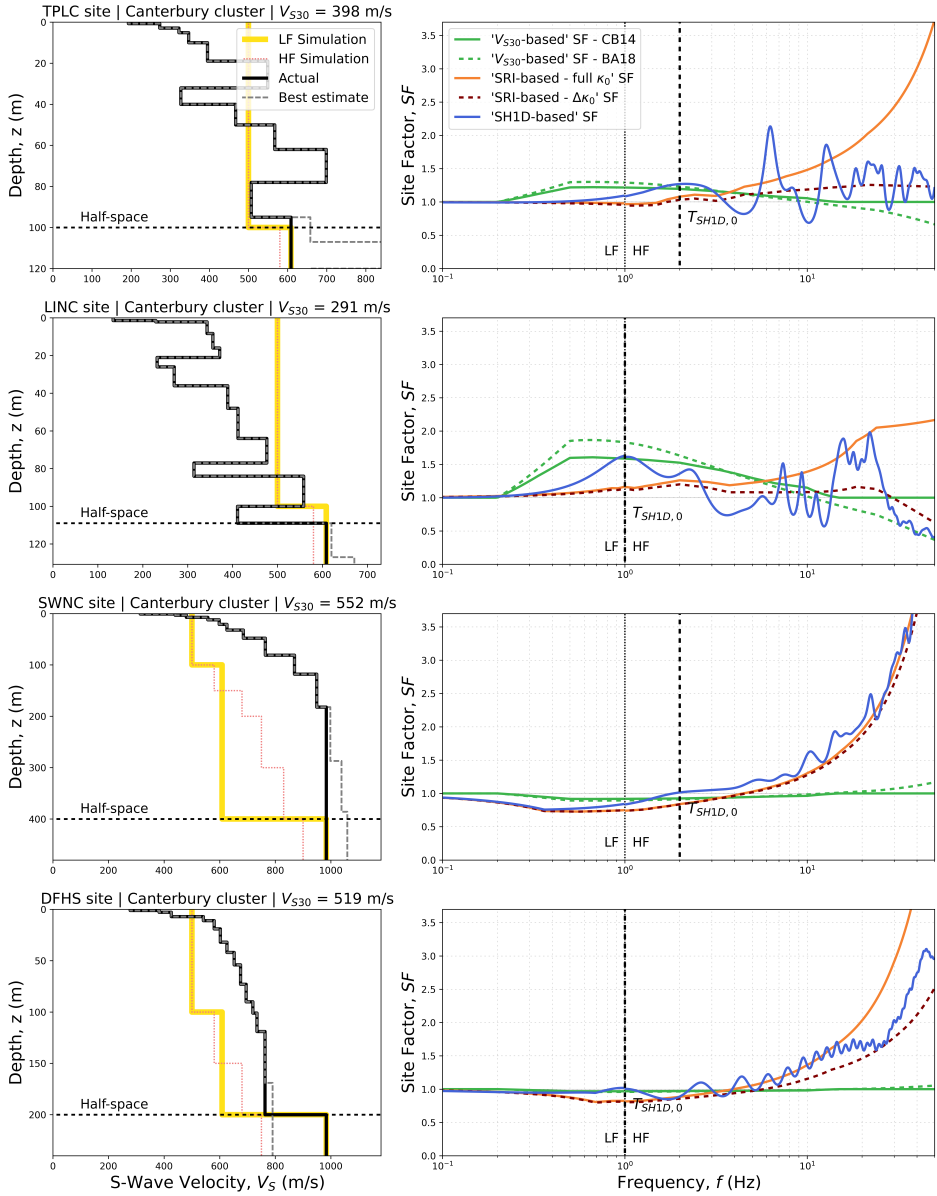

Figure C.9. V_S profiles considered and site factors obtained with the different methods, for the sites TPLC, LINC, SWNC, and DFHS. The site factors are computed for a HF PGA of 0.01g.

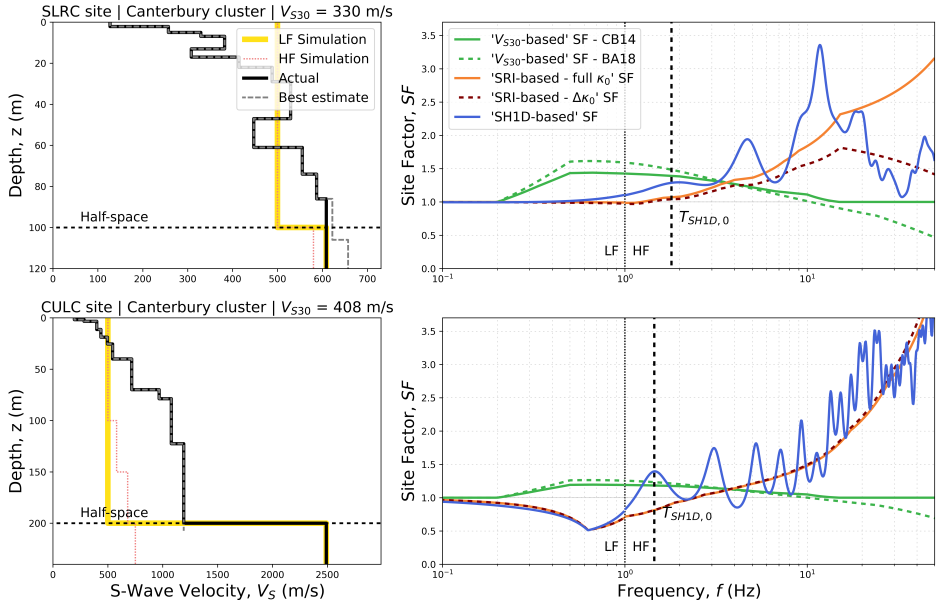

Figure C.10. V_S profiles considered and site factors obtained with the different methods, for the sites SLRC and CULC. The site factors are computed for a HF PGA of 0.01g.

D Electronic Supplement D: Systematic residuals for all sites

The following figures presents the systematic residuals obtained with the different methods for all sites considered.

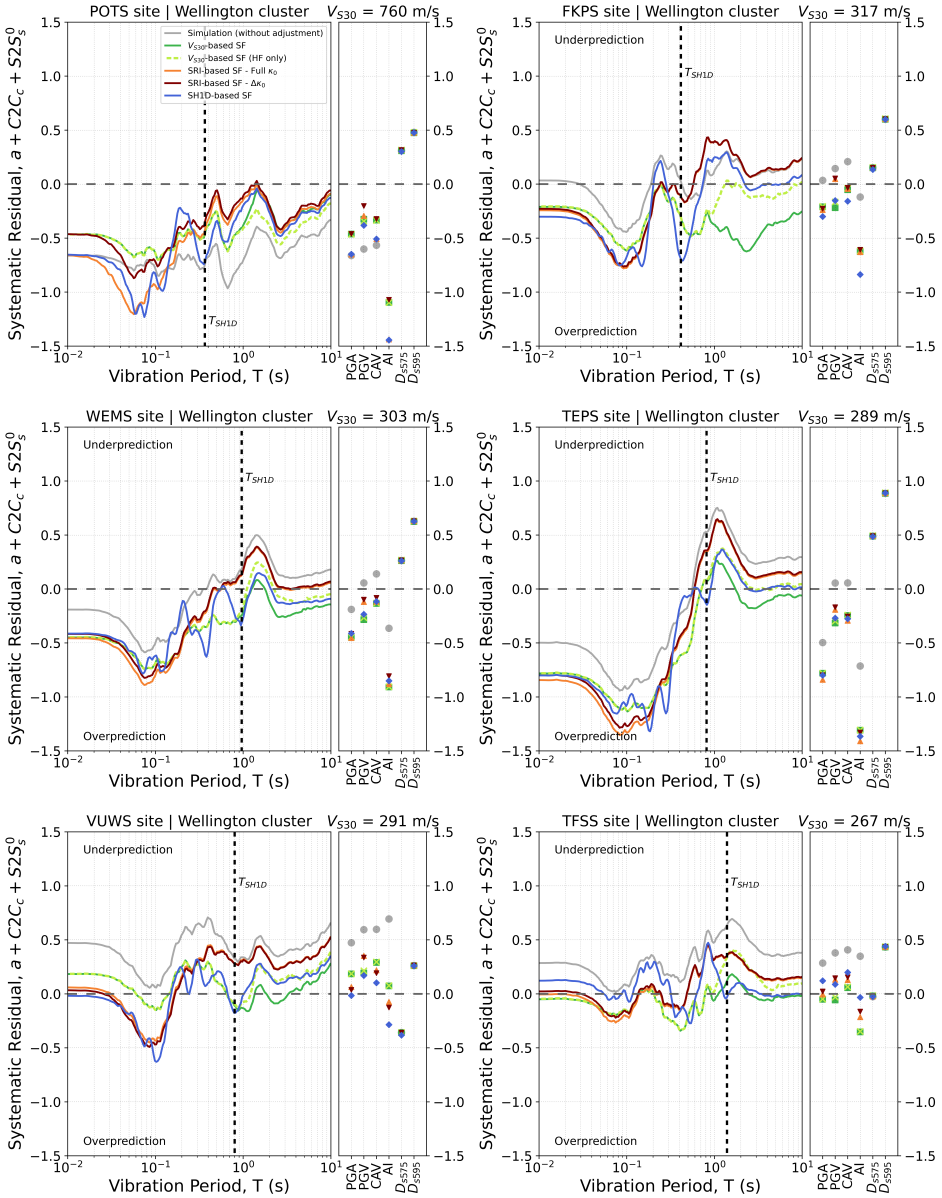

Figure D.1. Systematic residuals for the different methods, for the sites POTS, FKPS, WEMS, TEPS, VUWS, and TFSS.

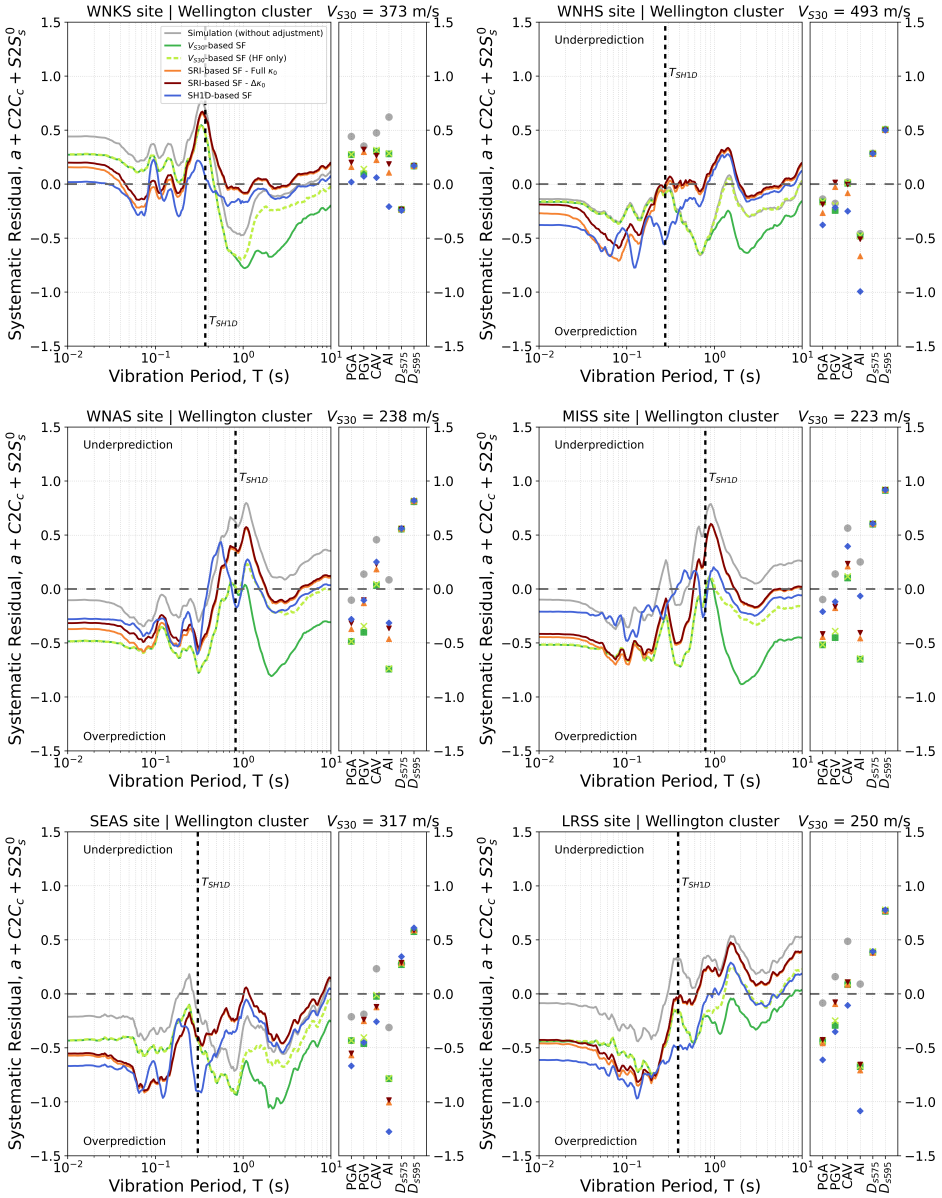

Figure D.2. Systematic residuals for the different methods, for the sites WNKS, WNHS, WNAS, MISS, SEAS, and LRSS.

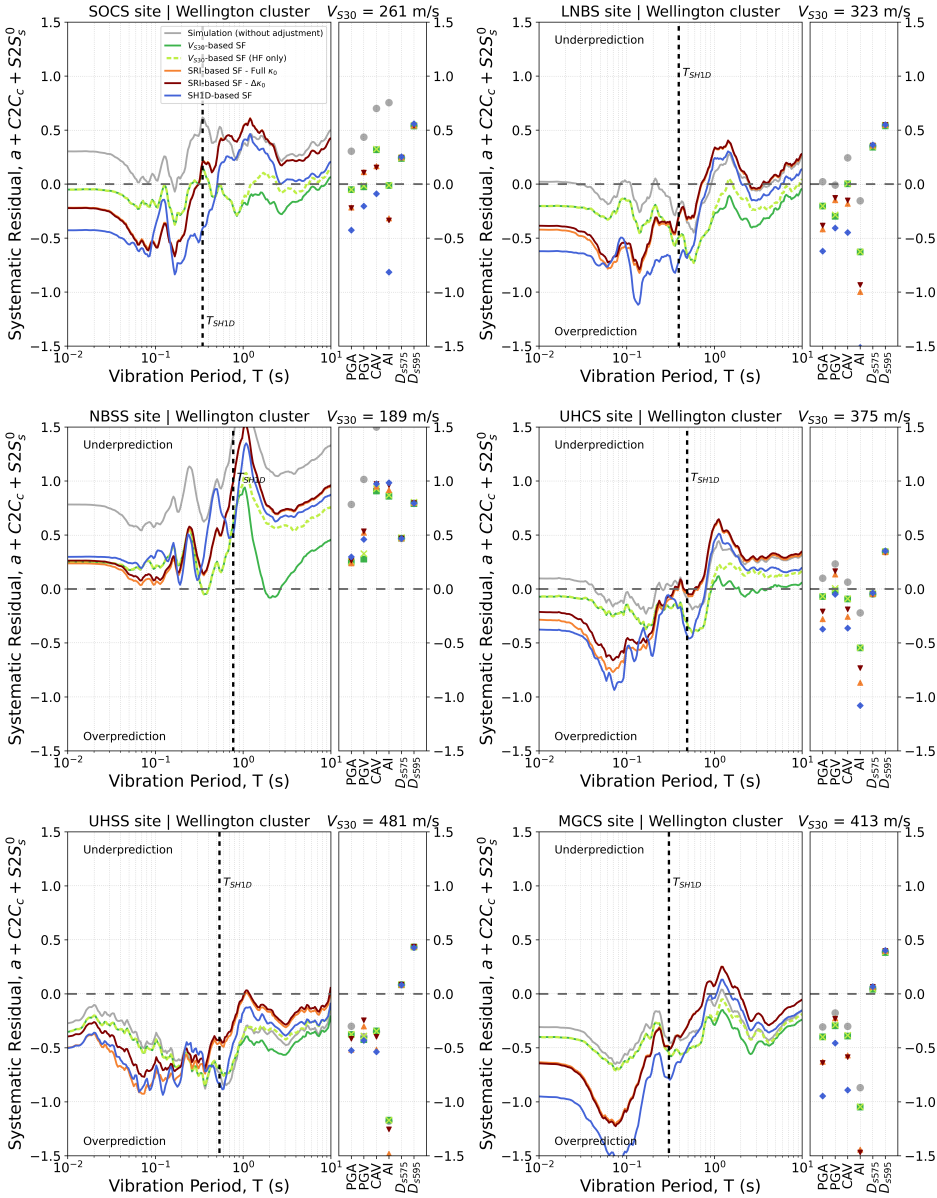

Figure D.3. Systematic residuals for the different methods, for the sites SOCS, LNBS, NBSS, UHCS, UHSS, and MGCS.

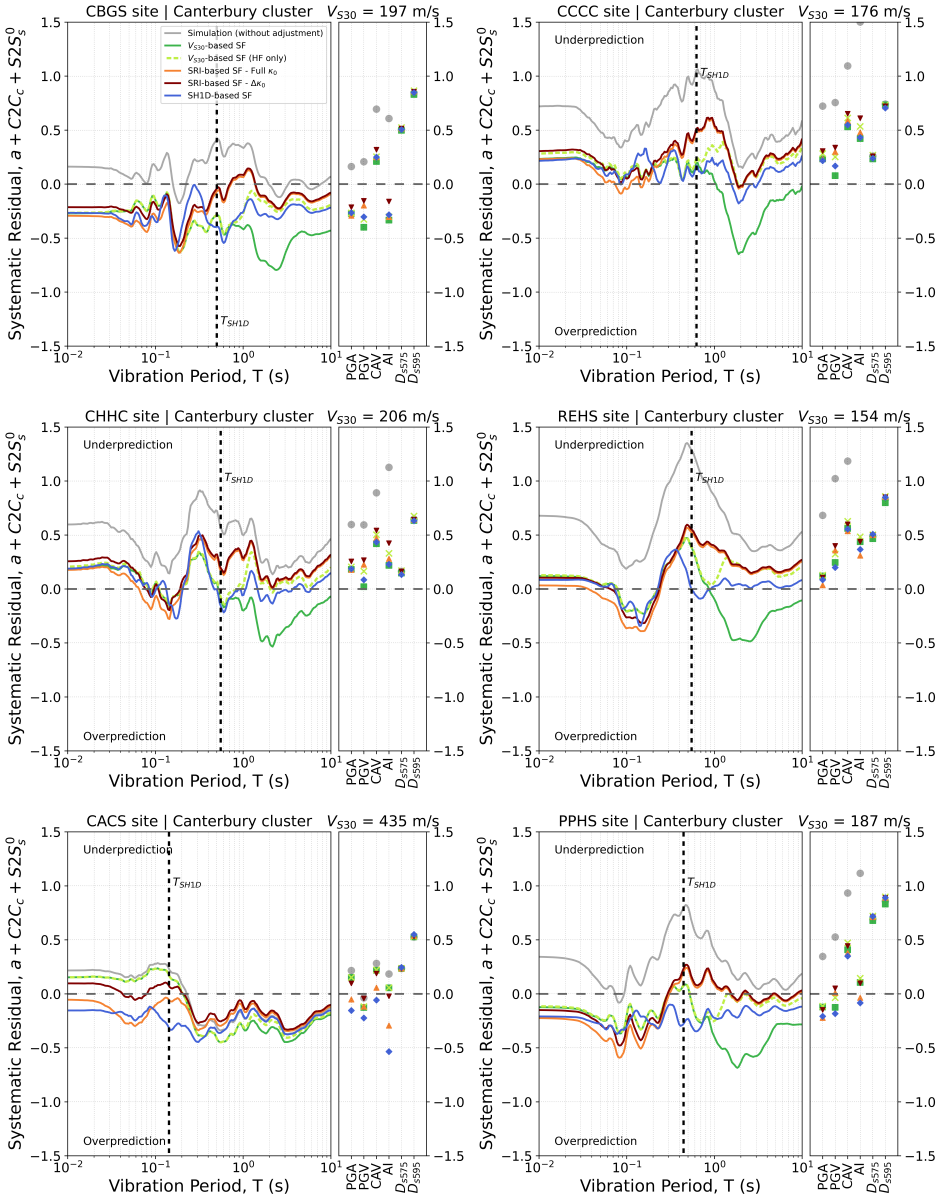

Figure D.4. Systematic residuals for the different methods, for the sites CBGS, CCCC, CHHC, REHS, CACS, and PPHS.

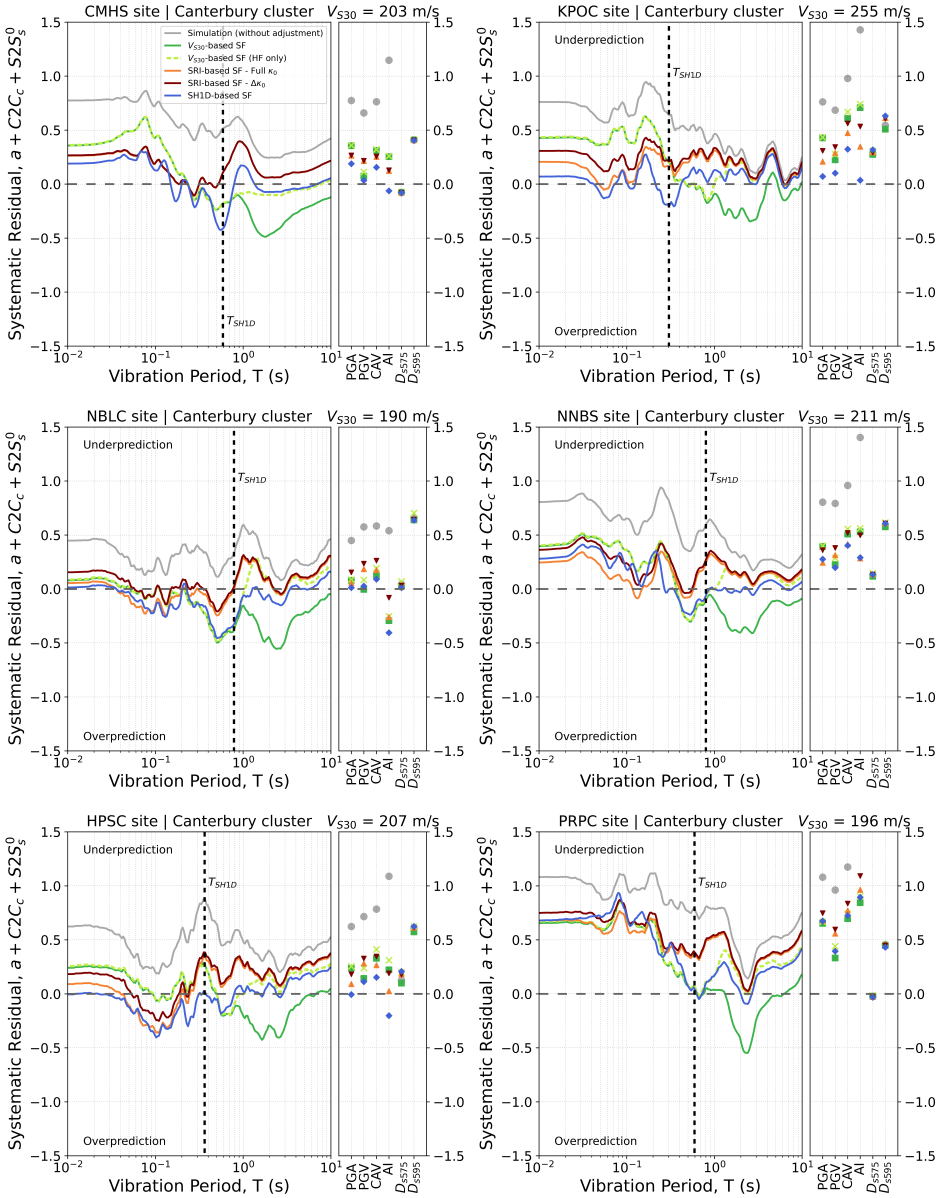

Figure D.5. Systematic residuals for the different methods, for the sites CMHS, KPOC, NBLC, NNBS, HPSC, and PRPC.

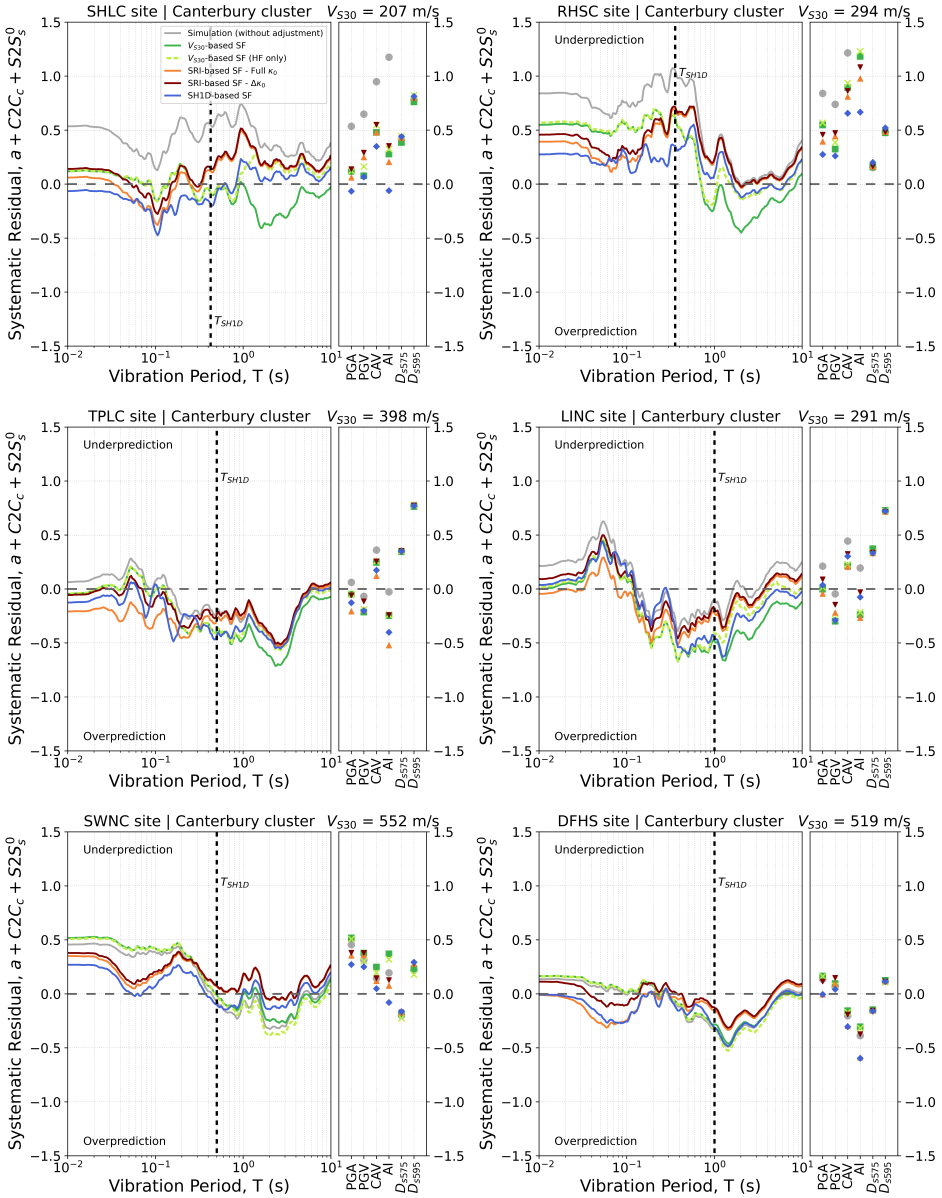

Figure D.6. Systematic residuals for the different methods, for the sites SHLC, RHSC, TPLC, LINC, SWNC, and DFHS.

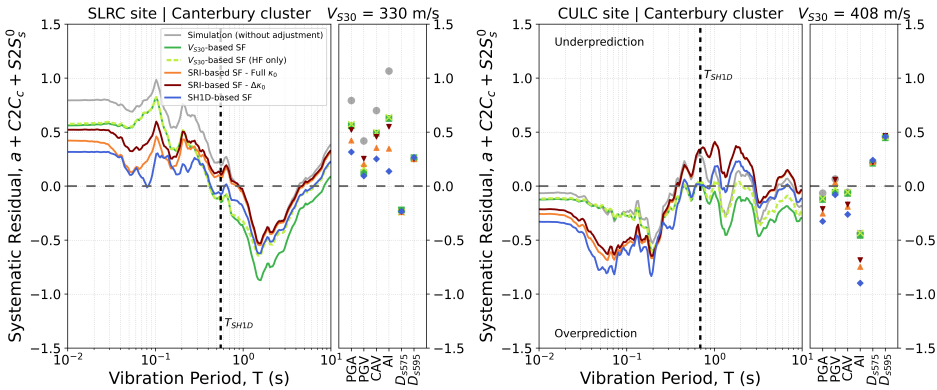

Figure D.7. Systematic residuals for the different methods, for the sites SLRC and CULC.

E Electronic Supplement E: Additional considerations and results

E.1 Illustration of the effect of the HF normalization factor

Figure E.1 illustrates the effect of the HF normalization factor (NF) for the CMHS and FKPS sites (also considered in Figure 7). CMHS is a site where the influence of NF is limited, whereas the site adjustment for FKPS is more significantly affected. The site factors are computed using the 'SH1D-based - $\Delta\kappa_0$' SF method, considering the "actual" and LF "simulation" profiles. The HF normalization factors are computed using the HF and LF "simulation" profiles. As shown in Figure 7, the stronger effect of NF for FKPS is due to larger differences between the LF and HF simulation profiles.

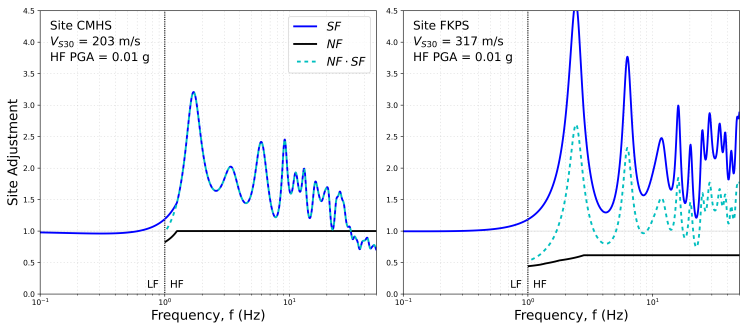

Figure E.1. Site factor (SF), HF normalization factor (NF), and their combined effect ($SF \cdot NF$) for the (a) CMHS and (b) FKPS sites. The site factors are computed with the 'SH1D-based - $\Delta\kappa_0$' SF method.

E.2 Evaluation of the NZVM in the Canterbury Region based on measured deep V_S profiles

Figure E.2 indicates the location of the nine stations in the Canterbury Plains where deep V_S profiles were developed by Deschenes et al. (2018).

Figure E.3 plots the nine profiles developed by Deschenes et al. (2018), and compares them with the corresponding NZVM profiles (and LF simulation profiles, adopting a grid spacing of 100 m and a minimum V_S of 500 m/s, as in this study). The figure illustrates that for the sites located further west (labelled as Gravel sites in Figure E.2), the measured V_S profiles are significantly stiffer than the NZVM profiles in the top 100-700 m. This indicates that the NZVM should be updated in this area, integrating this V_S information.

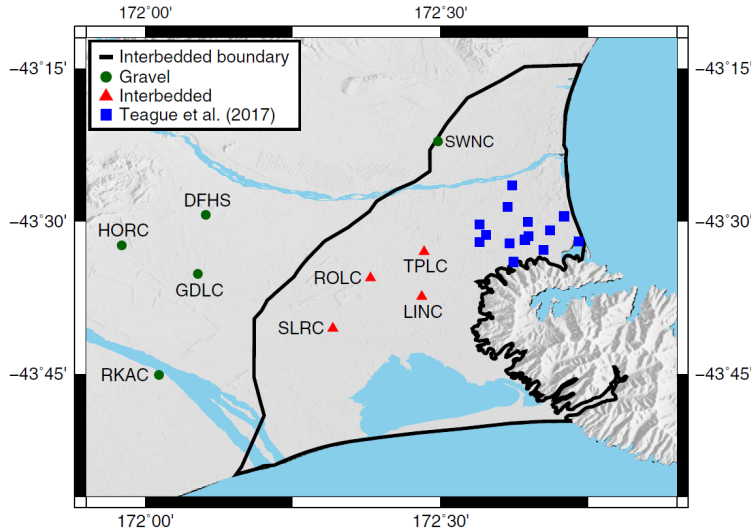

Figure E.2. Nine stations in the Canterbury Plains where deep V_S profiles were developed by Deschenes et al. (2018) (Figure 2 from Deschenes et al. 2018).

E.3 Comparison of site adjustments for soil sites in Wellington

Figure E.4 displays the linear SF computed with the alternative methods for 13 soil sites in the Wellington region with $V_{S30} = 223 - 375$ m/s, similar to Figure 12 for Christchurch. Strong discontinuities at $f = 1$ Hz in the V_S profile-based SFs are observed for several sites, due to the HF normalization factor being more influential in Wellington than in Canterbury (because the HF "simulation" profile deviates more substantially from the LF "simulation" profiles in Wellington). Similar to the Christchurch case, there are several sites where significant differences are observed between the V_{S30}- and V_S profile-based methods. In addition to sites with strong resonances (e.g., SOCS) and strong high-frequency amplification (e.g., UHCS), Figure E.4 illustrates another situation where large differences can occur: sites with $f_{SH1D,0}$ considerably lower than the transition frequency of 1 Hz (e.g., TFSS), where a significant amplification is predicted near $f_{SH1D,0}$ by the 'SH1D-based' SF methods and no amplification is considered by the (HF only) 'V_{S30}-based' SF method.

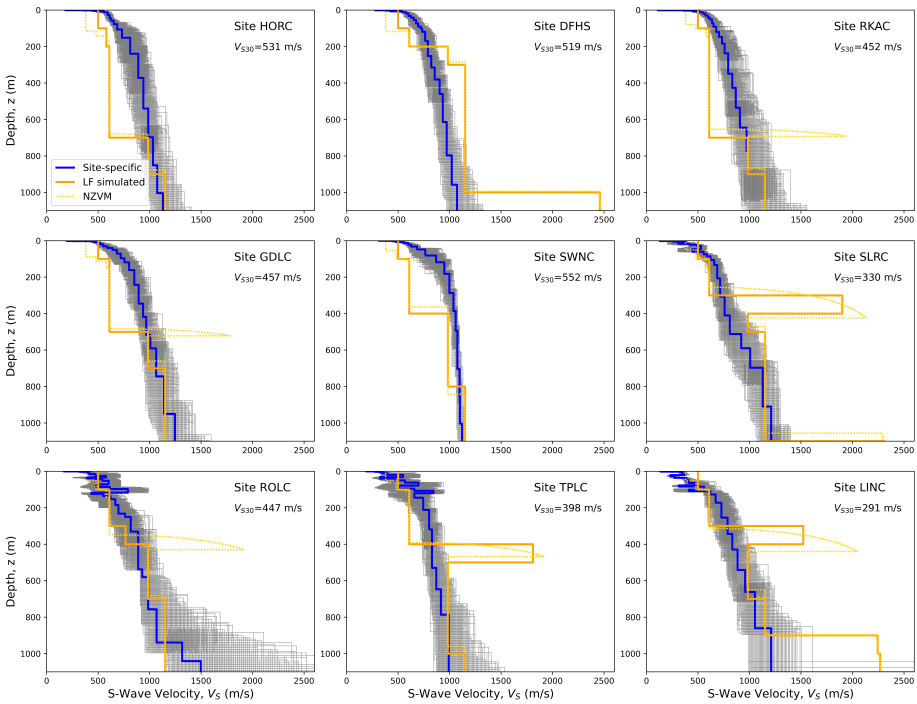

Figure E.3. Comparison between measured profiles (Deschenes et al. 2018) and NZVM/LF simulation profiles. The profiles in blue are the median profiles developed by (Deschenes et al. 2018) and the ones in gray, the 1000 lowest misfit models.

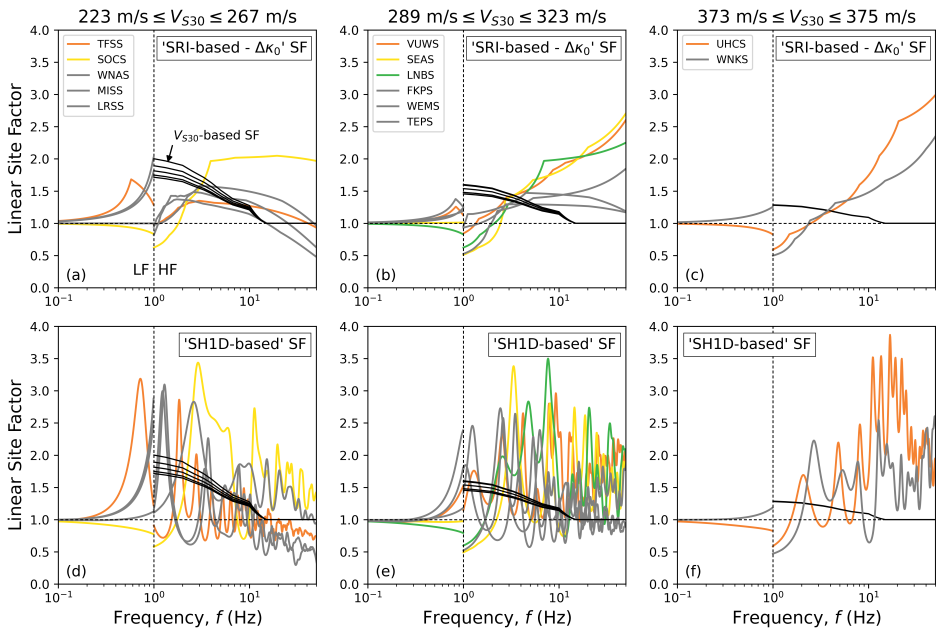

Figure E.4. Comparison between the (HF only) 'V_{S30}-based" linear SFs (computed with the CB14 model) and V_S profile-based linear SFs, for soil sites in Wellington grouped by different V_{S30} bins. Narrow V_{S30} ranges are considered such that the 'V_{S30}-based' SFs are practically equivalent within a bin. a - c represent low, intermediate, and high V_{S30} values, respectively, for the 'SRI-based - $\Delta\kappa_0$' SF method; and d - f represent low, intermediate, and high V_{S30} values, respectively, for the 'SH1D-based' SF method. The HF component of the V_S profile-based linear SFs is presented with the HF normalization factor applied (i.e., $NF\dot{S}F$).

E.4 Site response relative to nearby sites in Christchurch

Figure E.5 presents an analysis equivalent to that presented in de la Torre et al. (2020) (Figure 9), for the ground motions and methods considered in this article. The figure illustrates that the 'SH1D-based' SF method is able to capture the high site response at REHS (relative to three nearby sites).

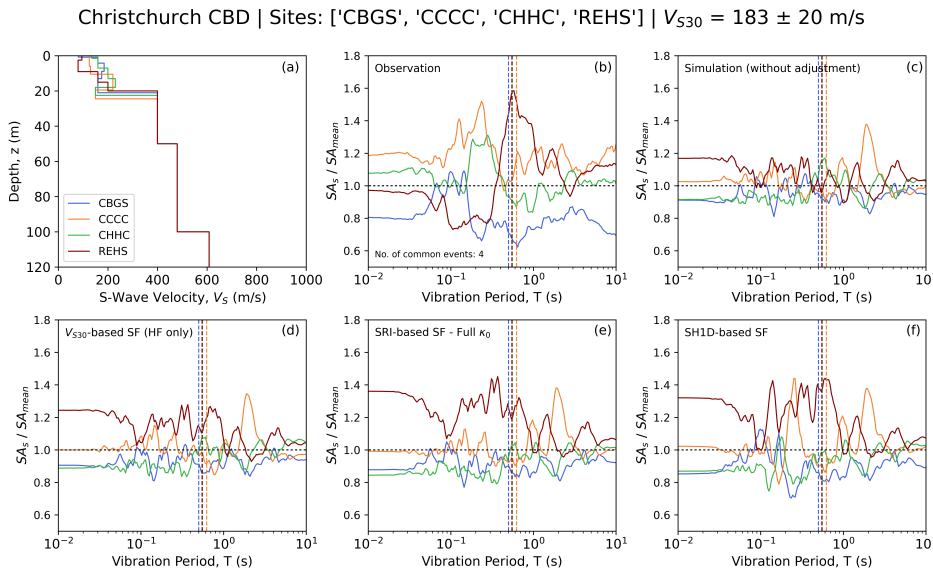

Figure E.5. Response spectral ratios for nearby sites within the Christchurch CBD. The ratio represents the average response of each site relative to the mean response from all sites in the group.

E.5 POTS V_S profile modification

A V_S profile measured close to POTS was modified in this study to better represent the site conditions at this station. POTS is located at the toe of the Wellington hills (Figure 1). As explained in de la Torre et al. (2024a), a V_S profile measured 15 m from the station (through downhole test) indicates a $V_{S30} = 453$ m/s (value considered in Wotherspoon et al. 2024). However, this measurement was performed in an in-filled gully adjacent to the station, which is believed not to be representative of POTS site conditions based on topographic and other considerations (de la Torre et al. 2024a), suggesting the presence of shallow weathered rock at the location of the instrument. Furthermore, residual analysis using semi-empirical GMMs and other similar evaluations (de la Torre et al. 2024a; Kaiser et al. 2024) suggest that $V_{S30} = 760$ m/s is likely a more realistic value for this site. Additional evidence of a rock-like response at POTS is given by the almost flat HVSR curve (Bradley et al. 2018) and GIT site response (Zhu et al. 2024); and the similarity of SA recorded at POTS and other rock stations in Wellington (Bradley et al. 2017). Based on this, in this study the nearby measured V_S profile was modified such that $V_{S30} = 760$ m/s. To do this, the top 13.1 m of the measured V_S were removed, which assumes that the site condition at 13.1 m depth is similar to the surficial condition at the location of the instrument. This heuristic modification of the V_S profile introduces additional uncertainty into the computation of SF for POTS, particularly at $f > 10$ Hz, where strong resonance peaks are predicted by the 'SH1D-based' SF due to the surficial softer layers.

E.6 LF simulation V_S profiles for POTS, WEMS, and TFSS

Figure E.6 shows the V_S profiles considered in the LF simulation for POTS, WEMS, and TFSS (whose relative locations are illustrated in Figure 3c), and the underlying V_S profiles extracted from the NZVM v2.02. The NZVM v2.02 model (Thomson et al. 2020) indicates a significantly lower near-surface V_S at POTS than that expected for a rock site. Also, the NZVM model indicates a greater rock depth (represented by $V_S > 1000$ m/s) at TFSS than at WEMS. However, due to the finite-difference grid spacing of 100 m and minimum V_S of 500 m/s, the depth to the rock that is effectively considered in the LF simulation, as well as the top layer V_S, is the same for the three sites (100 m and 500 m/s, respectively). Thus, the geometry of the relatively shallow Thorndon basin is not properly modeled in the LF simulation, explaining why 3D effects are not captured. As illustrated in the figure, the deep part of the actual profiles for WEMS and TFSS was constrained by the Hill et al. (2022) model. This model indicates considerable greater depths to rock for these sites than the NZVM v2.02.

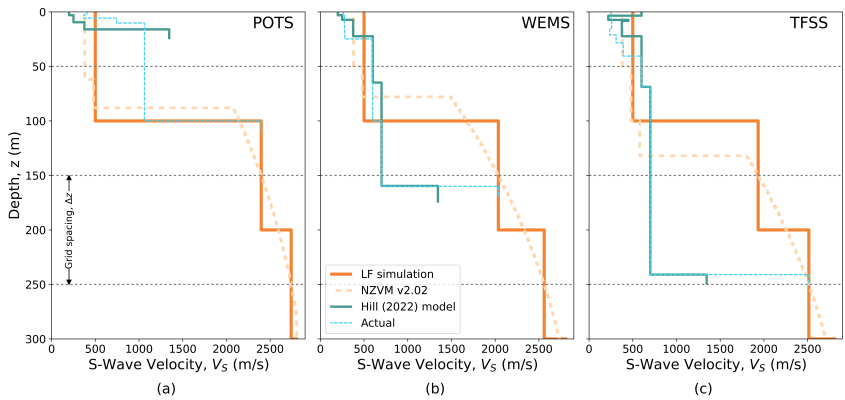

Figure E.6. Actual, NZVM v.2.02, and LF simulation V_S profiles considered for (a) POTS, (b) WEMS, and (c) TFSS. The NZVM v2.02 is implemented using a grid spacing $\Delta z = 100$ m in the LF simulation.